MECHANICALLY ROBUST INJECTABLE HYDROGEL SCAFFOLDS FOR THE INTRAMUSCULAR DELIVERY OF ADIPOSE-DERIVED STEM/STROMAL CELLS

by

Stuart Alexander Young

A thesis submitted to the Department of Chemical Engineering

In conformity with the requirements for

the degree of Doctor of Philosophy

Queen's University

Kingston, Ontario, Canada

(September 2017)

Abstract

An emerging treatment for peripheral arterial disease is the transplantation of adipose-derived stem/stromal cells (ASCs) by intramuscular (IM) injection to improve limb perfusion by paracrine-mediated angiogenesis and immunomodulation. However, effective clinical translation has been limited due to poor cell retention and survival in ischemic muscle. This thesis focused on the design and *in vitro*/*in vivo* evaluation of an injectable hydrogel to improve ASC retention and function following IM delivery.

Initial work developed an injectable, *in situ*-gelling hydrogel designed specifically to encapsulate ASCs and withstand the mechanical loading of the IM environment. The hydrogel consisted of two polymers: methacrylated glycol chitosan functionalized with a cell-adhesive RGD peptide, selected to support ASC retention and survival, and a triblock copolymer of poly(trimethylene carbonate)-*b*-poly(ethylene glycol)-*b*-poly(trimethylene carbonate) diacrylate, designed to improve mechanical resilience. Following *in vitro* injection and crosslinking within the hydrogel, encapsulated human ASCs demonstrated high viability (>90%) over two weeks under normoxic and hypoxic (2% O_2) conditions. The release of angiogenic and chemotactic cytokines from encapsulated ASCs was enhanced under hypoxia, suggesting that the hydrogel can support ASC retention and paracrine function under ischemic conditions.

Subsequent studies investigated the angiogenic and inflammatory responses to the IM injection of allogeneic rat ASCs in the hydrogel, the hydrogel alone, and ASCs in saline using a healthy, immunocompetent rat model. Immunohistochemical analysis over 4 weeks demonstrated that encapsulated ASCs were retained at a higher density and promoted $CD68^+$ macrophage recruitment, as well as M1 ($CD68^+CCR7^+$) macrophage infiltration and M2c ($CD163^+$) macrophage polarization at the hydrogel periphery. Coincident with enhanced macrophage infiltration, significantly more blood vessels were observed surrounding and within the hydrogels with ASCs compared to the hydrogels alone.

The therapeutic effects of the IM injection of human ASCs in the hydrogel, the hydrogel alone, ASCs in saline, and saline alone were compared in an immunocompromised NOD/SCID mouse model of hindlimb ischemia. While there were no differences observed in limb perfusion or function at 28 days,

immunohistochemical analysis revealed that hydrogel-delivered ASCs were well retained and significantly improved the IM capillary density and enhanced cell proliferation, indicating that the cell delivery approach stimulated localized angiogenesis.

Co-Authorship

Chapter 3 and sections of Chapter 5 have been submitted for publication in *Biomaterials* in August 2017, with the following co-authors: Stuart A. Young, Stephen E. Sherman, Tyler T. Cooper, Cody Brown, Fraz Anjum, David A. Hess, Lauren E. Flynn, and Brian G. Amsden. Dr. Fraz Anjum developed the original protocol for polymer peptide functionalization. Mr. Cody Brown performed the isolation and immunophenotyping of the adipose-derived stem/stromal cells used for *in vivo* experiments at Western University. Mr. Stephen Sherman and Mr. Tyler Cooper, of Dr. David Hess' lab at Western University, performed the microvascular surgeries and laser Doppler perfusion imaging. I planned and organized these experiments, assisted with the surgeries and imaging, and was solely responsible for the analysis and interpretation of the results.

Work from Chapter 4 has been submitted for publication in the *Journal of Tissue Engineering and Regenerative Medicine* in August 2017, with the following co-authors: Stuart A. Young, Lauren E. Flynn, and Brian G. Amsden.

Acknowledgements

I would like to express my sincere gratitude to my PhD supervisors, Dr. Brian Amsden and Dr. Lauren Flynn, for their guidance and encouragement, their thoughtful criticism, and their continued friendship. They have been invaluable role models as researchers, as collaborators, and as teachers – and I am thankful for every opportunity they have provided for me to grow in these roles.

I would also like to thank my colleagues, past and present, at Queen's University and the University of Western Ontario, without whom this work would have been impossible. Thanks especially to James Hayami, Thomas Rooney, Cody Brown, Valerio Russo, Claire Yu, Julian Chesterman, Moira Vyner, Fiona Serack, and Amanda Brissenden for many fond memories, both in and out of the lab.

I am grateful for the enthusiastic support and experienced guidance I received from Dr. David Hess, Stephen Sherman, and Tyler Cooper during my collaboration at the University of Western Ontario. Thank you also to my supervisory committee at Queen's University, Dr. Scott Parent and Dr. Katrina Gee, for their insight and direction throughout this project.

Finally, I would like to express my greatest appreciation to my friends and family for all their love and support during my PhD.

Table of Contents

List of Figures

List of Tables

List of Abbreviations

AC	Acryloyl chloride
APS	Ammonium persulfate
Arg-1	Arginase-1
ASC	Adipose-derived stem/stromal cell
bASC	Bovine adipose-derived stem/stromal cell
bFGF	Basic fibroblast growth factor
BMI	Body mass index
BMSC	Bone marrow-derived stem/stromal cell
CCL	Chemokine ligand
CCR	Chemokine receptor
CD	Cluster of differentiation
CT	Computed tomography
DAPI	4’,6-diamino-2-phenylindole
DCM	Dichloromethane
DMF	Dimethylformamide
DMSO	Dimethyl sulfoxide
DN	Double network
EC	Endothelial cell
ECM	Extracellular matrix
EdU	5-ethynyl-2’-deoxyuridine
EWC	Equilibrium water content
FBS	Fetal bovine serum
GAG	Glycosaminoglycan
GC	Glycol chitosan
GPC	Gel permeation chromatography
HA	Hyaluronic acid
hASC	Human adipose-derived stem/stromal cell
HGF	Hepatocyte growth factor
HI	Hindlimb ischemia
HUVEC	Human umbilical vein endothelial cell
IC	Immune complex
IFN-γ	Interferon-γ
IGF-1	Insulin-like growth factor-1
IHC	Immunohistochemistry
IL	Interleukin
IM	Intramuscular
iNOS	Inducible nitric oxide synthase
LDPI	Laser Doppler perfusion imaging
LPS	Lipopolysaccharide
M0	Non-activated macrophage
M1	Classically activated macrophage

M2	Alternatively activated macrophage
MCP-1	Monocyte chemoattractant protein-1
MGC	Methacrylate glycol chitosan
MGC-RGD	Methacrylated glycol chitosan functionalized with an RGD peptide
MI	Myocardial infarction
MMP	Matrix metalloproteinase
MSC	Mesenchymal stem/stromal cell
NC	Nanocomposite
NOD	Non-obese diabetic
NMR	Nuclear magnetic resonance
PAD	Peripheral arterial disease
PBS	Phosphate buffered saline
PDGF	Platelet-derived growth factor
PEG	Poly(ethylene glycol)
PEGDA	Poly(ethylene glycol) diacrylate
PlGF	Placental growth factor
PTMC	Poly(trimethylene carbonate)
rASC	Rat adipose-derived stem/stromal cell
RGD	Arginine-glycine-aspartic acid peptide sequence
RT	Room temperature
SCID	Severe combined immune deficiency
SD	Standard deviation
SDF-1α	Stromal cell-derived factor-1α
TCPS	Tissue culture polystyrene
TEA	Triethylamine
TEMED	*N*,*N*,*N'*,*N'*-tetramethylethylenediamine
TGF-β	Transforming growth factor-β
TIMP	Tissue inhibitor of metalloproteinase
TLR	Toll-like receptor
THF	Tetrahydrofuran
TMC	Trimethylene carbonate
TNF-α	Tumor necrosis factor-alpha
VEGF	Vascular endothelial growth factor
% w/v	Mass concentration (percent weight per volume)

Chapter 1

Introduction

1.1 Clinical Significance

Cardiovascular disease (CVD), including peripheral arterial disease (PAD) and myocardial infarction (MI), is the leading cause of mortality in the world, causing 17.3 million deaths annually in 2013, representing 31.5% of all deaths worldwide.[1] Current treatment strategies, including pharmacological therapy, artery bypass grafts, and endovascular angioplasty, have decreased mortality rates; however, the incidence of CVD is expected to rise as the population ages, and many patients are not eligible for existing therapies, motivating research into alternative treatment strategies.[2–4] Mesenchymal stem/stromal cell (MSC) transplantation has been proposed as a therapy for treating ischemic conditions including PAD[5,6] and MI.[7] In this role, it is postulated that MSCs act as trophic mediators in the ischemic environment,[8] modulating inflammation and promoting angiogenesis through the production of anti-inflammatory and pro-angiogenic factors.[9–11] While preclinical studies of MSC treatment have demonstrated therapeutic benefits,[12,13] clinical trials have largely failed to reproduce these effects.[7,14–16] A major limitation of this approach, and possible explanation for the issues in clinical translation, is the poor localization, retention, and survival of MSCs following injection in saline. In applications requiring intramuscular (IM) delivery, such as delivery to cardiac muscle in MI and skeletal muscle in PAD, the dynamic mechanical environment may exacerbate this problem, promoting the dispersal of injected MSCs from the target site.[17–20]

To address these challenges, injectable hydrogel delivery scaffolds have been widely investigated as a strategy to improve cell retention following intramuscular injection.[21,22] In this approach, cells are injected in a polymer solution that crosslinks *in situ* to form a hydrogel scaffold, encapsulating the cells at the site of delivery to minimize initial cell washout, prevent anoikis, and ideally enhance long-term cell function.[23] From within the hydrogel, MSCs may then promote angiogenesis and mediate inflammation in the ischemic environment through the sustained, localized generation and release of beneficial paracrine

factors.[24] By enhancing the therapeutic efficacy of the injected cells, it is postulated that injectable hydrogels could not only improve the clinical outcomes of MSC-based therapies, but also reduce the number of cells required. Further, in contrast to traditional surgical treatments of MI and PAD, minimally invasive injectable cell therapies would impose less damage to the already injured tissue and reduce procedure and recovery times.

1.2 Research hypotheses

Despite the potential for injectable hydrogels to enhance MSC-based angiogenic therapies, few hydrogel scaffold design approaches have addressed the specific requirements for minimally invasive intramuscular delivery. Specifically, application in the intramuscular environment necessitates a hydrogel scaffold with mechanical properties matched to the soft surrounding muscle tissue, while simultaneously withstanding the repetitive loading without undergoing material dispersal or brittle failure. Further, the crosslinking process must facilitate minimally invasive injection of cells suspended in the polymer solution, and subsequent stimuli-sensitive *in situ* crosslinking in the intramuscular space. Finally, the hydrogel and crosslinking system must support the viability, retention, and function of encapsulated cells in an ischemic environment. In pursuit of these criteria, the current work hypothesized that mixing and co-crosslinking synthetic copolymers with naturally-derived cell-supporting polymers can produce a mechanically robust hydrogel scaffold capable of supporting cell encapsulation following injection.

Adipose-derived stem/stromal cells (ASCs) have been identified as a promising source of MSCs due to their relative abundance and accessibility.[25,26] Further, ASCs have been identified as promising candidates to treat ischemic conditions due to the broad array of angiogenic and immunomodulatory paracrine factors in their secretome.[9,10,12,27,28] The current work hypothesizes that ASCs, encapsulated within the mixed polymer hydrogel, can respond to hypoxic conditions modeling ischemia by releasing therapeutic growth factors. Finally, this work further hypothesizes that the application of the mixed polymer hydrogel delivery scaffold can improve ASC retention following intramuscular injection *in vivo*, resulting in immunomodulatory and angiogenic effects.

1.3 Research objectives and thesis overview

Guided by these motivating hypotheses, this thesis describes the development of a hydrogel scaffold designed specifically for the intramuscular delivery of ASCs to treat peripheral limb ischemia. The work was divided into three main objectives:

1. Develop a mechanically robust, injectable hydrogel system for ASC encapsulation;
2. Assess the inflammatory and angiogenic response to the intramuscular delivery of ASCs within the hydrogel scaffold;
3. Evaluate the therapeutic effects of the delivery strategy in a model of hindlimb ischemia.

Towards objective 1, a library of synthetic copolymers of poly(trimethylene carbonate)-*b*-poly(ethylene glycol)-*b*-poly(trimethylene carbonate) (PEG-(PTMC-A)$_2$) was developed to produce soft, mechanically resilient hydrogels. PEG-(PTMC-A)$_2$ was mixed and co-crosslinked with methacrylated glycol chitosan, functionalized with a cell-binding RGD peptide (MGC-RGD), to produce a cell-supportive, mechanically robust hydrogel. An injectable crosslinking mechanism was optimized using thermally-sensitive radical initiators to provide *in situ*-gelling functionality. Finally, human ASCs (hASCs) were encapsulated within the hydrogel *in vitro*, and assessed based on viability, retention, metabolic activity, and growth factor release under hypoxic and normoxic conditions.

In objective 2, the mixed hydrogel scaffold was used to deliver rat ASCs (rASCs) by intramuscular injection to the hindlimbs of healthy, immunocompetent host rats, and compared to the delivery of rASCs in saline and the hydrogel alone. At 1, 2, and 4 weeks post-delivery, tissue explants were examined to semi-quantitatively assess the intramuscular retention and distribution of rASCs, which were fluorescently labeled prior to delivery. Immunohistochemical (IHC) staining was performed to assess the inflammatory response in terms of macrophage recruitment, phenotypic polarization towards inflammatory or regenerative subtypes, and enzymatic activity. Finally, angiogenesis in response to the ASCs and recruited macrophages was assessed based on changes in vessel density surrounding the ASCs and scaffolds.

In the final objective, the delivery of human ASCs (hASCs) within the hydrogel scaffold was evaluated in a model of acute hindlimb ischemia produced by femoral artery ligation in immune deficient NOD/SCID mice. The intramuscular injections of hASCs in the hydrogel, the hydrogel alone, and hASCs in saline were compared to a sham treatment of saline. IHC staining was used to visualize and quantify ASC retention and the effects on intramuscular capillary density and cell proliferation. The therapeutic effects of the treatments were compared in terms of recovery of hindlimb perfusion and function. This work was performed in collaboration with the labs of Dr. David Hess at the University of Western Ontario, relying on their expertise with the hindlimb ischemia model and medical imaging.

The thesis is presented in chapter format. Chapter 2 summarizes the relevant literature concerning the design of mechanically robust, injectable hydrogels for cell delivery; the use of encapsulated MSCs for therapeutic angiogenesis; and the role of macrophages in the host response to cell delivery scaffolds. Chapters 3 through 5 describe the methodology, results, and discussion of each research objective. Finally, Chapter 6 presents a concluding summary of the thesis and offers an outlook on future directions.

Chapter 2

Literature Review

2.1 Mechanically robust, injectable hydrogels for cell delivery

2.1.1 Design of hydrogels for load bearing tissue applications

Over the past two decades, hydrogels have emerged as one of the most studied classes of biomaterial. Composed of a crosslinked network of polymers swollen with aqueous medium, this basic composition can yield structures with a wide range of physical, mechanical, chemical, and biological properties. This diversity is made possible through a constantly expanding portfolio of crosslinking mechanisms and polymers, both natural and synthetic, available for hydrogel production.[29] Hydrogels have long been identified as promising materials for use as scaffolds for cell delivery in tissue engineering, due to their potential to improve cell engraftment and survival in the harsh environment of damaged and diseased tissue.[30] In this application, candidate hydrogels and crosslinking methods must meet very specific design criteria: they must support the retention and viability of encapsulated cells; facilitate the diffusion of nutrients, waste, and soluble growth factors; produce no toxic effects in surrounding tissues; and undergo degradation at a rate that facilitates their therapeutic purpose. In addition, the use of hydrogels as minimally invasive injectable scaffolds further necessitates that a prepolymer solution with suspended cells can be injected through a small diameter needle (ca. 25G), and that the prepolymer undergoes stimuli-sensitive *in situ* crosslinking to rapidly form a cell-encapsulating hydrogel upon injection.

Towards these goals, injectable hydrogels have been designed using synthetic polymers, naturally-derived polymers, decellularized extracellular matrix (ECM)-based materials, and combinations thereof.[31] While synthetic polymers offer advantages in terms of batch-to-batch consistency and the precise control over hydrogel properties (*e.g.* modulus, water affinity, degradation), they generally lack the chemical moieties and structural conformation of ECM polymers that are required to support cell adhesion and proliferation.[32] Conversely, naturally-derived polymers and solubilized ECM retain many of the bioactive

moieties present in the ECM, but require chemical modification to enable crosslinking into stable hydrogels.[32] Strategies to enhance the bioactivity of synthetic polymers have included functionalization with peptide sequences found in cell adhesion proteins such as the arginine-glycine-aspartic acid (RGD) sequence,[33] and combining with natural polymers with innate bioactivity (*i.e*. chitosan,[34] hyaluronan,[35] and gelatin[36]).

Many hydrogel systems have been developed that meet the aforementioned criteria; however, these systems have largely been limited to use in non-load bearing applications, as few cell-encapsulating hydrogels reproduce the tough, failure-resistant mechanical properties of the ECM. While strategies exist to produce hydrogels with extremely stiff, tough, or deformable mechanical properties, most rely on polymers, crosslinking mechanisms or fabrication techniques that preclude their use as cell-encapsulating or injectable systems.[37] Structural weakness has proven to be a major limitation in the application of injectable cell-laden scaffolds as therapeutic agents, as the targets of many such therapies are structural or load-bearing tissues that undergo the repetitive or continuous application of stress and strain. Conditions afflicting such tissues that could benefit from cell-laden scaffolds include tissue ischemia in cardiac and skeletal muscle[31]; osteoarthritis of articular cartilage[38]; and full thickness wounds in skin.[39] These target tissues have widely varying mechanical properties and experience diverse loading conditions such as strain magnitude, peak load, and loading frequency. In response to these material deficiencies, recent research has focused on developing mechanically robust hydrogel systems that are both injectable and cytocompatible. Although this combination of properties is represented by only a small subset of hydrogels, schematically illustrated in Figure 2-1, it has been the topic of intense research efforts as the need for such materials becomes apparent.

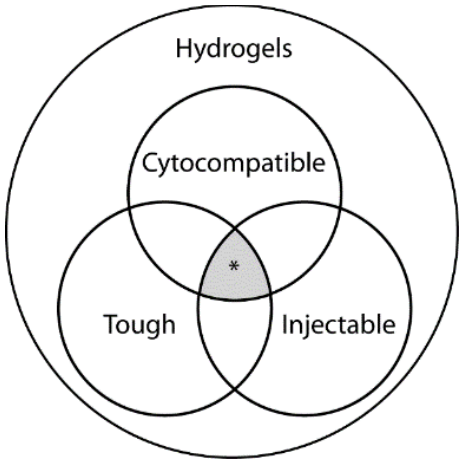

Figure 2-1: A schematic representation of hydrogel subsets based on select material properties. For the purpose of injectable cell delivery to mechanically dynamic tissue, hydrogel design has focused on the criteria of cytocompatibility, toughness, and injectability (*).

Towards developing hydrogels for cell delivery specifically to the intramuscular environment of the lower limb for treating peripheral arterial disease (PAD), important mechanical properties include a low compressive modulus matched to the surrounding soft tissue (ca. 15 kPa),[40] a high ultimate strain at failure (ca. 50% compression at 1 Hz[40,41]), and fatigue resistance under cyclic compression to withstand the repeated loading of muscle contraction.[40,41] To date, very few hydrogels have been designed to meet these criteria, while maintaining injectability, minimal swelling, and cell-encapsulation potential.

2.1.2 Structure-property relationships in hydrogels

The mechanical behavior of hydrogels is modeled based on the theory of rubber elasticity.[42] Similar to elastomers, deformation in hydrogels is facilitated by the uncoiling of polymer chains between network crosslinks or entanglements, and strain recovery is driven by regaining lost entropy.[43] The maximum strain achievable without network failure is therefore related to the ratio in dimensions of the initial random coil and the final extended chain. However, this theoretical ratio does not account for chain entanglements and network imperfections, which prevent the entire network from reaching strains that individual chains may be able to achieve. The network's initially linear resistance to applied strain, the Young's modulus of elasticity, is primarily influenced by the crosslink density. Networks with a higher polymer concentration

or a lower molecular weight between crosslinks have more networked chains per cross sectional area to resist deformation, resulting in a stiffer network and a higher modulus.[37,42]

Unlike elastomers, swelling is a significant factor in hydrogel properties. The degree of swelling with water is governed by the thermodynamic equilibrium between the driving force of water entering the network to dilute the polymers and the elastic force of the networked polymer chains stretching.[43] Swelling is therefore limited by crosslinks restricting network expansion, and related to the chemical nature of the polymers, where highly hydrophilic or charged polymers result in greater water uptake. Swelling has two primary effects on network mechanical properties: first, swelling induces considerable strain on the network, uncoiling the crosslinked segments such that the remaining capacity to withstand externally applied strain is diminished, and second, swelling typically reduces the modulus by diluting the crosslink density thereby resulting in fewer crosslinked polymer chains per cross sectional area to resist deformation. At extremely high degrees of swelling typical of networks of charged polymers, the network chains can become so highly extended that conformational limitations result in increased stiffness.[37]

Network failure is an important consideration in load-bearing applications of hydrogels, especially as hydrogels are typically susceptible to brittle failure. As cracks propagate through the hydrogel, energy is dissipated due to the extension and eventual fracture of network chains that span the crack. The toughness of the network depends on the amount of energy dissipated during this process.[37] This phenomenon is affected by the length of the network chains, as longer chains require more energy to extend, as well as the total polymer density, as more chains spanning the crack require more energy to extend and fracture.[44] Due to their swollen nature, hydrogels lack many of the typical means of energy dissipation found in elastomers. Specifically, swelling reduces the density of chains spanning the propagating crack, and therefore lowers the energy required for propagation.[37] Further, the separation of network chains with water reduces the ability of the chains to dissipate fracture energy through crystallization and viscoelastic effects.[37] Furthermore, the heterogeneous process of producing hydrogels via the crosslinking of aqueous prepolymer solutions results in network imperfections and inhomogeneity, which weaken the overall network. For

example, the commonly utilized free radical initiation process can result in the initial production of more densely crosslinked microgels, which are only later connected into a continuous hydrogel.[45] This process results in an inhomogeneous crosslink density distribution, in which areas of high crosslink density are more susceptible to fracture.[46]

The mode of crosslinking is also a factor in determining how hydrogel networks typically fail. Covalent crosslinking, though capable of producing a wide range of stiffness through permanent chemical crosslinks, typically produces fragile hydrogels that are susceptible to brittle failure and unable to absorb the energies or undergo the deformations characteristic of physiological loading.[47,48] Alternatively, physical crosslinking generally produces ductile rather than brittle networks due to the ability of physical crosslinks to "self-heal" (*i.e.* rapidly break and reform); however, physically crosslinked hydrogels often undergo pseudoplastic deformation and typically do not provide the required loading resistance for many physiological settings.[47,48]

2.1.3 Strategies for producing robust hydrogels for injectable cell encapsulation

The requirements of injectability and cytocompatibility limit the available strategies for producing robust hydrogels suitable for cell delivery to the intramuscular environment. Specifically, the need for injectability precludes the use of multi-step synthesis procedures or crosslinking methods that are slow or not stimuli-sensitive. Furthermore, cell encapsulation and use *in vivo* requires that the crosslinking reaction and polymers are non-cytotoxic, and do not rely on organic solvents or non-physiologic reaction conditions. Despite these restrictive criteria, several strategies have been developed, including *in situ*-forming double networks, nanocomposite networks, and single networks from high molecular weight amphiphilic copolymers.

2.1.4 Injectable double networks

Since their initial development by Gong *et al*.[49] in 2003, double network hydrogels (DNs), composed of two separate interpenetrating networks, have come to represent the toughest class of synthetic hydrogels produced.[37] Traditionally, the double network structure is prepared sequentially; the primary

network is crosslinked first then soaked in the pre-polymer solution of the secondary network, which is subsequently crosslinked within the first network (Figure 2-2). The primary network is typically a highly crosslinked, swollen fragile network, while the secondary network is a ductile network crosslinked with weak or recoverable "self-healing" bonds.[50,51] Other defining features contributing to the enhanced toughness of DNs include a high molar ratio of the secondary network to the primary,[49] and low levels of inter-network crosslinking.[52]

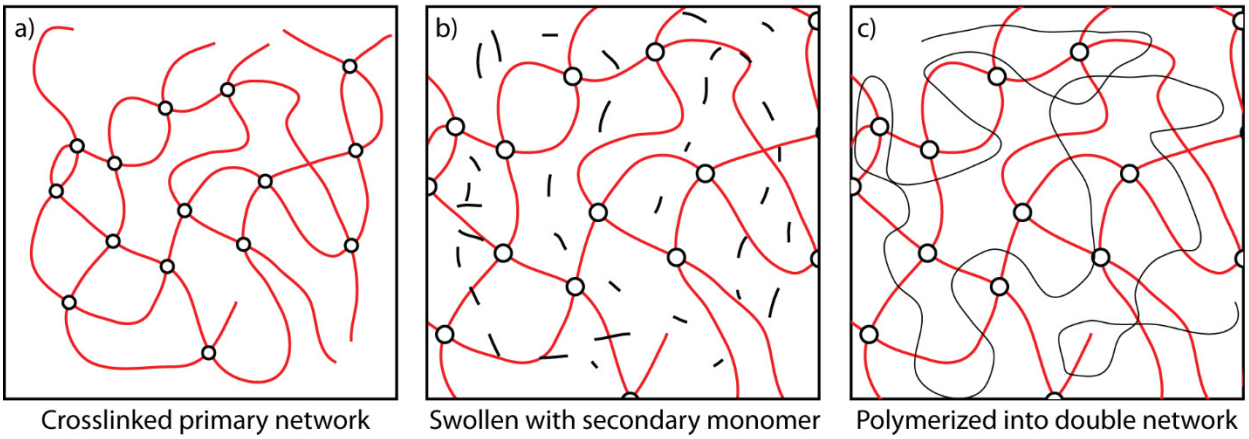

Figure 2-2: Schematic of double network hydrogel formation. a) The primary network (red) is prepared from a covalently crosslinked polymer network; b) the primary network is swollen with a monomer solution of the secondary network (black dashes); c) polymerization of the loosely crosslinked secondary network (black lines) results in a double network.

The strength of DNs is attributed to the ability of the loosely crosslinked chains of the secondary network to bridge and stabilize micro-cracks formed in the primary network. This bridging increases the number of strand fractures required for crack propagation, and further, distributes fracture forces across a wider damage zone, preventing the concentration of stress at the crack tip.[50,51] These mechanisms can result in a compression strength in the DN of 20 to 40 times the strength of the individual networks.[49] However, despite the self-healing nature of the secondary network, an accumulation of cracks in the primary network upon repeated mechanical loading can result in a loss of mechanical properties in a process termed the Mullins effect.[46] Further, the recovery of the secondary network often requires long time frames (2 h)[53] or high temperatures (> 50 °C).[54]

Recently, injectable, cell-encapsulating DNs have been developed by employing orthogonal crosslinking mechanisms to permit simultaneous formation of the primary and secondary networks. Truong *et al*.[55] utilized dual click chemistry mechanisms (thiol-yne addition and norborene-tetrazine cycloaddition) to provide rapid *in situ* crosslinking upon mixing of functionalized poly(ethylene glycol) (PEG) and chitosan that could encapsulate mesenchymal stem/stromal cells (MSCs) with high viability (99% after 48 h). Non-swollen, the network could undergo tensile extension over 550%, and withstand cyclic compression at 95% compression without hysteresis. However, given that swelling ratios between 200% and 400% were observed, these mechanical properties likely do not reflect the expected *in vivo* performance. In another approach, Rodell *et al*.[48] applied orthogonal crosslinking mechanisms (β-cyclodextrin with adamantane and thiol-ene addition) using a single polymer backbone of hyaluronic acid (HA) to encapsulate MSCs with sustained metabolic activity over 14 days. Non-swollen DNs could withstand approximately 250% extension and exhibited almost no Mullins-type softening (loss of moduli or strain energy with repeated loading); however, the approximate 4-fold swelling observed would likely compromise these properties when applied *in vivo*. Thus, while injectable DN have demonstrated outstanding ability to withstand tensile and compressive loading using cytocompatible polymers and reactions, the high degree of swelling following crosslinking is a yet unresolved issue hindering the translation of these mechanical properties into an *in vivo* setting.

2.1.5 Nanocomposite networks

Introduced by Haraguchi *et al*.[56] in 2002, nanocomposite (NC) hydrogels utilize nanoparticles, *i.e*. materials with extremely high surface area to volume ratios such as exfoliated clays, as multi-functional crosslinking sites within a polymer hydrogel network. In fabrication, the nanoparticles are distributed throughout a monomer solution that is subsequently crosslinked by free radical polymerization. The repeated absorption of polymer chains on the surface of multiple nanoparticles results in stable physical crosslinks reinforcing the hydrogel network (Figure 2-3). The resulting networks are extremely robust, typically withstanding elongation over 1000%.[56] The resistance to failure is attributed to the high molecular

weight of the polymers between the nanoparticles and the dissipation of fracture energy provided by the rearrangement of the absorbed polymers on the nanoparticle surface, allowing the network structure to re-organize under strain. As each nanoparticle is connected to multiple chains, and each chain to multiple nanoparticles, the breaking of individual bonds does not compromise the overall network, and these broken bonds can be recovered by neighboring polymers and nanoparticles.[57]

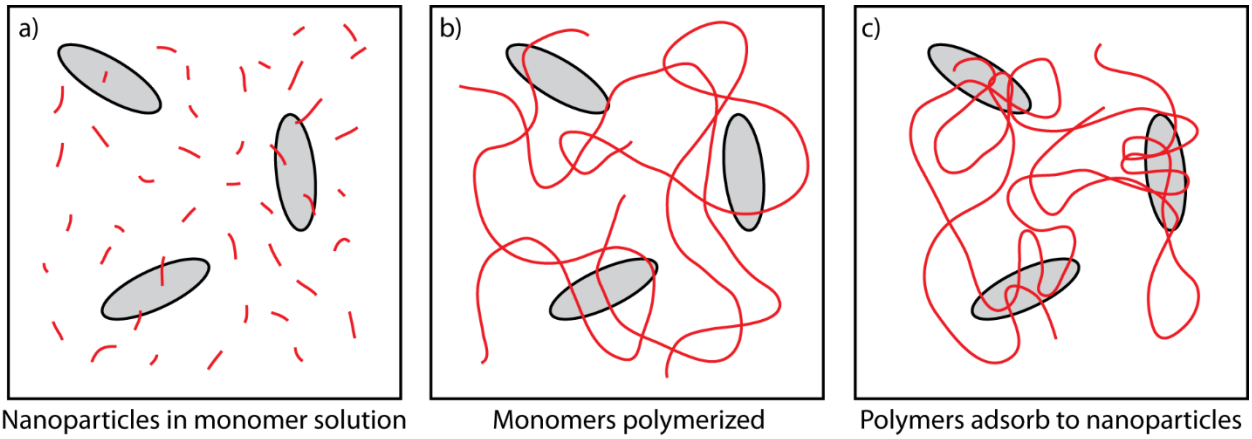

Figure 2-3: Schematic of nanocomposite hydrogel formation. a) Nanoparticles (grey) are dispersed in a solution of monomers (red); b) polymerization is initiated; c) polymer chains adsorb to multiple nanoparticle surfaces.

Simply mixing nanoparticles with polymer solutions does not result in networks that are as robust as those formed from the polymerization of monomer solutions with suspended nanoparticles, suggesting the effects depend on the polymerization of monomers from initiator absorbed to the nanoparticle surface.[57] This finding presents a challenge for cell encapsulation, as typically cells are suspended in a pre-polymer solution that is subsequently crosslinked, due to the cytotoxicity of low molecular weight monomers.[29] Furthermore, the recoverable nature of physical bonds between polymers and nanoparticles results in viscoelastic behavior, evident in hysteresis during repeated loading, and non-recoverable creep under sustained loading.[58] This behaviour may not be suitable for many load-bearing tissue applications where repeated loading is applied, or where creep resistance is essential for maintaining the tissue architecture.

NCs have been adapted for injectable cell encapsulation applications by using cytocompatible prepolymers, nanoparticles, and crosslinking methods. Gaharwar *et al.*[59] developed an elastomeric and highly extensible NC by photo crosslinking poly(ethylene glycol)-diacrylate (PEGDA) with hydroxyapatite

nanoparticles. The inclusion of nanoparticles allowed for the attachment and spreading of surface-seeded murine preosteoblasts. However, as the hydrogels were observed to swell between approximately 400% and 600% in phosphate buffered saline (PBS), it is expected that the performance of these systems *in vivo* would be compromised by network dilution. Jaiswal *et al*.[60] have prepared NC hydrogels from a network of methacrylated gelatin and functionalized iron nanoparticles that supported the encapsulation of murine preosteoblasts. Although the nanoparticles increased toughness by 17-fold, the degree of swelling was not reported, so the *in vivo* performance cannot be estimated. Overall, NC hydrogels represent a promising way to produce tough, cytocompatible hydrogels; however, the high degrees of swelling suggest that their mechanical properties would be severely compromised in the intramuscular environment. Further, there is concern regarding the potential toxicity of inorganic nanoparticles both locally and systemically, as well as to the encapsulated cells.[56,61]

2.1.6 High molecular weight amphiphilic prepolymer networks

A class of high molecular weight amphiphilic prepolymer precursors has been developed to address the fragile nature of highly swollen, highly crosslinked polymer networks. In this strategy, introduced by Zhang, *et al*.,[62] prepolymers with a well-defined structure of hydrophobic polymer blocks and high molecular weight (ca. >10 $kg \cdot mol^{-1}$) hydrophilic PEG blocks are crosslinked by radical polymerization of functionalized end groups. In such networks, the introduction of hydrophobic domains reduces network swelling, thereby preventing the complete extension of the polymer chains between crosslinks and preserving their random coil configuration (Figure 2-4).[62] Under strain, it is postulated that these domains are capable of absorbing the applied energy by uncoiling without any permanent effect on the underlying network, and upon unloading, entropic forces in the aqueous environment drive the recoiling of the hydrophobic domains (Figure 2-4c).[62] These effects are in contrast to typical hydrophilic networks in which swelling has extended the network chains and severely limited their ability to withstand deformation. Further, it is postulated that physical crosslinks are introduced in the form of entanglements of the high molecular weight PEG domains and in the interactions of the hydrophobic domains, capable of dissipating

energy during deformation without undergoing brittle failure.[62] These networks are particularly amenable to injectable cell encapsulation due to their simple, rapid, one-step preparation from a single precursor solution, and the ability to control the network swelling by adjusting the ratio of hydrophobic and hydrophilic components.

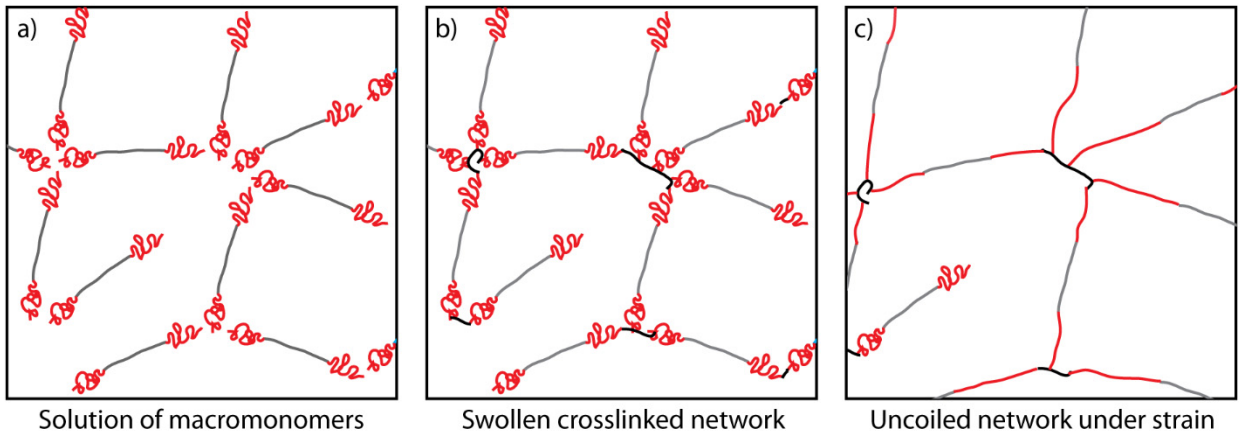

Figure 2-4: Schematic of high molecular weight amphiphilic copolymer hydrogel formation. a) Amphiphilic prepolymer precursors in solution (red: coiled hydrophobic domain; grey: extended hydrophilic domain); b) polymerization of end groups (black) produces a crosslinked network; c) upon application of strain, hydrophobic domains reversibly uncoil to allow network deformation.

In an initial study by Zhang *et al.*[62] using an amphiphilic α,ω-diacrylate poly(trimethylene carbonate)-*b*-poly(ethylene glycol)-*b*-poly(trimethylene carbonate) (PEG-(PTMC-A)$_2$) prepolymer, the introduction of the hydrophobic PTMC domains significantly increased the resulting network toughness and fracture stress compared to pure PEGDA networks. The networks could withstand large compressive strains of over 98% before failure, exemplifying the ability of crosslinked polymer chains to deform drastically without damaging the overall network. Importantly, these properties were measured on hydrogels swollen in PBS. MSCs encapsulated within the PEG-(PTMC-A)$_2$ networks were viable 24 h after crosslinking; however, the viability was not quantified. In subsequent studies, chondrocytes encapsulated within PEG-(PTMC-A)$_2$ hydrogels demonstrated *ca*. 80% viability, and produced significantly more collagen and glycosaminoglycans than those encapsulated within PEGDA hydrogels over three weeks of culture *in vitro*.[63]

Together, these studies have demonstrated potential for high molecular weight amphiphilic prepolymers to form mechanically robust networks. Importantly, in the context of *in vivo* use in load-bearing applications, these properties were maintained after network swelling. However, as purely synthetic polymers, these prepolymers lack the adhesive or instructive moieties that are present in the ECM and in hydrogels prepared from natural polymers.

2.2 Encapsulated mesenchymal stem cells for therapeutic angiogenesis

2.2.1 Mesenchymal stem cell sources

Beyond the design of the hydrogel scaffold, the main consideration of a cell-based treatment for PAD is the selection of a therapeutic cell source. To provide the estimated 10^7 to 10^9 cells required for angiogenic therapy[64] the cell source must be abundant, readily available, and ideally from the same patient to reduce concerns of immunogenicity and disease transfer. Embryonic stem cells and induced pluripotent stem cells have demonstrated substantial regenerative capacity; however, concerns over safety and ethics have limited their clinical application.[65] Alternatively, MSCs have been identified as one of the most promising candidates due to their autologous and allogeneic availability in adult tissues, as well as their immunomodulatory and angiogenic activities.[66,67] The first evidence of MSCs came from the work of Friedenstein *et al*.,[68] who identified bone marrow-derived stem/stromal cells (BMSCs) capable of clonal expansion and osteogenic differentiation. Since that discovery, numerous other adult tissue sources of MSCs have been identified, including adipose-derived stem/stromal cells (ASCs),[69] and cord and peripheral blood-derived mesenchymal stem/stromal cells.[70] Regardless of their tissue source, MSCs represent a heterogeneous population that is broadly characterized by their ability to adhere to tissue culture polystyrene, undergo *in vitro* expansion, and maintain the potential to differentiate into osteogenic, chondrogenic, and adipogenic lineages.[71] MSCs are also characterized by the expression of cell surface markers of the stromal cell phenotype (CD90, CD29, CD44, and CD73), and negative for hematopoietic (CD34, CD45, CD14) and endothelial (CD31) phenotypic markers.[71]

For the clinical application of MSCs, the ideal tissue source would be accessible by a minimally invasive procedure, and provide a high yield of cells that can be further expanded in culture without diminishing their regenerative capacity. Despite the extensive research into BMSCs for therapeutic applications, the invasive harvesting procedure, risks of donor site morbidity, and relatively low yields present challenges for deriving sufficient numbers of BMSCs for clinical application.[72,73] More recently, ASCs have been identified as an attractive source of regenerative cells, as ASCs can be isolated from adipose tissue collected by minimally invasive lipoaspiration with few adverse effects.[74] Furthermore, autologous ASCs can be isolated with a relatively high yield, as a typical 200 mL lipoaspirate yields approximately 10^6 stem cells, more than 40-fold more than is yielded from a typical 40 mL aspiration of bone marrow.[75] Both ASCs and BMSCs have a similar secretome of therapeutic growth factors,[9,76] the ability to migrate to sites of injury and ischemia,[13,77,78] and the capacity to enhance perfusion in ischemic tissue.[79] For these reasons, adipose tissue is increasingly being explored as a source of MSCs for treating vascular diseases.

2.2.2 Adipose-derived stem cells as trophic mediators of angiogenesis

Pre-clinical trials to investigate the potential of ASCs to promote therapeutic angiogenesis using murine models of PAD have generally demonstrated positive results.[12,13,79,80] To simulate the reduced limb perfusion of PAD, these models involve the induction of hindlimb ischemia (HI) of varying degrees of severity by ligating and potentially excising a segment of the femoral artery, as well as potentially the vein.[81] Typical assessments of vascular recovery include measuring the perfusion ratio (PR) of the ischemic versus contralateral non-ligated control limb, and immunohistochemical staining to identify capillary density in the treated limbs as a measure of collateral vessel formation. These assessments are made in comparison to sham treatments of saline injection. The results of pre-clinical trials of ASCs in murine models of PAD to date are summarized in Table 2-1.

Table 2-1: Pre-clinical trials of ASCs used to treat hindlimb ischemia as a model of PAD. IV: intravenous; IM: intramuscular; PR: perfusion ratio.

ASC source	Host Model	Delivery	Main results (relative to saline)	Ref.
Human	Nude mice (athymic)	5×10^5 ASCs injected IV 24 h post-ligation	↑PR (2.5× and 3×) after 5 and 10 days, respectively	[10]
Human	NMRI nude mice (athymic)	5×10^5 ASCs injected IV 24 h post-ligation	↑PR (3×); ↑ capillary density (1.25×) after 14 days	[80]
Human	Balb/C nude mice (athymic)	1-10×10^5 ASCs injected IM (3 sites) 24 h post-ligation	↑PR (up to 2.3×, proportional to number of ASCs delivered); reduced muscle fiber damage after 14 days	[13]
Human	Balb/C nude mice (athymic)	10^6 ASCs injected IM (3 sites) 24 h post-ligation	↑PR (2.7×); ↓injured muscle area (0.2×) after 14 days	[79]
Mouse (C57BL/6J)	C57BL/6J mice	1×10^6 ASCs injected IM (3 sites) 24 h post-ligation	↑PR (1.2×); ↑capillary density (1.25×) after 21 days	[12]

While these pre-clinical studies of ASCs in models of PAD have yielded positive results in terms of recovery of perfusion and often capillary density, none of the studies have quantified the retention of ASCs in the intramuscular environment. In studies that have tracked ASCs in the ischemic hindlimb by immunohistochemical staining, some have reported evidence that ASCs may differentiate into endothelial-like cells and incorporate into vascular structures.[13,80] However, the frequency of engraftment and differentiation is reported at less than 1%,[13] suggesting that ASCs are promoting vascular recovery through an alternate mechanism.

Current work suggests that the angiogenic activity of ASCs is largely due to paracrine mechanisms, where ASCs secrete factors in response to the ischemic and inflammatory environment to promote angiogenesis and modulate inflammation.[66,82] This theory is based on the limited evidence of injected MSCs engrafting directly into ischemic tissues or differentiating into vascular structures,[83–86] the dependence of therapeutic effects on growth factor production,[12,87,88] and the numerous reports documenting the angiogenic and immunomodulatory effects from MSC-conditioned medium alone.[89–92] This evidence has prompted interest in mapping the ASC secretome.

Table 2-2 presents a summary of select growth factors secreted by ASCs that are involved in the treatment of ischemic conditions.

Table 2-2: ASC secreted growth factors involved in angiogenesis and immunomodulation. Cell types: EC: endothelial cell; SMC: smooth muscle cell.

Growth factor	Function[93,94]	Reference
Angiogenin	Angiogenesis (vessel stabilization, EC migration and invasion), anti-apoptosis	[9,92]
Angiopoietin-1	Angiogenesis (EC migration, vessel stabilization)	[9,95]
Basic fibroblast growth factor (bFGF)	Anti-apoptosis, angiogenesis (EC proliferation and migration), anti-scarring	[10,92,95]
Hepatocyte growth factor (HGF)	Anti-apoptosis, anti-scarring	[8–10,76,92,95]
Insulin-like growth factor-1 (IGF-1)	Anti-apoptosis	[8,92]
Leptin	Angiogenesis (EC proliferation and vascular permeability)	[76]
Monocyte chemoattractant protein-1 (MCP-1)	Angiogenesis, chemoattraction (monocyte migration)	[8,9]
Placental growth factor (PlGF)	Angiogenesis (EC proliferation)	[9,95]
Platelet-derived growth factor-AA (PDGF-AA)	Angiogenesis (SMC proliferation and migration)	[8,9]
Stromal cell-derived factor-1α (SDF-1α)	Angiogenesis (EC migration), chemoattraction (progenitor cell homing)	[76,92]
Transforming growth factor-β (TGF-β)	Anti-apoptosis, angiogenesis (vessel maturation, EC proliferation), immunomodulation	[8–10,95]
Vascular endothelial growth factor (VEGF)	Anti-apoptosis, angiogenesis (EC proliferation, migration, tube formation)	[8–10,76,92,95]

2.2.3 Injectable scaffolds for improving mesenchymal stem cell therapy

Despite the demonstrated potential of MSCs to promote angiogenesis in ischemic tissues in pre-clinical studies, clinical trials using MSCs to treat PAD have largely failed to reproduce these effects.[5,6,14] To overcome this failed translation, several strategies have focused on enhancing the paracrine effects of MSCs, including hypoxic preconditioning[78,92,96–98] and genetic manipulation.[83,99] However, a major limitation to cell-based therapies and possible explanation for the issues in clinical translation is the poor localization, retention, and survival of cells delivered by intramuscular injection in saline.[30,100–102] Using this basic delivery approach, MSC retention rates have been reported to be below 10% as early as 24 h after injection into the ischemic heart [19,103], and as low as 2% at 24 h post-injection into the ischemic hindlimb.[20] These low rates of retention following injection in saline may be attributed to an initial cell washout that

occurs immediately upon injection, and the subsequent failure of the MSCs to adhere to the extracellular matrix, resulting in cell death due to anoikis and poor long-term retention.[23,102]

To overcome the limitations of poor cell retention, some preliminary studies have explored the use of injectable biomaterial scaffolds to deliver and retain cells intramuscularly.[30] In the context of PAD models, these studies have demonstrated the potential to enhance the efficacy of cell-based therapies. In a HI model in athymic rats, Suuronen *et al.*[104] compared the intramuscular injection of 3×10^5 human peripheral blood-derived MSCs using an injectable matrix of Type 1 collagen and chondroitin sulfate that underwent thermo-gelling at 37 °C to the injection of MSCs in saline, the matrix alone, and saline alone. Though retention was not quantified absolutely, over 2 times more MSCs were detected in the intramuscular tissue when the cells were delivered in the collagen matrix as compared to saline. The improved retention was associated with a higher capillary and arteriole density, although perfusion was not quantified. Tang *et al.*[105] similarly explored the use of non-crosslinked hyaluronan (HA) solutions, a natural polymer component of the ECM shown to have angiogenic activities. HA solutions were used to deliver 10^6 human umbilical vein endothelial (HUVECs) cells to a HI model in nude mice, and compared to the delivery of HUVECs in saline, HA alone, and saline alone. After 4 weeks, the recovery of perfusion was significantly higher in mice treated with HUVECs in HA compared to all other treatments, and capillary density was similarly improved. Tracking of HUVECs by green fluorescent protein transfection revealed no HUVECs were retained after 4 weeks when delivered in saline. HUVECs in HA were detected in the intramuscular space, though few were found in association with capillaries or arterioles.

Together, these works demonstrate the potential for injectable biomaterials to improve cell retention in the ischemic hindlimb, and subsequently enhance their therapeutic potential. However, these studies have not addressed key properties of the scaffold that could affect their performance *in vivo*, including crosslinking time and mechanical properties. Further, these works have not investigated the ability of cells to produce and release growth factors from within the scaffolds, an essential aspect of cell-mediated therapies for PAD. Such studies have been done for alginate-based hydrogel scaffolds,

demonstrating the release of angiogenin, angiopoietin-2, bFGF, HGF, PlGF, and VEGF from encapsulated BMSCs,[106] and the release of immune modulatory cytokines from encapsulated ASCs.[107] However, cytokine release from cells encapsulated in scaffolds used in HI models have not been similarly studied. Thus, given the integral role that paracrine mechanisms appear to play in MSC-based therapies, there is a paucity of data demonstrating the impact of encapsulation on MSC paracrine signaling mechanisms.

2.3 The host macrophage response to cell delivery scaffolds in angiogenic therapy

2.3.1 The macrophage response to biomaterials

While previous studies have focused on the angiogenic response to encapsulated MSCs, it is important to recognize that the success of any biomaterial-based strategy is also dependent on the host immune response to the material. The intramuscular implantation of any material, even those delivered non-surgically by minimally invasive injection, evokes a host immune response comparable to the process of wound-healing.[108] In general, the response begins within minutes with the adsorption of proteins on the surface of the material, including growth and chemoattractive factors.[108] Subsequently, within hours, peripheral blood mononuclear cells are recruited, exiting circulation via extravasation and migrating to the site of the implant and tissue damage. Neutrophils are the predominant cell type in the initial 24 h, responsible for the phagocytosis of necrotic tissue and other debris, and propagating a pro-inflammatory response through the release of reactive oxygen species and cytokines.[109] As the neutrophil population declines, monocyte-derived macrophages and tissue resident macrophages are recruited to the implant site within 24-48 h. Upon activation at the site of inflammation, the macrophages exhibit a range of phenotypic polarization, and subsequently represent an influential factor in the immunological response.[110] Macrophages play a role in the initiation of angiogenesis and extracellular matrix deposition at the implant site, and determine the outcome of the implant through either integration and remodeling or fibrous encapsulation.[108–110]

Contrary to traditional models of macrophage activation into discrete phenotypes, current evidence suggests that macrophages exist on a spectrum of polarization between a pro-inflammatory M1 phenotype,

and a series of regenerative M2 phenotype subtypes, broadly classified as M2a, M2b, and M2c.[111–113] While Murray *et al*.[114] have proposed a comprehensive nomenclature for the spectrum based on macrophage source, activating factors, and cellular markers, researchers still commonly refer to M1 and M2 polarization in the discussion of the macrophage response to biomaterials. The defining activators, markers, and expressed factors of macrophages in the M1-M2 spectrum are presented in Table 2-3, based on the classification proposed by Mantovani *et al*.[113] and Spiller *et al*.[115] However, these definitions are not discrete, as polarized macrophages may exhibit multiple aspects of these phenotypes at a given time, including transient levels of cytokine and enzyme expression, and it is postulated that macrophages may switch polarization states in response to environmental cues.[116]

Table 2-3: Defining activators, markers, and secreted factors of polarized macrophages. Adapted from Mantovani *et al*.[113] and Spiller *et al*.[115]

Phenotype	Activator	Key Markers	Secretions/Expression
M1	LPS, IFN-γ, TNF-α	CCR7	TNF-α; IL-1β, IL-6, IL-12, VEGF; iNOS
M2a	IL-4, IL-13	CD206	CCL18, CCL22, PDGF, TIMP3, IL-10; Arg-1
M2b	IC + antagonists of TLR4 or IL-1R	CD86	TNF-α, IL-1β, IL-10
M2c	IL-10	CD163	MMP9, TGF-β, IL-10

Arg-1: arginase-1; CCL: chemokine ligand; CCR: chemokine receptor; CD: cluster of differentiation; IC: immune complexes; IFN-γ: interferon-γ; IL: interleukin; iNOS: inducible nitric oxide synthase; LPS: lipopolysaccharide; MMP: matrix metalloproteinase; PDGF: platelet-derived growth factor; TGF-β: Transforming growth factor-β; TIMP: tissue inhibitor of metalloproteinases; TLR: toll-like receptor; TNF-α: tumor necrosis factor-α

In the timeline of normal wound healing, M1 macrophages appear initially within 1-5 days, followed by M2 macrophages within typically 7-10 days.[117] M1 macrophages, activated by pro-inflammatory signals such as interferon-γ (IFN-γ) and tumor necrosis factor-α (TNF-α), are initially predominant at implanted materials. M1 macrophages are responsible for the continued removal of necrotic and apoptotic cellular debris, and the propagation of inflammation through the production of pro-inflammatory cytokines. Depending on the nature of the material, M1 macrophages may initiate implant degradation through enzymatic activity and the production of reactive oxygen species from arginine via inducible nitric oxide synthase (iNOS).[110,115,118] While an M1 response is essential to the initiation of the

inflammatory response, a prolonged M1 response can lead to chronic inflammation associated with damage of the neighboring tissues, fibrotic encapsulation of the implant, and adverse tissue remodeling.[119,120]

Resolution of the initial pro-inflammatory phase and transition to a pro-regenerative remodeling phase is marked by a polarization of macrophages towards an M2 phenotype. Broadly, M2 macrophages play a role in immunoregulation and tissue remodeling. They produce anti-inflammatory cytokines; express scavenger (CD163) or mannose (CD206) receptors;[113] promote matrix remodeling through the expression of matrix metalloproteinases;[121] and stimulate cellular proliferation and matrix deposition through the hydrolysis of arginine via arginase-1 (Arg-1) into a precursor for polyamines used in collagen synthesis.[122] The M2 subtypes M2a (activated by IL-4 and IL-13) and M2b (activated by immune complexes and toll-like receptor agonists) are thought to be predominantly responsible for immune regulation via secretion of both pro- and anti-inflammatory cytokines. The M2c subtype (activated by IL-10) performs similar suppression of inflammation, but is thought to be predominantly involved in tissue remodeling and matrix deposition.[113,118]

Many biomaterial design factors have been employed to modulate the M1:M2 macrophage polarization ratio in attempts to avoid a persistent inflammatory state and promote positive integration and remodeling outcomes rather than fibrous encapsulation.[118,120] A predominant factor dictating the long-term macrophage response is material degradability.[123] However, other important factors for hydrogels include stiffness, where softer materials have been found to reduce macrophage activation (both M1 and M2) and fibrous encapsulation[124].

2.3.2 Macrophages in angiogenesis

Angiogenesis is a critical process in most tissue engineering strategies, especially those with the goal of improving blood flow to ischemic tissues. Macrophages, as part of the overall inflammatory response, play a major regulatory role in the process of angiogenesis during development,[125] wound healing,[126] and in response to implanted materials.[115] While initial theories proposed that M2 macrophages, and not M1, were pro-angiogenic,[127,128] recent evidence suggests that angiogenesis is regulated by the

coordinated activities of both M1 and M2 macrophages.[115,121] In this model, M1 macrophages, via the secretion of pro-angiogenic factors including VEGF and bFGF, are thought to initiate sprout formation by endothelial cells. Subsequently, M2 macrophages contribute to vessel maturation. M2a macrophages, via secreted PDGF-BB, recruit pericytes to stabilize the nascent vessels and promote anastomosis. M2c macrophages, via MMP9 secretion, enable vascular remodeling.[121,129] This theory implies that the temporal distribution of macrophage phenotypes is important for angiogenesis, specifically the transition from an early M1 response to a subsequent M2 response. If the transition is disrupted, where M1 macrophages persist as the dominant phenotype, the wound or biomaterial implant could suffer from not only chronic inflammation, but also inhibited angiogenesis.[130]

2.3.3 Mesenchymal stem cells and macrophages

MSCs have demonstrated broad immunoregulatory effects on both the adaptive and innate immune system, motivating their use in treating immune-based disorders in addition to cardiovascular diseases.[131] To explain these effects, Waterman *et al*.[132] have proposed a model in which MSCs in a pro-inflammatory environment (high IFN-γ, TNF-α) adopt an anti-inflammatory immune-suppressive MSC2 phenotype, and in the absence of inflammatory signals (low IFN-γ, TNF-α) MSCs adopt an inflammation-permissive MSC1 phenotype that can enhance lymphocyte recruitment. Although seemingly contrary, these roles establish a balance between promoting host defenses, while also limiting the extent of inflammation to prevent excessive tissue damage.[133] Importantly, this model acknowledges the cross-talk between MSCs and cells of the immune system, including macrophages.

Numerous *in vitro* studies of MSCs in co-culture with macrophages have demonstrated the immunomodulatory interactions between MSCs and macrophages. In co-culture with M1 macrophages, ASCs have been shown to promote an immune regulatory M2-like macrophage phenotype with increased CD163 and CD206 marker expression, high Arg-1 activity, increased IL-10 production, and reduced TNF-α production.[134–136] The effect was bi-directional, as co-cultured ASCs increased expression of M2-inducing cytokines TGF-β1, IL-4 and IL-13.[135,137] ASCs may also enhance macrophage recruitment during

inflammation. When exposed to pro-inflammatory TNF-α, ASCs upregulated the production of macrophage chemoattractants IL-6, IL-8, and MCP-1.[138]

These findings have motivated the use of MSCs to modulate the macrophage response to implanted biomaterials. *In vitro* studies have demonstrated conflicting trends, where MSCs encapsulated in gelatin/PEG scaffolds can reduce TNF-α production in macrophages,[139] while MSCs encapsulated in gelatin/hyaluronic acid increase TNF-α production.[140] These results suggest that encapsulation of MSCs may alter the interaction with macrophages, with the effects potentially dependent on the specific properties of the engineered cellular microenvironment. *In vivo*, studies of implanted fibrin[141] and collagen[142] scaffolds have shown that the inclusion of MSCs significantly promotes M1 infiltration into the scaffolds, suggesting that MSCs can alter the macrophage recruitment and response to biomaterials. In contrast, in a study of ASCs delivered subcutaneously in a decellularized adipose tissue scaffold, while there were no differences observed in macrophage recruitment or infiltration in ASC-seeded implants versus unseeded controls, enhanced M2 ($CD163^+$) polarization was observed in response to the ASCs at 12 weeks.[143] Overall, these results indicate that while MSCs have the potential to significantly alter the macrophage response to implanted biomaterials, the effects are likely dependent on the interaction between the material itself, the MSCs, and host macrophages, leading to outcomes that are diverse and difficult to predict.

2.4 Summary

Despite the potential that MSCs have demonstrated for treating vascular diseases such as PAD in pre-clinical trials, the success in the clinical translation of these cell-based approaches has been modest.[5,144] The limited efficacy has been attributed to the low rates of cell retention and survival at the site of delivery following injection in saline. In response, research has focused on developing injectable hydrogel scaffolds to improve MSC delivery, with some pre-clinical evidence that suggests scaffold-based delivery approaches can enhance MSC therapeutic efficacy. However, a review of the literature indicates that there remains a lack of hydrogels that are designed specifically for this application, combining injectability, cell-encapsulation, and robust mechanical properties appropriate for use in the mechanically dynamic

intramuscular environment. While several strategies have been developed to produce robust hydrogels, including double networks, nanocomposites, and amphiphilic prepolymer networks, these types of networks are rarely applied in applications requiring cell encapsulation and injectability *in vivo*. This lack of appropriate biomaterials motivated the current work of developing a robust hydrogel scaffold for the injectable delivery of MSCs to the intramuscular environment.

The success of such biomaterial-based strategies ultimately depends on the angiogenic and inflammatory responses to the combined scaffold and MSCs *in vivo*. Recent literature indicates that the process of angiogenesis is closely linked to the activities of macrophages, and furthermore, that the angiogenic potential of MSCs is at least partially linked to their immunomodulatory interactions with macrophages. These relationships motivated the investigation in the current work on the interactions between host macrophages and the hydrogel scaffolds with and without MSCs to help better understand the role of each component in mediating the host response.

Chapter 3

Development of a mechanically robust, injectable hydrogel system for adipose-derived stem cell encapsulation

3.1 Introduction

A promising strategy for treating peripheral arterial disease (PAD) involves intramuscular (IM) or intra-arterial (IA) injection of autologous mesenchymal stem/stromal cells (MSCs) into the ischemic regions of the affected limbs to stimulate revascularization and functional recovery.[144] Adipose-derived stem/stromal cells (ASCs) are an attractive MSC source due to their relative abundance and accessibility in the autologous setting.[25,26] Further, ASCs have been shown to enhance angiogenesis in ischemic limbs,[10,12,13,80] a process largely mediated by the secretion of an array of pro-angiogenic cytokines and growth factors.[12,27,28] However, a major obstacle in maintaining paracrine-mediated cell therapy is the poor retention of cells delivered in saline to ischemic regions via IM or IA injection, which is consistently below 10% at 1 week post-transplantation.[18–20]

By providing a matrix that supports cell adhesion and survival, biomaterial scaffolds may overcome the challenge of retaining cells delivered to ischemic tissues.[31,145] Previous studies have indicated this strategy can improve the efficacy of cell therapies in treating PAD in animal models.[105,146] However, the approaches examined to date have not addressed key material requirements for minimally invasive IM delivery of cells to the lower limb. The ideal material for this application would closely reproduce the properties of skeletal muscle in terms of mechanical properties, cellular support, and integration with the surrounding tissue, while facilitating injectable delivery and encapsulation of therapeutic cells. Specifically, the mechanically dynamic intramuscular environment demands an elastic modulus matched to the surrounding soft muscle tissue (ca. 15 kPa[40]), as well as the ability to undergo repeated compressive strain typical of muscle contraction (ca. 50% compression at 1 Hz[40,41]). Furthermore, *in situ* formation via a rapid, stimuli-sensitive, cytocompatible mechanism is desirable to facilitate minimally invasive injectable

delivery, minimize cell loss after injection, and allow for the hydrogel to spread and conform to the available intramuscular space. Finally, the physical and electrostatic nature of the hydrogel must facilitate the exchange of growth factors between encapsulated cells and the surrounding environment without swelling. Hydrogels developed to date have failed to achieve this combination of highly robust mechanical properties and injectability, while facilitating cell encapsulation and growth factor release.

In this work, a library of high molecular weight amphiphilic prepolymers was prepared, designed specifically to be co-crosslinked with a cell-supportive prepolymer in order to produce mechanically resilient, cell-supporting hydrogels. Amphiphilic prepolymers of poly(trimethylene carbonate)-*b*-poly(ethylene glycol)-*b*-poly(trimethylene carbonate) diacrylate (PEG-(PTMC-A)$_2$) were designed to provide a soft, yet highly deformable and minimally swelling structural component.[62,63,147–149] PEG-(PTMC-A)$_2$ prepolymers were prepared with a range of PEG and PTMC block molecular weights (4 to 20 kg·mol^{-1} and 0 to 5 kg·mol^{-1}, respectively) with low dispersity by using HCl as a monomer activator in place of a traditional metal catalyst.[150–152] When referring to a specific formulation, the prepolymer is referred to as PEG$_m$-(PTMC$_n$-A)$_2$, where the subscripts m and n specify the approximate PEG and PTMC block lengths in kg·mol^{-1}, respectively. The previously developed *N*-methacrylated glycol chitosan functionalized with the cell-adhesive integrin-specific peptide motif GGGG**RGD**S (MGC-RGD) was chosen as the cell-supportive prepolymer component based on its demonstrated ability to support the viability and retention of encapsulated ASCs.[153,154] Furthermore, chitosan and its degradation products have been found to scavenge reactive oxygen species in ischemic tissues and protect cells from oxidative stress[155,156], making chitosan-based materials advantageous for treating ischemic conditions.

In initial materials characterization studies, hydrogels were prepared from only PEG-(PTMC-A)$_2$ to assess the effect of PEG and PTMC block lengths on equilibrium compressive modulus, maximum compressive strain at failure, swelling, and sol content. Compositions with stiffness comparable to the target muscle tissue along with a high resiliency to compressive strain were combined with MGC to form

composite hydrogels, which were tested under cyclic compressive strain to determine the effects of repeated loading on gel stiffness and integrity.

Cell encapsulation using acrylate- and methacrylate-functionalized prepolymers is commonly achieved by photo-initiated crosslinking[157,158]; however, this approach is poorly suited to applications where light access is limited, such as deep-tissue intramuscular injection. As an alternative, this study investigated the potential of radical initiation with ammonium persulfate (APS) and *N*,*N*,*N'*,*N'*-tetramethylethylenediamine (TEMED). Dynamic shear rheometry was used to measure crosslinking kinetics with a range of initiator concentrations. The gelation times at 20 °C and 37 °C were compared to determine an initiator concentration that allowed for adequate pre-injection handling time, while providing rapid post-injection crosslinking.

In subsequent *in vitro* studies, ASCs isolated from human tissue (hASCs) were encapsulated within the mixed hydrogel and cultured under normoxic (~20% O_2) or hypoxic (2% O_2) conditions to model the reduced partial pressure of oxygen in ischemic muscle.[159] hASC density, viability, metabolic activity, and fraction of dead/damaged cells were quantified over 14 days. The release of nine growth factors involved in angiogenesis from both encapsulated hASCs and control hASCs grown on tissue culture polystyrene (TCPS) was quantified to evaluate the effects of hypoxic culture within the hydrogels on paracrine factor production.

3.2 Materials and Methods

3.2.1 Materials

Water used was of type 1 purity, obtained from a Millipore Milli-Q Plus ultrapure water filtration system. Glycol chitosan (GC) (minimum number average molecular weight (M_N) = 82 kg·mol^{-1}, 85% degree of deacetylation) was obtained from Wako Chemicals Inc. GGGG**RGD**S peptide (RGD peptide, 94% purity) was obtained from CanPeptide Inc., and used as received. Trimethylene carbonate (TMC) was obtained from Leapchem (Hangzhou, China). Deuterium oxide (D_2O) for ^{1}H NMR was obtained from Cambridge Isotope Laboratories Inc. PEG with M_N = 4 kg·mol^{-1} (PEG_4) and HCl (1 M in diethyl ether)

were obtained from Acros Organics. Triethylamine (TEA), dichloromethane (DCM), tetrahydrofuran (THF), dimethylformamide (DMF), dimethyl sulfoxide (DMSO), toluene, methanol, ethyl acetate, dialysis membrane, phosphate buffered saline pH 7.4 (PBS), 3-(4,5-dimethylthiazol-2-yl)-2,5-diphenyltetrazolium bromide (Vibrant® MTT), and a LIVE/DEAD™ cell viability kit were obtained from Thermo Fisher Scientific. A ToxiLight™ assay was obtained from Lonza. A custom Luminex® assay was obtained from R&D Systems. Unless specified, all other reagents were obtained from Sigma Aldrich Ltd.

3.2.2 Preparation of PEG-(PTMC-A)$_2$

PEG_4, PEG_{10}, and PEG_{20} diols were used as initiators for the ring opening polymerization of TMC. The polymerization was carried out in DCM at room temperature, using HCl as a monomer activator.[150–152] All glassware was flame-dried before use. The following is a representative procedure: PEG_{20} (5.0 g, 0.25 mmol) was first dissolved in 60 mL toluene in a round-bottom flask, after which the toluene and residual water from PEG_{20} were removed by azeotropic distillation at 100 °C under reduced pressure. TMC (2.5 g, 24.5 mmol) was dissolved in 5 mL anhydrous DCM, added to the PEG_{20} and stirred under an inert argon atmosphere. A 1 M solution of HCl in diethyl ether (5.0 mL, 5.0 mmol) was added and the solution was stirred for 24 h. The polymer was recovered by a series of three precipitations from DCM using a ten-fold volumetric addition of a 9:1 mixture of hexanes and methanol. Finally, remaining solvent was removed under rotary evaporation.

3.2.3 Acrylation of PEG and PEG-(PTMC)$_2$

Both PEG and PEG-(PTMC)$_2$ used for acrylation were dried by azeotropic distillation in toluene as previously described. In a typical reaction, dried PEG or PEG-(PTMC)$_2$ was dissolved in anhydrous DCM at 0.1 g/mL under an inert argon atmosphere at room temperature. 4-(dimethylamino)pyridine (DMAP) was added as a catalyst (1:1000 molar ratio to terminal hydroxyl groups). Triethylamine (TEA) was added to scavenge hydrochloric acid formed during the reaction (1.5:1 molar ratio to terminal hydroxyl groups). Acryloyl chloride (AC) was dissolved in anhydrous DCM at 0.05 g/mL and slowly added over 2 h (2:1 molar ratio to terminal hydroxyl groups). The reaction was stirred at room temperature for 24 h.

Following acrylation, DCM was removed under rotary evaporation. The polymer was dissolved in ethyl acetate and insoluble triethylamine hydrochloride salt formed during the reaction was removed by three repeated steps of centrifugation and filtration of the supernatant. The acrylated PEG-(PTMC-A)$_2$ polymer was recovered by a series of three precipitations using methanol at -20 °C, after which residual solvent was removed by rotary evaporation.

For hASC encapsulation experiments (Section 3.2.12), PEG$_{20}$-(PTMC$_2$-A)$_2$ was further purified to remove residual TEA-HCl salt. Following rotary evaporation, the dried polymer was dissolved in water, and the pH was adjusted to 8.0 with sodium hydroxide to regenerate TEA from any residual TEA·HCl salt. The solution was heated to 40 °C under rotary evaporation for 5 min, then neutralized with HCl and dialyzed against distilled water using a 6 kDa molecular weight cut-off membrane for 2 days. The product solution was then lyophilized to recover diacrylated PEG$_{20}$-(PTMC$_2$-A)$_2$.

3.2.4 Characterization of PEG-(PTMC-A)$_2$

A Bruker Avance-400 MHz spectrometer was used to measure ^{1}H spectra of PEG and PEG-(PTMC-A)$_2$ in dimethyl sulfoxide-d$_6$ (DMSO-d$_6$) (20 mg/mL) at room temperature. The polymer composition and number average molecular weight per block were calculated based on the integration of TMC methylene protons (δ = 1.95, 4.15 ppm) relative to the methylene protons of the ethylene oxide repeating units of PEG (δ = 3.52 ppm). The degree of acrylation was calculated from the average integration of the three vinyl protons of the terminal acrylate groups (δ = 5.94 – 6.36 ppm), relative to the methylene protons of PEG.

Prior to acrylation of the PEG-(PTMC)$_2$, the molecular weight dispersity was determined by gel permeation chromatography (GPC) using THF as the eluent. Polymer solutions were prepared in THF and filtered with 0.2 μm filters. The GPC system consisted of a Waters 2690 separation module equipped with four Waters Styragel HR columns in series. Refractive index measurements were collected at 35 °C and calibrated to polystyrene standards.

3.2.5 Methacrylation and RGD functionalization of glycol chitosan

GC was purified and reacted with glycidyl methacrylate to form MGC as previously reported.[153] Briefly, GC was dissolved in water at 10 mg/mL, filtered to remove insoluble impurities, dialyzed using a 50 kg·mol^{-1} molecular weight cutoff membrane for 24 h, and lyophilized to obtain purified GC. Purified GC was dissolved at 20 mg/mL in a 0.2 M sodium phosphate buffer at pH 9. Glycidyl methacrylate was added dropwise at a 0.15 molar ratio to free amine of GC and stirred for 24 h, according to a previous report.[31] The reaction was neutralized with 1.0 M hydrochloric acid and dialyzed using 12-14 kg·mol^{-1} molecular weight cutoff membrane against distilled water for three baths over 48 h, and lyophilized to obtain purified MGC.

The GGGGRGDS peptide was dissolved at 20 mg/mL in 0.15 M sodium phosphate buffer at pH 5.5. *N*-acryloxysuccinimide (2.3 molar equivalents) was dissolved in DMF and added dropwise to the GGGGRGDS solution, accounting for 10% of the final reaction volume. The reaction was stirred at 4 °C for 2 h, then diluted by half with water and dialyzed using a 0.5 kg·mol^{-1} molecular weight cutoff membrane over 24 h. The purified solution was lyophilized to obtain *N*-terminal acrylated GGGGRGDS (Acr-RGD).

MGC was dissolved at 5 mg/mL in a 0.2 M sodium phosphate buffer at pH 8.5. Acr-RGD was added at a rate of 62.5 mmol of acrylate group per mole of MGC residue, and the solution was stirred at 37 °C for 24 h. The solution was then dialyzed using a 6-8 kg·mol^{-1} molecular weight cutoff membrane against 0.2 M NaCl for 8 h, and against distilled water for 24 h, with replacement of the water after 8 h. The purified solution was lyophilized to obtain MGC functionalized with the GGGGRGDS peptide (MGC-RGD). For all physical and mechanical characterization, MGC without RGD functionalization was used. For cell encapsulation and subsequent *in vivo* studies, MGC-RGD was used.

3.2.6 Characterization of Acr-RGD and MGC-RGD

A Bruker Avance-400 MHz spectrometer was used to measure ^{1}H NMR spectra of samples of Acr-RGD, MGC, and MGC-RGD in D_2O (10 mg/mL) at 80 °C. The degree of acrylation of RGD was determined from the average integration of the vinyl protons of the acrylate group (δ = 6.84, 6.76, and 6.34

ppm) relative to the average integration of the gamma protons (δ = 2.47 and 2.36 ppm) and delta protons (δ = 2.21 ppm) of arginine. All functionalization of GC was calculated relative to the total integration of anomeric protons of both acetylated and deacetylated GC residues (δ = 5.18 and δ = 5.00 ppm, respectively). The degree of *N*-methacrylation was determined from the average integration of vinyl protons of the methacrylate groups (δ = 6.70 and δ = 6.30 ppm). The degree of RGD functionalization was determined by the average integration of the gamma protons and delta protons of arginine.

3.2.7 Hydrogel formation for physical and mechanical testing

Hydrogels were initially prepared using PEG-(PTMC-A)$_2$ at 10% w/v without MGC to assess the influence of PEG and PTMC block lengths and overall molecular weight on swelling and mechanical properties. Subsequently, based on this analysis, mixed hydrogels of PEG-(PTMC-A)$_2$ and MGC were prepared using one of two PEG-(PTMC-A)$_2$ formulations: PEG$_{10}$-(PTMC$_1$-A)$_2$ and PEG$_{20}$-(PTMC$_2$-A)$_2$. These hydrogels were prepared at 1% w/v MGC with either 2% w/v or 4% w/v PEG-(PTMC-A)$_2$. MGC-only hydrogels were prepared at concentrations of 2, 3, and 5% w/v for comparison with the mixed hydrogels.

To prepare the hydrogels, PEG-(PTMC-A)$_2$ and/or MGC were dissolved in PBS. Solutions of APS and TEMED at 20 times the final required concentration were added sequentially at a volumetric ratio of 5 APS : 5 TEMED : 90 polymer solution, with thorough mixing after each addition. The final concentrations of APS and TEMED were 5.0 mM, except as noted in the crosslinking kinetic studies. The polymer solution was transferred to a 1 mL syringe (Becton Dickinson), sealed on both faces with flat-ended plungers to form a cylindrical mold (4.5 mm diameter x approximately 3.0 mm height) and incubated at 37 °C for 15 min to initiate crosslinking. Hydrogels used for sol content and equilibrium water content determination were prepared in water instead of PBS.

3.2.8 Physical characterization of hydrogels

The sol content and equilibrium water content of hydrogel samples (N = 4-5 gels per type) was determined as previously described.[149,153] Briefly, hydrogels were weighed immediately after crosslinking

($m_{wet\ initial}$), frozen in liquid nitrogen, and lyophilized to determine the total dry mass ($m_{dry\ total}$). Dried samples were soaked in water for 24 h to extract non-crosslinked material, and then weighed in their swollen state ($m_{wet\ final}$). Extracted samples were frozen and lyophilized to determine the total dry network mass ($m_{dry\ network}$). The sol content was calculated as:

$$sol\ content = \frac{m_{dry\ total} - m_{dry\ network}}{m_{dry\ total}} \quad \textbf{Eq. 3-1}$$

The equilibrium water content (EWC) was calculated as:

$$EWC = \frac{m_{wet\ final} - m_{dry\ network}}{m_{wet\ final}} \quad \textbf{Eq. 3-2}$$

The swelling ratio of hydrogels (N = 4-5 per group) prepared and swollen in PBS was calculated as:

$$Swelling\ ratio = \frac{m_{wet\ final}}{m_{wet\ initial}} \quad \textbf{Eq. 3-3}$$

3.2.9 Mechanical characterization of hydrogels

Hydrogels for mechanical testing were prepared in PBS, swollen to equilibrium in PBS, and then maintained in PBS during testing at room temperature (N = 4-5 gels per group). The height and diameter of the swollen cylindrical hydrogels were measured using digital calipers immediately before testing. Unconfined stress-relaxation measurements were conducted using a micromechanical tester with a 1 kg load cell (MACH-1, Biomomentum Inc., QC, Canada) equipped with an upper steel platen and an advancing steel base. Samples were first preconditioned with 0.5 g axial compressive force held until equilibrium was reached (defined as a change in force less than 0.1 g per minute). Subsequently, axial compression was applied at step strain increments of 4% at a rate of $10\%\cdot s^{-1}$ to a total strain of 40%, based on the protocols of Hayami *et al.*[160] At each step, the resulting force decay was recorded until an equilibrium load was reached. Nominal stress was calculated from the applied force divided by the initial cross-sectional area of the sample. The equilibrium modulus was obtained from the slope of the linear region of the nominal equilibrium stress-stain curve. Samples were tested for compressive failure immediately following stress-relaxation measurements. Samples were again preconditioned with 0.5 g axial compressive force, and axial

compression at 1%·s^{-1} was applied until sample failure. From the resulting stress-strain data, a value of maximum compressive strain at failure was recorded.

Fatigue measurements were performed with a Bose ElectroForce 5500 micromechanical testing system, equipped with an actuated upper steel platen and a flat steel base. Three hydrogel formulations were tested: 2% w/v MGC; 4% w/v PEG_{10}-$(PTMC_1$-$A)_2$ + 1% w/v MGC; and 4% w/v PEG_{20}-$(PTMC_2$-$A)_2$ + 1% w/v MGC, prepared as previously described, swollen to equilibrium in PBS, and maintained under PBS during the course of testing (N = 4 gels per group). Cyclic compressive strain was applied at 3 Hz and 50% amplitude to model the maximum expected intramuscular strain conditions that would be expected in the lower limb at a 180 step per minute gait cycle.[40,41] The instantaneous compressive moduli were calculated from the linear region of the resulting stress-strain curves at every 50th compressive cycle.

3.2.10 Rheological determination of crosslinking

An AR2000 rheometer (TA Instruments) equipped with a cone geometry (40 mm diameter, 0.5°) was used to monitor the storage and loss moduli of polymer solutions during gelation (N = 3 per group). The temperature of the rheometer stage was controlled at either 20 °C or 37 °C, and the cone geometry was allowed to reach equilibrium with the stage temperature before testing. The linear viscoelastic region of a polymer solution without initiator was first determined by performing a strain rate sweep. APS and TEMED solutions at 20× the required final concentration (2.5, 5.0, and 10.0 mM) were sequentially added to a polymer solution of 4% w/v PEG_{20}-$(PTMC_2$-$A)_2$ + 1% w/v MGC immediately before testing, with brief mixing after each addition. The polymer solution was then transferred to the rheometer stage and covered with a humidity chamber to prevent dehydration. The storage modulus (G') and loss modulus (G") were monitored under time sweep oscillatory shear at constant 10% strain (within the linear viscoelastic region). Gelation was defined as the point at which G' equaled G".

3.2.11 Isolation, culture, and immunophenotyping of ASCs

Primary hASCs were isolated from freshly excised adipose tissue samples obtained from female patients undergoing elective breast reduction surgery at the Kingston General Hospital or Hotel Dieu

Hospital in Kingston, ON, Canada using published methods.[161] Human research ethics board approval for this study was obtained from Queen's University (REB# CHEM-002-07, see Appendix A.2). hASCs were expanded on TCPS under standard culture conditions (37 °C, 5% CO_2 in air) in complete medium (DMEM:Ham's F12 medium supplemented with 10% fetal bovine serum, 100 U/mL penicillin, and 0.1 mg/mL streptomycin), replaced every 2-3 days. Upon reaching 80% confluence, hASCs were trypsin-released, washed, counted, and re-plated at 5000 cells/cm^2. hASCs used in this study were isolated from three donors (age 59.3 ± 5.5 years; BMI 36.6 ± 9.4 kg/m^2) and frozen at passage 0. The hASCs were thawed and expanded concurrently, and an equal number of passage 2 hASCs from each donor was pooled immediately before encapsulation in order to reduce the impact of donor variability on hASC activity. Pooled hASCs were used for the assessment of survival, retention, metabolism, and growth factor release under normoxic and hypoxic conditions.

To confirm the immunophenotype of the pooled passage 2 hASCs used in the studies, single colour flow cytometry analysis was performed in triplicate using a Guava easyCyte 8HT Benchtop flow cytometer (EMD Millipore, Billerica, MA, USA) as previously reported.[162] The cells were incubated with the following monoclonal, fluorochrome-conjugated antibodies from eBioscience (San Diego, CA): the mesenchymal markers CD29-PE (β1-integrin), CD34-APC (progenitor associated marker), CD44-PE-Cyanine7 (hyaluronic acid receptor), CD73-FITC (ecto-5'-nucleotidase), CD90-FITC (Thy-1), CD105-PE (endoglin), and CD146-FITC (melanoma cell adhesion molecule), as well as negative markers CD31-PE (endothelial) and CD45-FIT (hematopoietic).[163,164] All samples were stained for 30 min at 4 °C and protected from light. Unstained and isotype controls were included in every trial.

3.2.12 Encapsulation of hASCs

Encapsulation studies using hASCs were performed to measure the viability, cell density, metabolic activity, cell damage, and cytokine release from encapsulated hASCs over 14 days. These studies were performed without repetition, using the pooled passage 2 hASCs described in 3.2.11. The number of replicate hydrogels (N) and number of repeated measurements are noted in the subsection of each assay.

Dry MGC-RGD and PEG_{20}-$(PTMC_2\text{-}A)_2$ were disinfected by exposure to low intensity UV irradiation for 30 min. The two polymers were dissolved together in sterile PBS. hASCs suspended in complete medium at room temperature were added to the polymer solution and thoroughly combined by gentle mixing with a spatula for approximately 30 seconds until the suspension was visibly homogenous. Concentrated solutions of APS and TEMED were sterile filtered and added sequentially with thorough mixing between each addition, to provide a final concentration of 5 mM each of APS and TEMED, selected based on the crosslinking kinetics and previous studies encapsulating ASCs in similar hydrogels.[149] The volumetric ratio was 70 polymer solution : 20 hASC suspension in complete medium : 5 APS solution : 5 TEMED solution, providing a final polymer concentration of 1% w/v MGC-RGD + 4% w/v PEG_{20}-$(PTMC_2\text{-}A)_2$ with 10×10^6 hASCs/mL, and 5 mM of APS and TEMED. No colour change of the phenol red media was observed upon mixing, suggesting the pH was maintained between 6.8 to 8.2. The polymer solution with suspended cells was drawn into a syringe, then injected via a 25G × 5/8" needle into a 0.3 mL syringe barrel (Becton Dickinson) and sealed on both faces with flat-ended plungers to form a 10 µL cylindrical mold (3.0 mm diameter x approximately 1.4 mm height). The molds were incubated at 37 °C for 15 min. After crosslinking, the gels were transferred to individual wells of a 12-well plate containing 2 mL of complete medium. hASCs were also plated in T75 culture flasks at 5000 cells/cm^2 as a 2-D TCPS control. Complete medium was replaced after 30 min and 1 h to aid in the clearance of residual initiator, and then every 48 h for up to 14 days. All samples were incubated at 37 °C under either normoxic (5% CO_2 in air) or hypoxic (5% CO_2/2% O_2 in N_2) conditions. Hypoxic conditions were maintained in a hypoxic chamber (ProOx C21, BioSpherix Ltd.).

3.2.13 Determination of cell viability and density

The viability and density of encapsulated hASCs was determined semi-quantitatively using the LIVE/DEAD staining assay (N = 6-8 gels per group). The hydrogels were rinsed with PBS then incubated in a staining solution containing 4 µM ethidium homodimer-1 and 2 µM calcein-AM in PBS at 37 °C for 45 min. The hydrogels were then rinsed in PBS and imaged on an inverted Olympus FV1000 laser scanning

confocal microscope with a 10× objective. Mosaic z-stack images were generated of the entire cross section of the gel. Cell viability was determined from counts of the total number of live (green) and dead (red) cells (ImageJ software v. 1.46r). Total cell density was estimated by extrapolating the cell density from z-stacks separated by 25 μm, representing distinct layers of seeded cells. Viability and density of TCPS-seeded hASCs were determined by trypan blue staining and hemocytometer counts (N = 4 TCPS flasks per group).

3.2.14 MTT metabolic assay

The metabolic activity of encapsulated hASCs was determined using an MTT assay (N = 4 gels per group per time point). Hydrogels without ASCs were cultured in complete medium and similarly tested as a negative control. Briefly, medium was replaced with 2 mL of complete medium with 0.5 mg/mL MTT. The samples were incubated for 4 h, then rinsed in PBS. The water insoluble formazan product was extracted from the cells with 0.6 mL of DMSO. Three 1-second bursts of probe sonication (Sonic Dismembrator, Fisher Scientific) on ice were used to disrupt the hydrogel in DMSO. The DMSO solution was centrifuged at 1200 × g to remove any insoluble hydrogel or cellular components before sampling the formazan-containing supernatant solution in triplicate. Sample absorbance was measured at 540 nm, and background absorbance at 690 nm was subtracted (EnSpire multimode plate reader, Perkin Elmer). The average normalized absorbance of the negative controls was subtracted from the normalized absorbance of the sample measurements. The metabolic activity of TCPS-seeded hASCs was similarly measured (N = 4 TCPS flasks per group).

3.2.15 ToxiLight assay

The activity of adenylate kinase (AK) released from compromised cell membranes was quantified as an indirect measure of the number of dead or damaged cells, as described previously for ASCs encapsulate in Type II collagen gels.[165] Briefly, complete culture medium that had been conditioned by the encapsulated hASCs or TCPS-seeded hASCs for 24 h (N = 4 gels or TCPS flasks per group per time point) was collected and centrifuged at 1200 × g. This protocol does not consider AK enzyme retained in the hydrogels. The supernatant was frozen in liquid nitrogen and stored at -80 °C. To generate a standard curve

of AK enzyme activity, a suspension of hASCs was lysed by sonication and used to generate a 6-point serial dilution (10^6 - 0 lysed cells/mL), then similarly centrifuged and frozen. Medium samples were thawed and analyzed together in duplicate for AK enzyme activity using the ToxiLight assay kit according to the manufacturer's instructions. The background AK activity in media from control hydrogels without hASCs was subtracted from the sample measurements. AK enzyme activity was converted to an estimate of the number of dead or damaged cells using a 4PL regression of lysed hASC standards, and expressed as a fraction of the total cells in each gel or TCPS flask.

3.2.16 *In vitro* cytokine release

48 h prior to the collection of media for cytokine analysis from encapsulated and TCPS-seeded hASCs, the complete medium was replaced with low serum medium (DMEM:F12 supplemented with 2% fetal bovine serum, 100 U/mL penicillin, and 0.1 mg/mL streptomycin). The conditioned medium was centrifuged at 1200 × g to remove cells and debris. The supernatant was frozen in liquid nitrogen and stored at -80 °C (N = 4 gels or TCPS flasks per group). Unconditioned low serum medium was similarly incubated and collected. Immediately prior to the assays, the samples were thawed at room temperature and centrifuged at 10,000 × g. A custom Luminex multiplex magnetic bead assay and a Bio-Plex® 200 suspension array system (Bio-Rad) were used to quantify the concentration of the following cytokines in the supernatant release medium: VEGF-A, PlGF, HGF, angiopoietin-1, angiogenin, leptin, PDGF-AA, and MCP-1. ELISA (Peprotech) was used to quantify the concentration of SDF-1α. All samples were measured in duplicate. The background of each cytokine present in the medium from unseeded controls was subtracted from sample measurements, and the values were then normalized to the live cell number as determined by LIVE/DEAD staining or trypan blue staining of the TCPS samples. The result was expressed as cytokine released per 10^6 cells per 24 h.

3.2.17 Statistical analysis

All data is presented as the group mean ± standard deviation. All statistical analyses were performed using GraphPad Prism 7. Significant differences between group means were determined by ANOVA with

Tukey's test for multiple comparisons. This post-hoc comparison was selected to allow comparison between all group means.

3.3 Results

3.3.1 Characterization of PEG-(PTMC-A)$_2$ copolymers and MGC-RGD

^{1}H NMR of the PEG-(PMTC-A)$_2$ copolymers demonstrated an 80-95% conversion of TMC using HCl as a monomer activator, and a high degree of acrylation (>90%) (Figure 3-1). TEA-HCl salts in the PEG-(PTMC-A)$_2$ sample prior to purification, evident at δ = 1.17 ppm (Figure 3-1a), were absent following purification (Figure 3-1b), indicating removal of residual TEA-HCl. NMR spectra of the other PEG-(PTMC-A)$_2$ formulations are given in Appendix A.1.

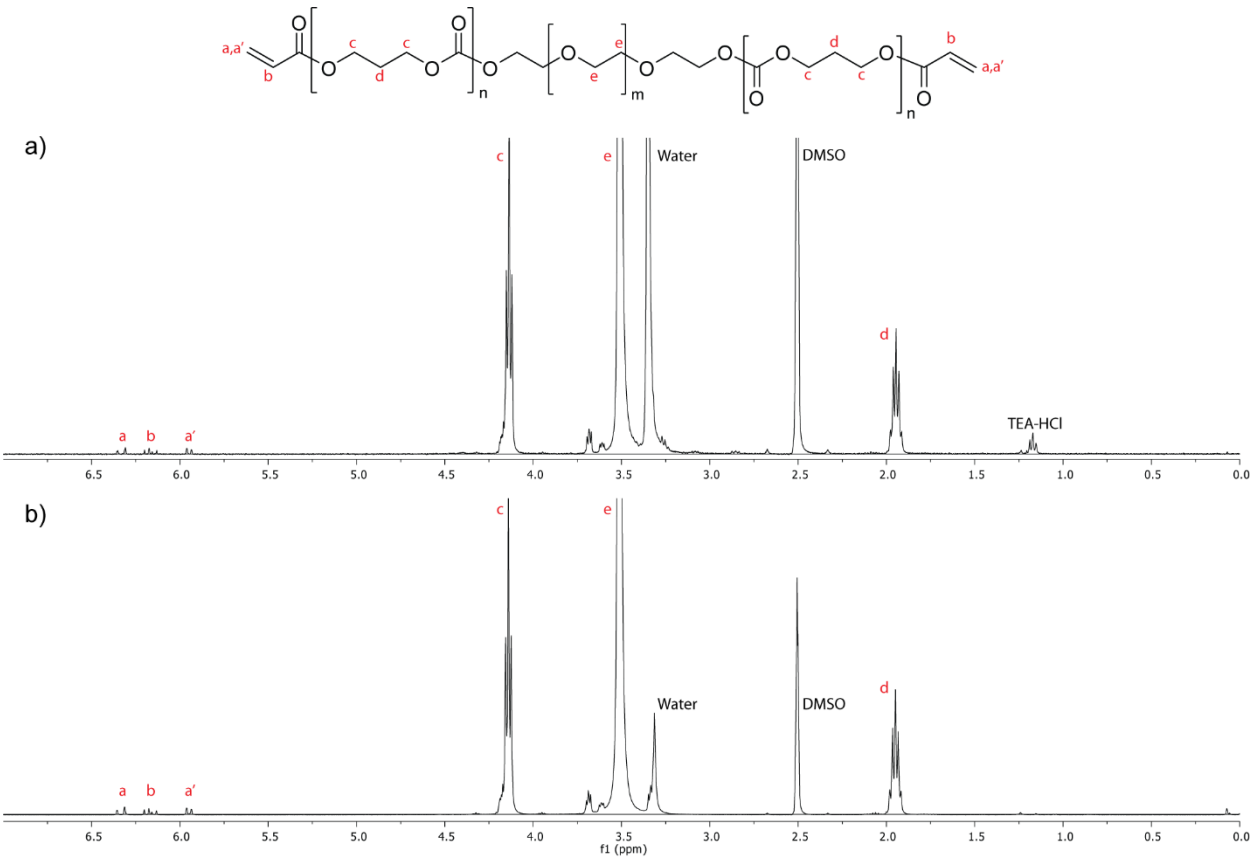

Figure 3-1: Chemical structure and ^{1}H NMR spectrum of PEG$_{20}$-(PTMC$_2$-A)$_2$. a) Prior to and b) after the removal of residual TEA-HCl salts.

The PEG-(PTMC-A)$_2$ copolymers had a uniformly low dispersity (1.02-1.04) determined by GPC. A summary of the PEG-(PTMC-A)$_2$ copolymer properties determined by ^{1}H NMR and GPC is presented in Table 3-1.

Table 3-1: Summary of PEG-(PTMC-A)$_2$ copolymer properties.

	PEG initiator M_N ($kg \cdot mol^{-1}$)	**Target PTMC M_N** ($kg \cdot mol^{-1}$)	**PTMC M_N[a]** ($kg \cdot mol^{-1}$)	**Total M_N[a]** ($kg \cdot mol^{-1}$)	**Dispersity[b]**	**Acrylation[a]** (%)
PEG_4-($PTMC_0$-A)$_2$	4	0	0	4	1.02	91
PEG_4-($PTMC_1$-A)$_2$	4	2	1.9	5.9	1.02	100
PEG_{10}-($PTMC_0$-A)$_2$	10	0	0	10	1.03	100
PEG_{10}-($PTMC_1$-A)$_2$	10	2	1.6	11.6	1.02	98
PEG_{10}-($PTMC_{2.5}$-A)$_2$	10	5	4.4	14.4	1.02	100
PEG_{20}-($PTMC_0$-A)$_2$	20	0	0	20	1.04	93
PEG_{20}-($PTMC_1$-A)$_2$	20	2	1.8	21.8	1.04	100
PEG_{20}-($PTMC_2$-A)$_2$	20	4	3.7	23.7	1.05	99
PEG_{20}-($PTMC_5$-A)$_2$	20	10	8.7	28.7	1.03	100

[a] By ^{1}H NMR integration; [b] By GPC relative to polystyrene standards

The GGGGRGDS peptide was 50% acrylated by reaction with *N*-acryloxysuccinimide (Figure 3-2a). To allow crosslinking, glycol chitosan was *N*-methacrylated to a degree of molar substitution of 5% to form MGC (Figure 3-2b). To improve cell survival and retention after crosslinking, MGC was functionalized with RGD to a degree of molar substitution of 5% (Figure 3-2c). The degrees of *N*-methacrylate and RGD substitution were selected based on previous reported correlations with hydrogel stiffness and cell survival, respectively.[154]

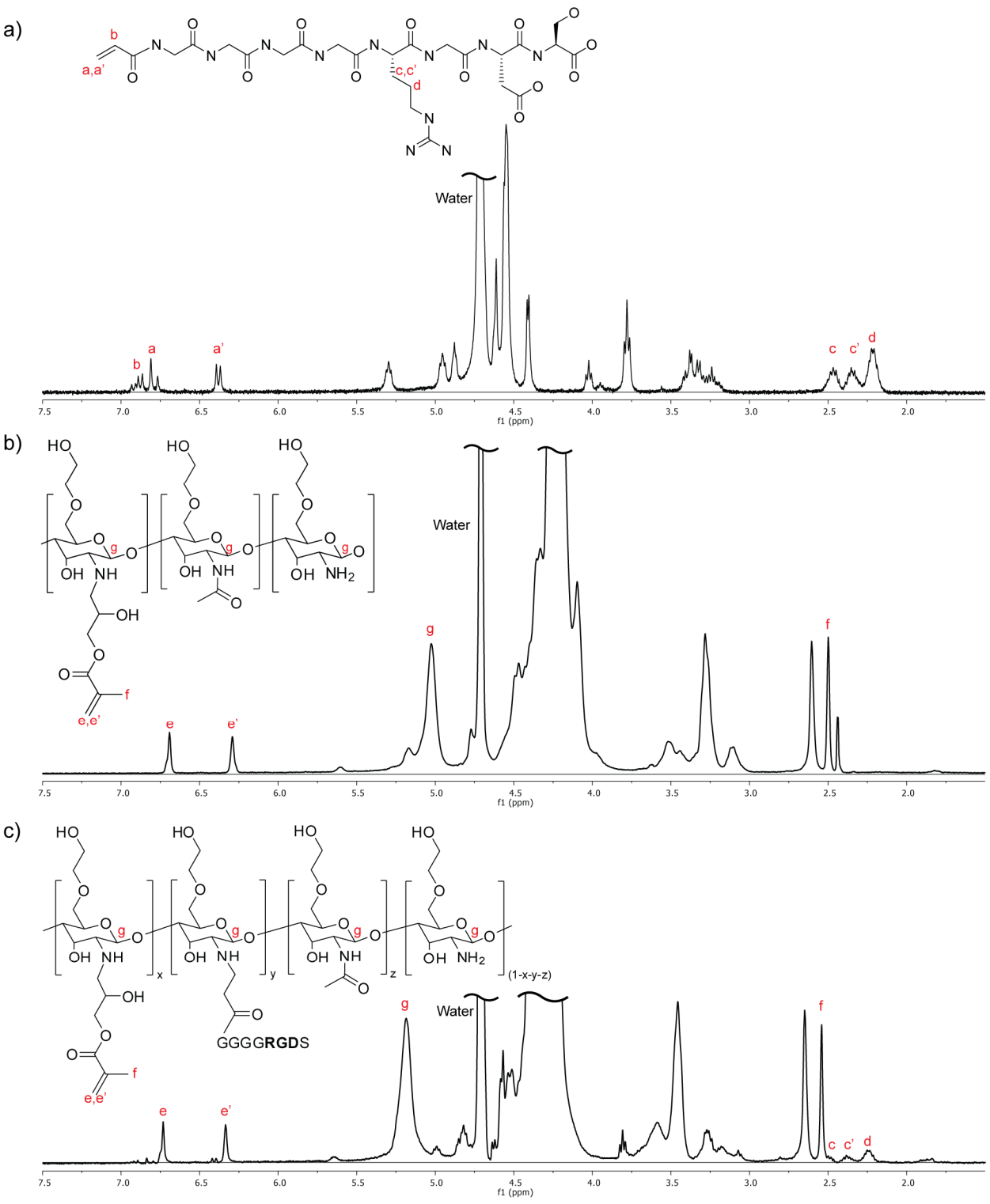

Figure 3-2: Chemical structures and ^{1}H NMR spectra of MGC-RGD synthesis. a) Acrylated GGGGRGDS peptide, b) MGC, and c) MGC-RGD. The degree of acrylation of the peptide was ca. 50%. For MGC-RGD, the degree of *N*-methacrylate substitution (x) was 5%; the degree of RGD functionalization (y) was 5%, as determined by ^{1}H NMR. The fraction of residual acetyl groups (z) was 15%, as reported by the supplier.

3.3.2 Physical characterization of PEG-(PTMC-A)$_2$ hydrogels

Initially, hydrogels were prepared from PEG-(PTMC-A)$_2$ alone to investigate the impact of PEG and PTMC block length on physical and mechanical properties (Figure 3-3). This initial screening process was performed to identify the block length of PEG and PTMC that could provide a soft, highly resilient, and minimally swelling polymer component for eventual mixing with MGC.

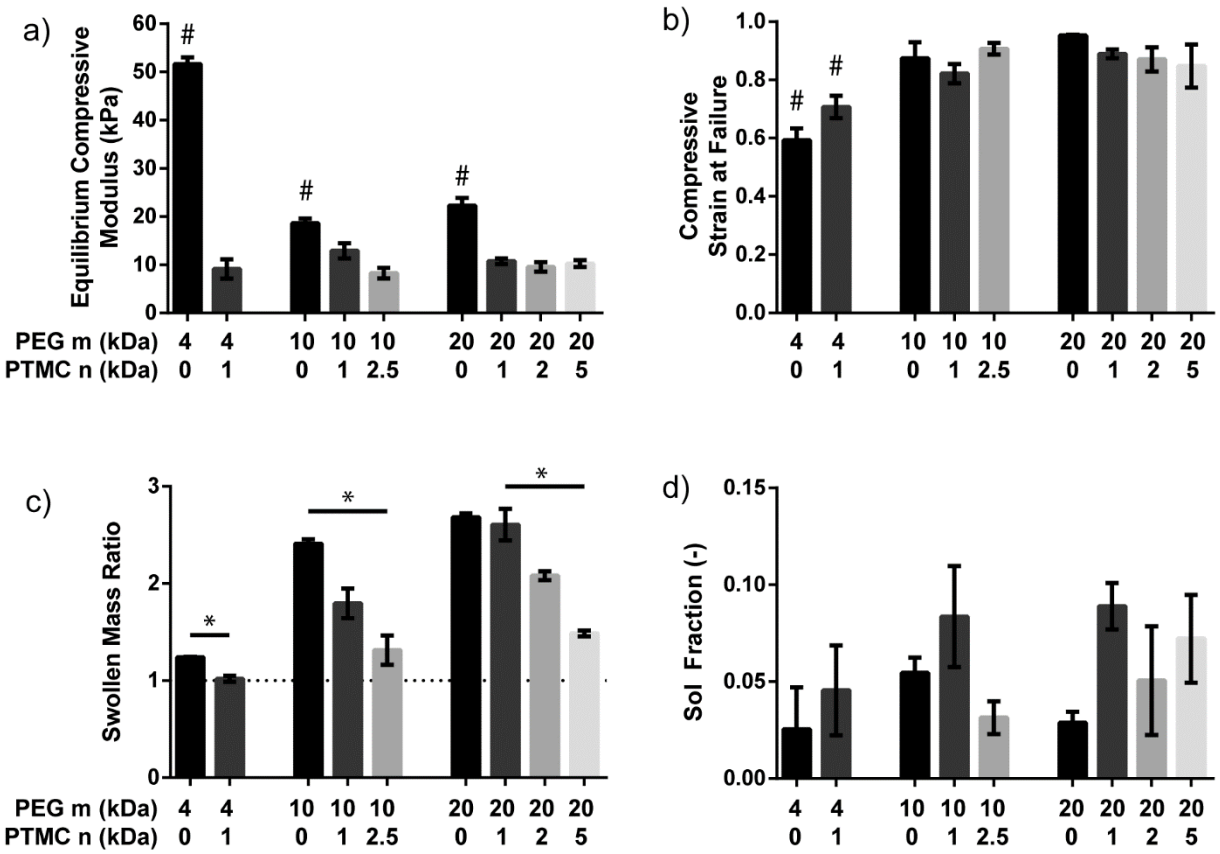

Figure 3-3: Properties of hydrogels prepared from 10% w/v PEG-(PTMC-A)$_2$. a) Equilibrium compressive modulus; b) compressive strain at break; c) as-made to swollen mass ratio; d) sol fraction after crosslinking with 5.0 mM APS and TEMED. (N = 4 - 5 gels, mean ± SD). Differences between groups were determined by one-way ANOVA with Tukey's correction for multiple comparisons; * denotes a significant difference between all indicated groups; # denotes significant difference between the indicated group and all other groups ($p < 0.05$).

The equilibrium compressive modulus (Figure 3-3a) was dependent on the molecular weight of PEG-(PTMC-A)$_2$, where greater molecular weight prepolymers resulted in a higher molecular weight between crosslinks in the hydrogel network, and therefore, in general, a lower modulus. However, comparing PEG$_{10}$-(PTMC$_0$-A)$_2$ with PEG$_{20}$-(PTMC$_0$-A)$_2$, the higher molecular weight polymer resulted in

a stiffer hydrogel, likely due to the effect of chain entanglements acting as physical crosslinking points. Further, comparing the three groups without PTMC to the other formulations, it was evident that the introduction of PTMC blocks reduced the equilibrium compressive modulus. This property may be due to the hydrophobic nature of the PTMC blocks, which causes the polymer chains to adopt a less expanded random coil conformation in the aqueous environment.[62] These hydrophobic domains may uncoil under applied stress, resulting in a lower overall network stiffness compared to PEG diacrylate networks without the hydrophobic blocks. The hydrogels prepared from pre-polymers greater than 10 $kg \cdot mol^{-1}$ were capable of undergoing compressive strain of over 90% of their original height (Figure 3-3b). This combination of resilience to compressive strain with lower equilibrium modulus is well suited for use in intramuscular environments, which undergo repetitive strain with muscle contraction.

Despite increasing the overall molecular weight and therefore decreasing the crosslink density of the initial network, the introduction of hydrophobic PTMC domains significantly reduced the swelling ratio of the PEG-$(PTMC\text{-}A)_2$ hydrogels, with progressively higher PTMC:PEG weight ratios resulting in correspondingly lower swelling ratios (Figure 3-3c). The observed reduction in swelling supports the concept that the PTMC domains reduce polymer chain extension in the aqueous environment. Thus, despite reducing swelling and therefore increasing the effective polymer and crosslink concentration in the network, the PTMC domains reduce the compressive modulus by uncoiling under compressive strain.

The low sol content for all groups indicates that the APS/TEMED system of initiators was an effective means of crosslinking these diacrylated polymers resulting in a low fraction of unreacted components (Figure 3-3d). Further, the differences observed in the mechanical properties of the PEG-$(PTMC\text{-}A)_2$ hydrogels were unlikely to be due to differences in crosslinking efficiency, since all groups had similar sol contents (*ca*. 5 – 10%).

3.3.3 Physical characterization of mixed PEG-$(PTMC\text{-}A)_2$ + MGC hydrogels

PEG_{10}-$(PTMC_1\text{-}A)_2$ and PEG_{20}-$(PTMC_2\text{-}A)_2$, both with a total PTMC:PEG weight ratio of 1:5, were selected for mixing with 1% w/v MGC based on their equilibrium compressive moduli (5 – 15 kPa)

and high maximum compressive strain (80 — 90%) appropriate for the intramuscular environment, as well as reduced swelling compared to formulations without PTMC. For comparison, pure MGC hydrogels were prepared at concentrations chosen to span the lowest that would form a stable gel to the highest that was readily injectable. Representative plots of the equilibrium compressive stress and the compressive loading to failure are presented in Appendix 1 (Figure A-10).

Even at the lowest polymer concentrations, pure MGC hydrogels had an equilibrium compressive modulus higher than the desired maximum of 15 kPa (Figure 3-4a). Though the moduli of mixed hydrogels prepared with only 2% w/v PEG-(PTMC-A)$_2$ were below the target physiological range of 5-15 kPa, MGC mixed with 4% w/v PEG-(PTMC-A)$_2$ resulted in hydrogels with moduli within this target range. Combining MGC with PEG-(PTMC-A)$_2$ significantly increased the resistance to compressive strain. Mixing with 4% w/v PEG-(PTMC-A)$_2$ had the greatest effect, increasing the ultimate compressive strain at failure to over 75% (Figure 3-4b), well above the expected strain conditions of the intramuscular environment. Thus, the mechanical properties of the mixed 1% w/v MGC + 4% w/v PEG-(PTMC-A)$_2$ hydrogels were highly suitable for the target application, both in terms of modulus and resistance to failure under compressive strain.

When equilibrated in PBS, all tested MGC hydrogels exhibited no swelling, while mixed gels underwent swelling between 1.2 and 1.4 times their original mass (Figure 3-4c). This effect may be attributed to the increase in the aggregate molecular weight between crosslinks when PEG-(PTMC-A)$_2$ is added to the network, as well as the hydrophilic nature of the PEG block. Further, the equilibrium water content of both MGC and mixed hydrogels was 95% or greater after swelling (Figure 3-4d), suggesting that cell nutrient and waste diffusion should not be limited by the polymer network.[166]

Based on mechanical properties, the combination of 1% w/v MGC with 4% w/v PEG-(PTMC-A)$_2$ was selected for further testing under cyclic compressive fatigue. MGC at 2% w/v was selected for comparison, as it was the softest and most resilient to compressive strain of all the MGC concentrations.

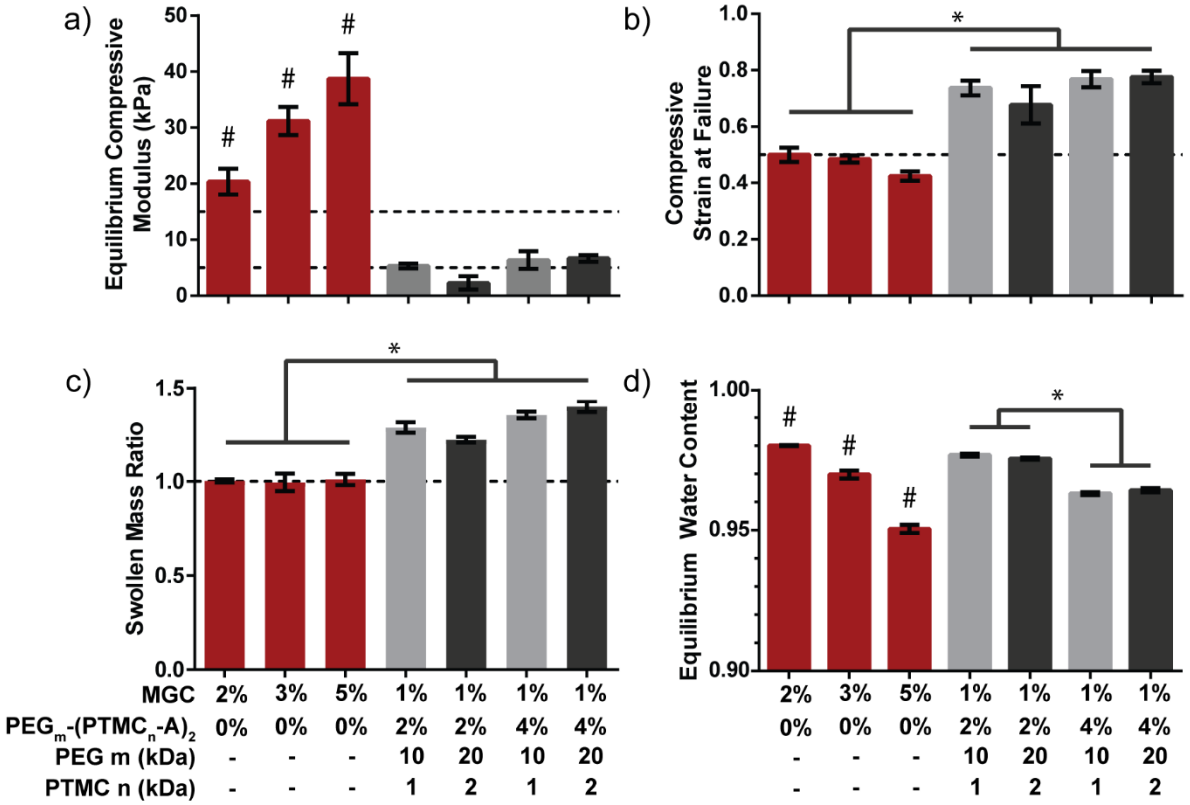

Figure 3-4: Properties of hydrogels prepared from MGC with and without PEG-(PTMC-A)$_2$. a) Equilibrium compressive modulus; b) compressive strain at break; c) as-made to swollen mass ratio; d) equilibrium water content. The dashed lines represent the target range for the given properties, based on physiological conditions. (N = 4 - 5 gels, mean ± SD). Differences between groups were determined by one-way ANOVA with Tukey's correction for multiple comparisons; * denotes a significant difference between all indicated groups; # denotes significant difference between the indicated group and all other groups ($p < 0.05$).

3.3.4 Fatigue testing under cyclic compression

Hydrogels swollen to equilibrium were compressed to 50% strain at 3 Hz for 1000 cycles, during which the instantaneous modulus of the hydrogel was monitored (Figure 3-5). While the 2% w/v MGC hydrogels underwent brittle failure in under 200 cycles (marked by the end of the red lines), mixing MGC with PEG-(PTMC-A)$_2$ allowed the hydrogels to maintain their initial instantaneous compressive modulus without significant change over 1000 compression cycles. At the tested 50% strain rate, elastic recovery was observed in the mixed polymer hydrogels. 1% w/v MGC + 4% w/v PEG$_{20}$-(PTMC$_2$-A)$_2$ was selected for further study, as it demonstrated the most promising combination of static and dynamic mechanical properties, while also introducing fewer acrylate groups at a given concentration of PEG-(PTMC-A)$_2$ that can potentially be cytotoxic for cells.[167]

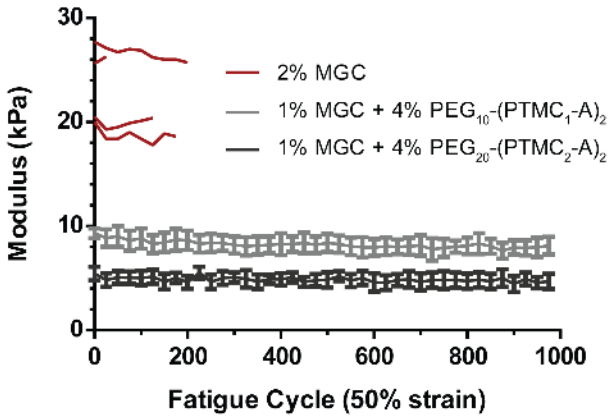

Figure 3-5: Hydrogel fatigue testing under cyclic compression. Instantaneous compressive modulus of hydrogels under cyclic compression. The moduli of 2% MGC hydrogels are plotted individually (red lines) up to the point of failure; the moduli of mixed hydrogels are plotted as the mean ± SD (N = 4).

3.3.5 Thermally stimulated chemical crosslinking kinetics

The evolution of the storage modulus (G') and loss modulus (G") of a solution of 1% w/v MGC + 4% w/v PEG_{20}-$(PTMC_2$-$A)_2$ initiated with 5 mM APS/TEMED was measured by rheometry (Figure 3-6). The rapid increase and subsequent plateau of G' suggests a complete, single-step gelation process. The crosslinking time, determined as the point at which G' = G" according to the approach proposed by Winter and Chambon[168] was compared at 20 °C and 37 °C for varying APS and TEMED concentrations (2.5, 5.0, and 10.0 mM). Representative plots of G' and G" are shown in Figure 3-6a-c, and average crosslinking times are summarized Figure 3-6d. A sufficient crosslinking time prior to injection is essential for clinical application, as the material must remain uncrosslinked during handling. At 20 °C, APS and TEMED concentrations of 2.5 and 5.0 mM allow for periods of handling without crosslinking of approximately 28 and 9 min, while still crosslinking rapidly at 37 °C within 6 and 3 min, respectively. Thus, for this polymer system, initiator concentrations in the range of 2.5 and 5.0 mM provided appropriate crosslinking times for material handling and *in situ* gelation.

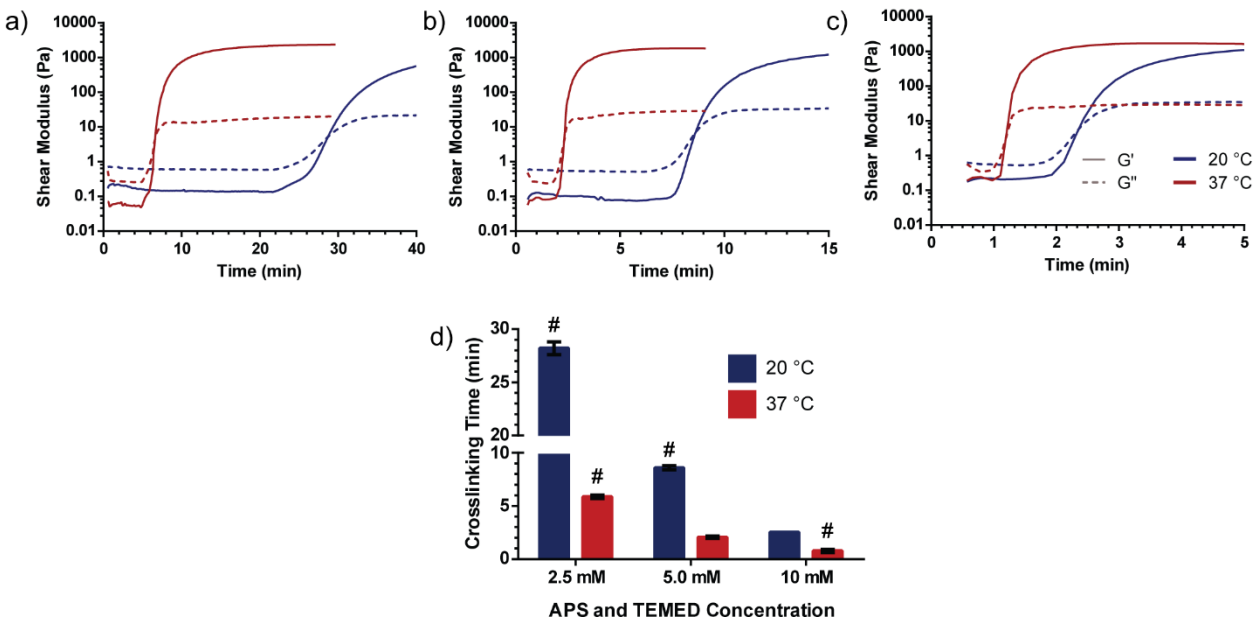

Figure 3-6: Rheometric monitoring of crosslinking using APS and TEMED initiators. Representative traces of storage (G', solid line) and loss (G", dashed line) moduli of 1% w/v MGC + 4% w/v PEG_{20}-$(PTMC_2$-$A)_2$ during crosslinking using a) 2.5 mM, b) 5.0 mM, and c) 10.0 mM APS and TEMED at 20 °C (blue) and 37 °C (red). d) Summary of crosslinking times (mean ± SD, N = 3 trials per group). # denotes significant difference between the indicated group and all other groups ($p < 0.05$ with Tukey's post-hoc correction for multiple comparisons).

3.3.6 Immunophenotype of hASC used for *in vitro* encapsulation

Passage 2 hASCs, pooled from three donors, exhibited the expected positive and negative expression of surface markers (Table 3-2), confirming that the cells had a stromal cell phenotype.

Table 3-2: Immunophenotype of hASCs used for *in vitro* encapsulation. Percent of cells positive for each marker is presented as the average ± SD from n = 3 repeated measurements from pooled hASCs from three donors.

Surface Marker	Expected phenotype[163,164]	Percent positive
CD90	>80%	99.01 ± 0.25
CD29	>80%	99.96 ± 0.01
CD44	>80%	99.96 ± 0.03
CD105	>80%	99.13 ± 0.26
CD73	>80%	99.64 ± 0.03
CD34	Variable	25.44 ± 0.22
CD146	Variable	0.16 ± 0.04
CD31	<2%	0.05 ± 0.05
CD45	<2%	0.20 ± 0.03

3.3.7 Viability and growth of encapsulated hASCs

hASCs that had been injected and encapsulated in the mixed hydrogel (1% w/v MGC-RGD + 4% w/v PEG_{20}-$(PTMC_2\text{-}A)_2$, purified to remove residual TEA-HCl) and cultured in both hypoxia and normoxia exhibited viability of approximately 90% after 3 days (Figure 3-7a). The cell suspension in prepolymer solution was easily injected through a 25G × 5/8" needle. Under normoxic conditions, the viability increased significantly to ~95% and ~98% at days 7 and 14; however, under hypoxia, the viability remained unchanged over time (ca. 90%), and was significantly lower than under normoxic conditions at day 7 and 14. Beyond subtle differences in viability, significant differences in hASC density within the hydrogels were observed (Figure 3-7b). At day 3, the cell density under both conditions was similar to the original density (10×10^6 hASCs/mL), and this density was maintained over time under normoxia. Under hypoxia, the hASC density at days 7 and 14 were significantly reduced compared to day 3 (~75% and ~65% of the day 3 density, respectively), and significantly lower than the densities observed under normoxia.

The metabolic activity of the encapsulated hASCs (Figure 3-7c) was significantly lower under hypoxia at all time points, consistent with the reduced number of viable cells in this group. Between days 3 to 7, hASCs in both conditions exhibited a significant reduction in MTT metabolism that plateaued between day 7 to 14. However, the LIVE/DEAD imaging results (Figure 3-7a-b) suggest that this initial drop may reflect a change only in metabolic activity as the cells adapt to the 3-D microenvironment, rather than a change in cell viability or density.

The analysis of AK enzyme in the conditioned media (Figure 3-7d) indicated that approximately 5% of the encapsulated hASCs were damaged or dying under hypoxia, significantly more than under normoxia at day 3. Generally consistent with the viability data, the AK levels under normoxic conditions at day 3 and 7 were below the threshold of detection from the background in complete media, although there was an increase in AK activity observed at 14 days.

In comparison to encapsulated hASCs, the control hASCs cultured on TCPS demonstrated similar trends in normoxic versus hypoxic culture. Specifically, relative to the normoxic conditions, hASCs cultured under hypoxia exhibited reduced viability by day 14 (Figure 3-7e) and lower cell density by day 7

(Figure 3-7f). While the metabolic activity of hASCs under normoxia increased significantly over 14 days, under hypoxia it remained unchanged (Figure 3-7g). Similar to encapsulated hASCs, those under hypoxia demonstrated a higher initial rate of cell damage (~5%) (Figure 3-7h).

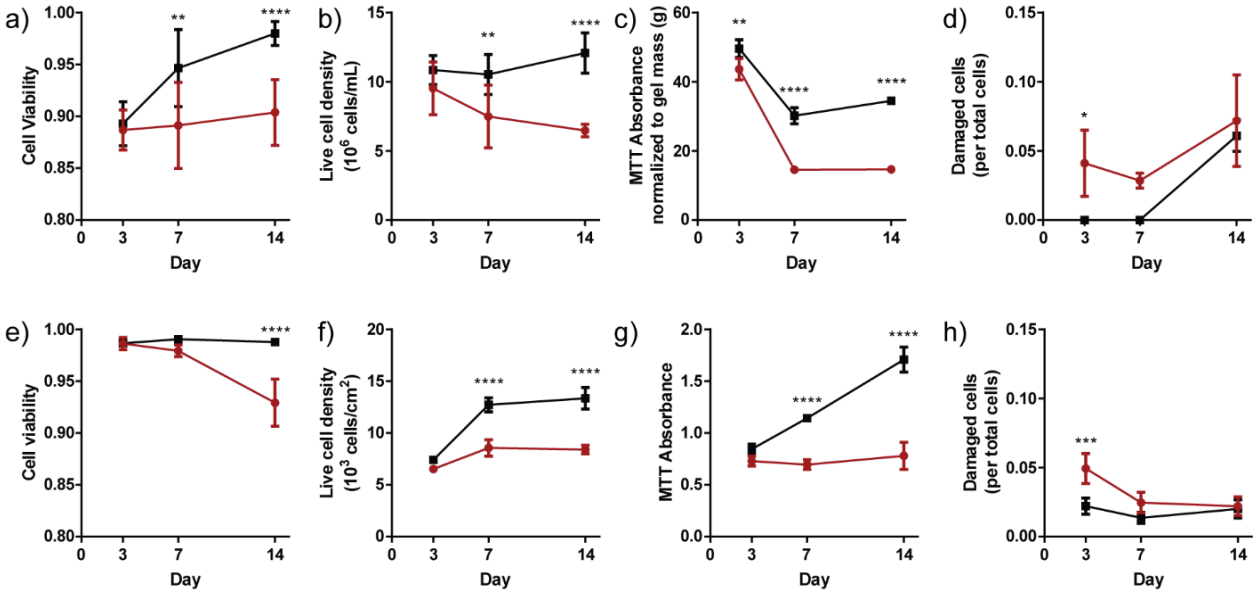

Figure 3-7: *In vitro* culture of hASCs in mixed hydrogels and on TCPS. hASCs were cultured under normoxia (20% O_2, black) and hypoxia (2% O_2, red), encapsulated in PEG-(PTMC-A)$_2$ + MGC-RGD (a-d) and on TCPS (e-h). a,e) hASC viability; b,f) live hASC density; c,g) metabolic activity by MTT (normalized to gel weight for encapsulated hASCs); d,h) dead/damaged cells as a fraction of total cells. All data presented as mean ± SD. Differences between hypoxic and normoxic groups at a given time point were determined by two-way ANOVA of group means with Tukey's correction for multiple comparisons. Significant differences are indicated (* $p<0.05$; ** $p<0.01$; **** $p<0.0001$).

Differences were also noted in the morphology of the encapsulated hASCs, where a more spindle-like morphology was observed under normoxia after 7 days (Figure 3-8a), compared to the same time point under hypoxic conditions (Figure 3-8b).

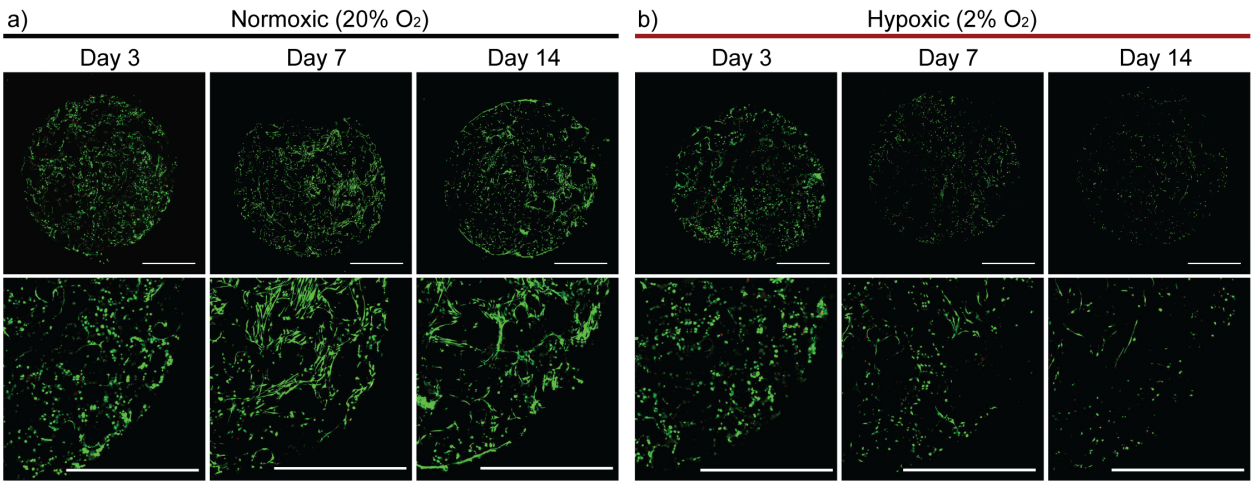

Figure 3-8: Mosaic confocal images of hASCs encapsulated in PEG-(PTMC-A)$_2$ + MGC-RGD. hASCs, cultured under normoxia (20% O_2) and hypoxia (2% O_2) were stained with calcein-AM (live cells, green) and ethidium homodimer-1 (dead cells, red). Scale bar = 1 mm.

3.3.8 Growth factor release from encapsulated and TCPS cultured hASCs

The production of a range of pro-angiogenic, anti-apoptotic, or chemoattractant factors (VEGF-A, angiopoietin-1, angiogenin, HGF, PlGF, PDGF-AA, leptin, SDF-1α, and MCP-1) was quantified within the conditioned media of encapsulated hASCs (Figure 3-9a) and hASCs on TCPS (Figure 3-9b) cultured under normoxic and hypoxic conditions. Of note, this quantification does not consider the fraction of cytokines that may be retained in the hydrogel. In the encapsulated hASCs, all cytokines were detected at levels exceeding the background level, with the exception of HGF at day 7 under hypoxia. Although there was no evidence of hypoxic upregulation for any factors at 7 days, by 14 days, all cytokines measured were significantly increased under hypoxia conditions. All of the factors were also detected in the TCPS controls, typically at lower levels at 14 days as compared to the gels, with the exception of leptin. Unlike encapsulated hASCs, hypoxic upregulation of many factors at day 7 was observed in the TCPS-seeded hASCs (VEGF-A, angiopoietin-1, angiogenin, PlGF, and MCP-1).

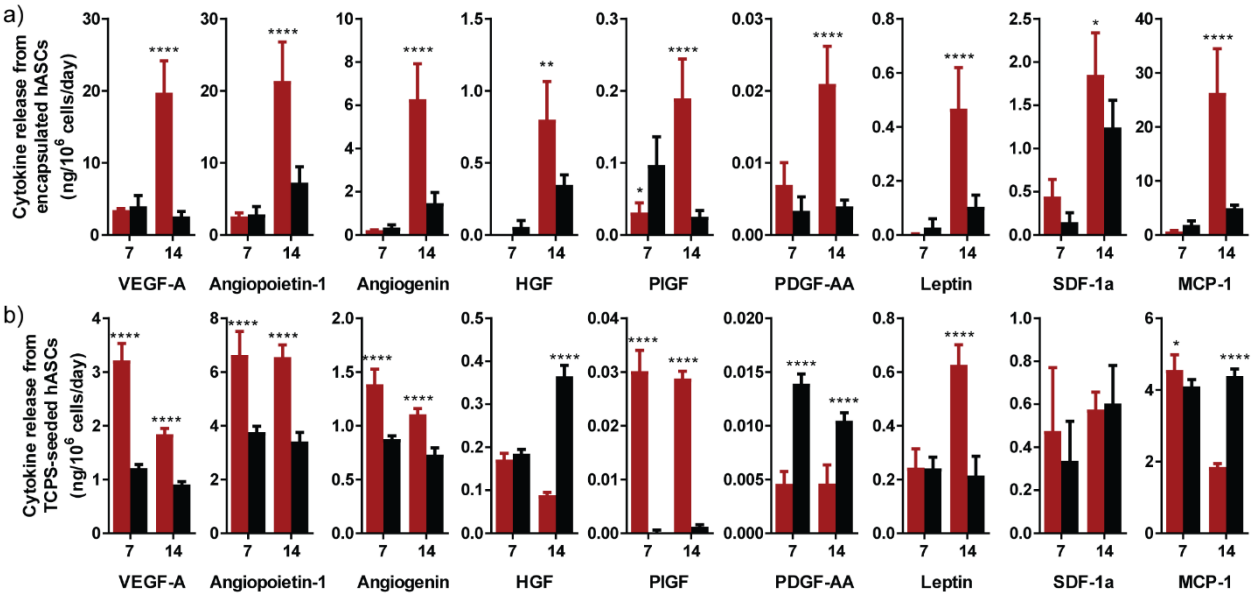

Figure 3-9: Growth factor release measured in the cell culture media of hASCs. Growth factor concentrations were measured in the media of a) encapsulated hASCs and b) hASCs on TCPS, cultured under normoxic (20% O_2, black) and hypoxic (2% O_2, red) conditions. Growth factor concentrations were normalized to live cell number and release period. All data presented as mean ± SD. Differences between hypoxic and normoxic groups at a given time point were determined by two-way ANOVA of group means with Tukey's correction for multiple comparisons. Significant differences are indicated (* $p<0.05$; ** $p<0.01$; **** $p<0.0001$).

3.4 Discussion

As cellular delivery scaffolds, hydrogels have the potential to enhance the efficacy of cellular therapies for treating ischemic conditions by improving cell retention and survival at the site of delivery. In the case of PAD, however, the intramuscular delivery site presents a dynamic mechanical environment, undergoing cyclic loading with repeated muscle contractions. For such applications, there is an unmet need for hydrogel scaffolds combining soft, robust mechanical properties with non-invasive injectability and viable cell encapsulation capacity.

While there are many approaches for producing mechanically robust hydrogels,[169] most are unsuitable for injectable cell delivery. Interpenetrating double network hydrogels, for instance, typically require one gel component to be cast into another pre-formed gel,[49,170] making injectable delivery unfeasible. Recent work using orthogonal crosslinking reactions has produced robust double network hydrogels able to withstand injection[48]; however, these materials undergo an approximate four-fold swelling in culture conditions. In addition to the corresponding loss in mechanical stiffness, such swelling

could have adverse effects in the intramuscular space. Alternatively, the reversible associations of purely ionically-crosslinked systems allow for crosslinks to reform after mechanical stress; however, the process is dependent on local ion concentrations,[171] which are not readily controlled *in vivo*, and such hydrogels often undergo plastic, rather than elastic deformation.[48] While nanocomposite hydrogels exhibit remarkable toughness and resiliency to strain, these materials are often too stiff for the IM environment,[60,147] and the inclusion of inorganic nanoparticles presents issues of potential toxicity to the encapsulated and surrounding cells.[56,61]

In the present work, PEG-(PTMC-A)$_2$ copolymers were developed as a modular additive to enhance the mechanical properties of an MGC-RGD based cell-supportive hydrogel. The PEG-(PTMC-A)$_2$ copolymers were designed to provide a high equilibrium water content, a high molecular weight between crosslinks, and a coiled hydrophobic domain that is capable of uncoiling under strain. The goal of this design was to produce hydrogels with minimal swelling, a low compressive modulus, and a high resiliency to compressive strain tuned to the target intramuscular environment. The use of HCl as a monomer activator in the preparation of the PEG-(PTMC-A)$_2$ was advantageous as it did not require elevated temperatures or the use of potentially toxic metal catalysts, such as the commonly used tin (II) ethylhexanoate.[172] Further, the monomer activation method provided a very low dispersity of molecular weights (1.02 – 1.04), facilitating the investigation of the effect of block length on mechanical properties.

Compared to hydrogels prepared from MGC alone, the addition of PEG-(PTMC-A)$_2$ produced hydrogels with tailored mechanical properties: lower modulus, greater ultimate compressive strain, and more resilience to cyclic compressive loading. These results may be caused by the increase in the effective molecular weight between crosslinks caused by introducing PEG-(PTMC-A)$_2$ into the MGC network. From the current work, it is unclear whether PEG-(PTMC-A)$_2$ and MGC crosslink independently or in a continuous network; however, the true network architecture is likely an intermediate of these two extremes. In an intramuscular environment, the reduced modulus further implies that the mixed hydrogels would exert lower resistance forces during muscle contraction, potentially reducing the chances for interfering with

contraction or disrupting the interface between the hydrogel and the surrounding tissue. These results suggest that the system is well suited to the mechanically dynamic environment of the lower limb.

A thermally-sensitive redox initiator system of APS with TEMED was adapted for *in situ* crosslinking under physiological conditions. This system has previously been used to initiate crosslinking of other polymers for the encapsulation of MSCs,[149,173–175] fibroblasts,[176] and chondrocytes[177,178] with high cell viability, as well as acellular scaffolds *in vivo*.[179,180] For a given polymer system, a concentration of APS and TEMED must be determined that provides i) rapid crosslinking at 37 °C to prevent material and cell dispersion; ii) sufficient handling time at 20 °C to prevent premature crosslinking; and iii) a non-toxic radical concentration. A final APS and TEMED concentration of 5 mM provided adequate handling time prior to injection (> 9 min), and rapid gelation at 37 °C (< 3 min). The gelation time was similar to that found by Temenoff *et al*.,[173] who used 25 mM APS and TEMED to crosslink an oligo(poly(ethylene glycol) fumarate) and PEGDA prepolymer solution. The difference in required initiator concentration suggests that crosslinking time is dependent on the nature and concentration of crosslinking groups, in addition to the initiator concentration. The 5 mM concentration used in the current study resulted in a low sol content in PEG-(PTMC-A)$_2$ hydrogels (ca. 5-10%), which is beneficial in terms of limiting the exposure of encapsulated cells to unreacted acrylate or methacylate groups and preventing the diffusion of unreacted and potentially immunogenic components into the surrounding tissue when eventually applied *in vivo*. While some studies have reported a high cytotoxicity following cell encapsulation using APS and TEMED initiators,[181] the current work supports the findings of many others that indicate this initiator system is cytocompatible.[173–178] These differences likely arise due to differences in required initiator concentrations, the rates of initiator consumption and diffusion in the individual polymer systems, as well as the cell types encapsulated.

The *in vitro* assessment of hASC encapsulation using purified PEG-(PTMC-A)$_2$ indicated that under both hypoxia and normoxia, post-crosslinking viability was high (approximately 90% after 3 days), supporting that the process of injection through a minimally invasive 25G needle and crosslinking with

APS and TEMED had no major cytotoxic effects. Under normoxia, hASC density remained relatively constant, cell viability increased significantly from day 3 to 14, and the cells transitioned to a spindle-shaped morphology. Under hypoxia, the hASCs exhibited lower density and metabolic activity at later time points and less spindle-shaped morphology; however, the hASCs still exhibited high (ca. 90%) viability, suggesting that the delivery system could support viable cell retention and function even within an ischemic environment. Under both conditions, metabolic activity was significantly lower after day 3; however, this result was not reflected in reductions in either cell density or viability, suggesting that it could be due to a metabolic adaptation of the cells to a 3-D environment, though additional studies would be required to confirm this hypothesis.

Critical to the proposed strategy of using encapsulated hASCs to treat ischemic conditions is the production and release of growth factors in response to low oxygen tension. The effects of encapsulation and hypoxia on growth factor release were evaluated by comparing the release rate of angiogenic cytokines from encapsulated and TCPS cultured hASCs under normoxia and hypoxia. The observed rates of cytokine release by hASCs cultured under normoxia on TCPS closely support the previous findings of Amable *et al.*[9] in terms of VEGF-A, angiopoietin-1, angiogenin, and PDGF-AA secretion. However, in the current study, lower levels of PlGF, and higher levels of HGF and MCP-1 were observed, potentially due to cell donor variability. The hypoxic upregulation of VEGF-A and angiopoietin, but not HGF or SDF-1α, also supports previous studies of TCPS cultured hASCs.[10,92,182] These findings confirm that the hASCs in the current study exhibited a pro-angiogenic secretome, while also providing a baseline of growth factor production for comparison with encapsulated hASCs.

Encapsulated hASCs released significantly higher levels of all the studied cytokines under hypoxia compared to normoxia at day 14. This included HGF, PDGF-AA, SDF-1α, and MCP-1, which were not enhanced by hypoxia in TCPS cultured hASCs. While TCPS cultured hASCs demonstrated hypoxic upregulation of VEGF-A, angiopoietin-1, angiogenin, PlGF, and MCP-1 by day 7, no upregulation was observed from encapsulated hASCs until day 14. This delayed onset may reflect a ‘recovery period’

following crosslinking during which hASCs adapt to the 3-D environment, though additional studies would be required to confirm this hypothesis. These differences between encapsulated and TCPS cultured hASCs may have arisen due to differences in matrix stiffness and the presence of RGD as an integrin binding ligand, factors which have previously been demonstrated to affect MSC angiogenic cytokine profiles.[183] Of note, this investigation only quantified the level of cytokines released from the hydrogels. As diffusional limitations and electrostatic interactions caused by the hydrogel network may have inhibited the release of cytokines produced by encapsulated hASCs, this assessment likely underestimates the level of cytokine production. Furthermore, this also suggests that there existed an elevated concentration of cytokines within the hydrogel, resulting in a concentration difference driving diffusion from the hydrogel into the release medium, and potentially enhancing the paracrine effects of the cytokines on the encapsulated hASCs. Overall, however, the production and release of these angiogenic cytokines from encapsulated hASCs is a promising indication that the encapsulation strategy may be effective for promoting angiogenesis in ischemic tissues.

3.5 Conclusions

The use of hydrogel delivery scaffolds has the potential to improve the efficacy of many cell-based therapies by overcoming the high rates of cell washout upon delivery, as well as poor long-term cell retention and survival. However, their use in treating conditions affecting mechanically dynamic tissues has largely been limited due to a lack of hydrogels that combine cell encapsulation, injectable delivery, and robust mechanical properties. In this work, PEG-(PTMC-A)$_2$ copolymers were developed as a mechanically reinforcing component in a modular polymer hydrogel system, whereby adjusting the copolymer block lengths and polymer mixing ratios can be used to tune the modulus, increase toughness, and improve the resistance to strain and fatigue of the composite hydrogels, while still maintaining their elastic and minimal swelling nature.

Though demonstrated here in combination with MGC-RGD, the PEG-(PTMC-A)$_2$ system has the potential to be applied more broadly to reinforce the mechanical properties of the vast library of existing

acrylate or methacrylate-based hydrogels for cell encapsulation, such as hydrogels derived from chondroitin sulfate, hyaluronic acid, and gelatin. By reinforcing typically weak hydrogels, PEG-(PTMC-A)$_2$ could potentially expand the application of these materials as injectable hydrogel scaffolds to include a range of mechanically dynamic soft tissues targets including skeletal and cardiac muscle, cartilage, adipose tissue, and skin. Further, the adaptation of the APS/TEMED crosslinking system facilitates use in applications requiring *in situ* crosslinking for minimally invasive or defect-filling delivery.

The cytocompatibility of the proposed encapsulation system was demonstrated by the encapsulation and retention of viable hASCs capable of producing and releasing growth factors over 14 days, with a generally enhanced angiogenic response under the environmental cue of hypoxia. These results are a promising indication that the proposed hydrogel system may overcome the challenges of poor cell localization, retention, and survival following injection. Further, this work demonstrated the ability of encapsulated ASCs to release angiogenic growth factors at rates equal to or exceeding rates from TCPS cultured ASCs, suggesting that the hydrogel scaffold could facilitate the function of encapsulated ASCs as trophic mediators in the ischemic environment of PAD. Compared to the delivery of growth factors directly, the use of encapsulated hASCs as "paracrine factories" has the advantage of providing an array of complementary growth factors simultaneously, delivered in a temporally regulated manner that is continuous and sensitive to environmental stimuli such as hypoxia.

Chapter 4

Immunological and angiogenic response to the intramuscular injection of adipose-derived stem/stromal cells in a hydrogel scaffold

4.1 Introduction

Adipose-derived stem/stromal cells (ASCs) have received increasing attention as an abundant and readily accessible source of mesenchymal stem/stromal cells (MSCs) for the treatment of ischemia not only due to their angiogenic potential,[9,10,12,13] but also their potent immunomodulatory effects.[134,135,137,184] *In vitro,* ASCs promote a regenerative phenotype and the production of anti-inflammatory cytokines in peripheral blood mononuclear cells[137] and macrophages.[134,135] *In vivo*, delivery of allogeneic ASCs has been shown to induce a more pro-regenerative macrophage phenotype and increased systemic anti-inflammatory cytokine levels following liver transplantation in rats,[184] as well as in diabetic mice.[135] These properties make ASCs a promising candidate for modulating both the pro-inflammatory microenvironment within tissues impacted by chronic ischemia, as well as the host response to implanted biomaterial scaffolds.

Inflammation is a fundamental response to implanted biomaterials that ultimately determines the fate and efficacy of such scaffolds.[185] Moreover, inflammation is also closely linked to angiogenesis.[128,186] Both processes are governed by the activity of macrophages, through their long-term interactions with the biomaterial and their role in the recruitment and direction of endothelial cells.[115] As such, modulating the macrophage response to biomaterials is an important strategy to promote wound-healing and angiogenic activity, the retention and survival of encapsulated cells, and the remodeling and eventual clearance of the scaffold.[187–191]

Specifically, strategies for treating ischemic conditions have focused on balancing the responses of M1 and M2 macrophages,[121,130,192] which represent the pro-inflammatory and pro-regenerative phenotypes along the spectrum of macrophage polarization, respectively.[112] The role of M1 and M2 macrophages in the process of biomaterial vascularization is the subject of ongoing study, but evidence suggests that M1

macrophages are involved in the initiation of angiogenesis at early time points, while M2 macrophages later stabilize nascent vessels.[121] Specifically, M2 subtypes M2a and M2c promote vessel anastomosis and aid in vascular remodeling of the extracellular matrix (ECM), respectively.[121]

In this chapter, an injectable hydrogel delivery scaffold was evaluated *in vivo* for the delivery of allogeneic rat adipose-derived stem/stromal cells (rASCs) to the adductor muscle of healthy immune-competent rats. The scaffold was composed of two polymers: a triblock copolymer of poly(trimethylene carbonate)-*b*-poly(ethylene glycol)-*b*-poly(trimethylene carbonate) diacrylate (PEG-(PTMC-A)$_2$) and methacrylated glycol chitosan functionalized with an RGD-containing peptide (MGC-RGD). The PEG-(PTMC-A)$_2$ component was used to modify the mechanical properties of the hydrogel to withstand the mechanical loading conditions of the lower limb, based on previous work.[149] The MGC-RGD component was selected to support ASC retention, viability, and activity.[33,149,193]

Immunohistochemical analysis was performed at 1, 2, and 4 weeks to compare the host response to intramuscularly injected composite PEG-(PTMC-A)$_2$ + MGC-RGD hydrogel scaffolds incorporating allogeneic rASCs relative to control groups of hydrogels without rASCs and rASCs delivered in saline. Intramuscular allogeneic rASC density was semi-quantitatively analyzed through PKH26 fluorescent cell tracking to determine the impact of the scaffold on cell retention. To assess the effects of rASCs on the macrophage response to the scaffolds, macrophage infiltration and polarization towards M1 and M2 phenotypes were probed using a range of macrophage markers. Finally, the angiogenic response to the encapsulated rASCs was assessed in comparison to the controls based on the blood vessel density at the site of each treatment.

4.2 Materials and methods

4.2.1 Materials

PEG$_{20}$-(PTMC$_2$-A)$_2$, referred to as PEG-(PTMC-A)$_2$ in this chapter, and MGC-RGD were prepared and characterized as described in Chapter 3. Phosphate buffered saline pH 7.4 (PBS), tris-buffered saline pH 7.4 (TBS), Cryomatrix frozen embedding resin, and HyClone fetal bovine serum (FBS) were obtained

from Fisher Scientific. Collagenase (Worthington Type 1) was obtained from Cedarlane. Unless specified, all other materials were obtained from Sigma Aldrich, Ltd.

4.2.2 Isolation, culture, and immunophenotyping of rASCs

All studies involving animals followed the Canadian Council on Animal Care guidelines and were reviewed and approved by the Animal Care Committee at Queen's University (protocols Amsden 2015-1628 and Amsden 2013-048). rASCs were isolated from the epididymal fat pad using methods adapted from protocols for the isolation and culture of human ASCs.[161] In brief, male Wistar rats (aged 10-12 weeks) were euthanized by CO_2 overdose and the epididymal fat pad was extracted and finely minced. The minced tissue was digested in Kreb's Ringer Buffer solution with 2 mg/mL type I collagenase, 1% bovine serum albumin, 2 mM glucose, and 25 mM HEPES at 37 °C for 45 min. The tissue digest was filtered through a stainless steel mesh and the mature adipocytes were removed following gravity separation. The sample was centrifuged (1200 × g, 5 min) and the cell pellet was re-suspended in erythrocyte lysis buffer (0.15 mM NH_4Cl, 10 mM $KHCO_3$, and 0.1 mM EDTA) for 10 min at room temperature. The cell suspension was filtered through a 40 micron cell strainer, then washed twice in complete medium (DMEM:Ham's F12 with 10% FBS and 1% pen/strep). The cells were plated at 5000 cells/cm^2 in complete medium. The adherent ASCs were cultured at 37 °C with 5% CO_2, and were passaged at 80% confluence. Passage 2 cells were used for the study.

To confirm the immunophenotype of the passage 2 rASC used in the studies, single colour flow cytometry analysis was performed in triplicate using a Guava easyCyte 8HT Benchtop flow cytometer (EMD Millipore, Billerica, MA, USA) as previously reported.[162] The cells were incubated with the following monoclonal, fluorochrome-conjugated antibodies from eBioscience (San Diego, CA): the mesenchymal markers CD90-FITC, CD29-PE, and CD44-PE-Cyanine7, as well as the negative markers CD31-PE (endothelial) and CD45-FITC (hematopoietic). All samples were stained for 30 min at 4 °C and protected from light. Unstained controls were included in every trial.

4.2.3 PKH labeling of rASCs

To enable *in vivo* cell tracking, donor rASCs were labelled with the lipophilic membrane dye PKH26 according to the manufacturer's instructions two days prior to intramuscular delivery. rASCs were trypsin-released, washed with serum-free medium, and re-suspended at 2×10^7 cells/mL in Diluent C. The cell suspension was mixed with an equal volume of Diluent C containing 4 μM PKH26 for 4 min. Dye binding was terminated by adding an equal volume of FBS, then the cell suspension was centrifuged (400 × g for 10 min) and washed with complete medium three times, transferring to a new tube after each centrifugation (400 × g for 5 min). The rASCs were re-plated at their original density and the adherent cells were washed with PBS after 24 h.

4.2.4 Intramuscular injection

Intramuscular injections were administered to healthy female Wistar rats aged 8 weeks (N = 4 per treatment type, per time point). The rats were anesthetized with isoflurane, and given subcutaneous injections of meloxicam (2 mg/kg) as a pre-operative analgesic and bupivacaine (2 mg/kg) as a local anesthetic. Three treatment groups were tested:

i) Gel + rASCs: rASCs (2×10^7 cells/mL) in hydrogel prepared from mixed solutions of 4% w/v PEG-$(PTMC\text{-}A)_2$ + 1% w/v MGC-RGD, dissolved in PBS;

ii) Gel alone: hydrogel prepared from mixed solutions of 4% w/v PEG-$(PTMC\text{-}A)_2$ + 1% w/v MGC-RGD, dissolved in PBS;

iii) rASCs + saline: rASCs (2×10^7 cells/mL) suspended in PBS.

All polymers were disinfected by exposure to low intensity UV light in a biological safety cabinet for 40 min before dissolving in sterile PBS. For hydrogels with rASCs, a suspension of PKH-labelled rASCs in sterile PBS was thoroughly mixed into the polymer solution. To initiate polymerization of both hydrogel groups, sterile filtered 100 mM solutions of ammonium persulfate (APS) and tetramethylethylenediamine (TEMED) were added sequentially to the polymer solutions immediately

before administration, with thorough mixing between each addition, providing a final concentration of 5 mM each of APS and TEMED.

The treatments were administered by injecting a total volume of 50 µL divided evenly over two injection sites 5 mm apart centred along the length of the adductor muscle using a 25G × ½" needle. After injection, the animals were maintained under anesthesia for 5 min to prevent muscle contractions from dispersing the delivered material or cells. Rats were sacrificed by CO_2 overdose at 1, 2, and 4 weeks post-injection. A 15 mm long section of the adductor muscle group, centred on the injection sites, was carefully excised. The tissue was embedded in Cryomatrix frozen embedding resin and snap frozen in liquid nitrogen.

4.2.5 Immunohistochemical analysis

The characterization studies focused on immunohistochemical (IHC) staining to be able to assess the spatial distribution of rASCs, macrophages, and blood vessels relative to the hydrogels and surrounding tissue. Frozen tissue was cryo-sectioned perpendicular to the muscle fibre orientation at 5 µm thickness. Sections were taken at the injection sites, as identified by the presence of PKH^+ cells and/or the hydrogel.

4.2.6 PKH^+ rASC retention

To quantify PKH^+ rASC density, unfixed sections from three depths across the injection site were mounted in fluoroshield mounting medium with 4',6-diamidino-2-phenylindole (DAPI) (Abcam) and all nucleated PKH^+ cells across the entire section were imaged with a Zeiss Axio Imager M1 microscope with a 20× objective. The total number of PKH^+ cells was normalized to the total muscle cross sectional area. Identification of PKH^+ rASCs was performed on unfixed, unstained tissue sections, as the process of fixation and permeabilization reduced the PKH staining fidelity.

4.2.7 Macrophage response and angiogenesis

Sections were fixed with 4% paraformaldehyde, rinsed with TBS, and blocked with 5% goat serum in TBS with 0.2% Tween-20 (TBS-T) for 1 h at room temperature. The serum solution was replaced with primary antibodies diluted in TBS-T with 1% bovine serum albumin per Table 1 and incubated overnight

at 4 °C. Anti-CD31 was applied alone; anti-CD163 and anti-CD68 were applied alone to serial sections to facilitate comparison of $CD163^+$ and $CD68^+$ cell densities; anti-CCR7, anti-arginase-1 (Arg-1), and anti-inducible nitric oxide synthase (iNOS) were each paired with anti-CD68. Following primary incubation, the sections were rinsed three times with TBS and incubated with appropriate secondary antibodies diluted in TBS-T with 1% bovine serum albumin per Table 4-1 for 1 h at room temperature. The secondary antibody solutions were rinsed three times with TBS and the sections were mounted with fluoroshield mounting medium with DAPI. All imaging was performed with a Zeiss Axio Imager M1 microscope. Negative primary controls were included for each stain, following the exact same staining procedure, but without primary antibodies added to the dilution buffer for incubation; positive tissue controls were performed where available (see Appendix A.4)

Table 4-1: Summary of primary and secondary antibodies used for IHC.

Antibody	Clone	Supplier (Cat. #)	Dilution	Conc. (µg/mL)
Mouse anti-CD31	TLD-3A12	Bio-Rad (MCA-1334G)	1:250	4.0
Mouse anti-CD68	ED1	Bio-Rad (MCA341R)	1:400	2.5
Rabbit anti-CCR7	Y59	Abcam (ab32527)	1:250	4.2
Mouse anti-CD163	ED2	Bio-Rad (MCA342GA)	1:250	2.0
Rabbit anti-arginase-1	Polyclonal	Abcam (ab91279)	1:200	5.0
Rabbit anti-iNOS	Polyclonal	Abcam (ab15323)	1:50	4.0
Goat anti-mouse Alexa Fluor 488	Polyclonal	Abcam (ab150113)	1:500	4.0
Donkey anti-rabbit Alexa Fluor 647	Polyclonal	Abcam (ab150063)	1:250	8.0

The maximum penetration depth of $CD68^+$ cells into each hydrogel was measured perpendicular to the border from five points (10× magnification) using Zeiss Zen software (v. 2.3). The fractional area of the gels staining $CD68^+$ was determined by converting the images (10× magnification) to binary and measuring the ratio of $CD68^+$ area within the gel to total gel area using ImageJ software (v. 1.46r). To assess

macrophage polarization, a minimum of four non-overlapping images per hydrogel were analyzed (40× magnification, centered on hydrogel border). The total number of cells that were $CD68^+$ and $CD68^+$ $CCR7^+$ were counted; the number of $CD163^+$ cells was similarly counted on images taken from serial sections to the CD68 images, and matched in terms of location at the gel border. CCR7 and CD163 expression was quantified as the fraction of $CD68^+$ cells that were co-stained $CCR7^+$ or $CD163^+$. To assess enzymatic expression, at least four images per hydrogel were used (40× magnification, taken from areas within the hydrogel), and the total number of cells that were $CD68^+$, $CD68^+$ $iNOS^+$ and $CD68^+$ Arg-1^+ were counted (ImageJ v. 1.46r and Zeiss Zen v. 2.3 software). iNOS and Arg-1 expression were quantified as the fraction of $CD68^+$ cells that were co-stained $iNOS^+$ or Arg-1^+.

$CD31^+$ vessel density was quantified in all treatment groups, using at least 6 non-overlapping images from each sample (20× magnification) at the border of the hydrogels or at the site of PKH^+ cells, when delivered in saline. The minor diameter of all $CD31^+$ blood vessels was measured using AxioVision software (v. 4.9.1).

4.2.8 Statistical analysis

All data are presented as the mean ± SD. Comparisons were made by two-way ANOVA. Differences between groups at given time points and differences within groups across time points were determined by Sidak's multiple comparisons test. All analysis was performed using GraphPad Prism 7.

4.3 Results

4.3.1 Injection using hydrogel scaffolds improves rASC retention at the delivery site

Passage 2 rASCs isolated from the epididymal fat pad exhibited the expected positive and negative expression of surface markers (Table 4-2), confirming the cells had a stromal cell type. PKH^+ rASCs delivered by IM injection in the hydrogel scaffold and in saline were identified in the adductor muscle of all recipient rats at 1, 2, and 4 weeks post-injection. rASCs delivered in the hydrogel were observed

predominately within the gel, located in the intramuscular space (Figure 4-1a). When delivered in saline, rASCs were largely found along the subdermal fascia (Figure 4-1b).

Table 4-2: Immunophenotype of rASCs used for *in vivo* delivery. Percent of cells positive for each marker is presented as the average ± SD from n = 3 repeated measurements.

Surface Marker	Expected phenotype[163]	Percent positive
CD 90	+	91.14 ± 0.23
CD 29	+	99.25 ± 0.15
CD 44	+	70.52 ± 0.48
CD 31	-	1.97 ± 0.15
CD 45	-	0.21 ± 0.10

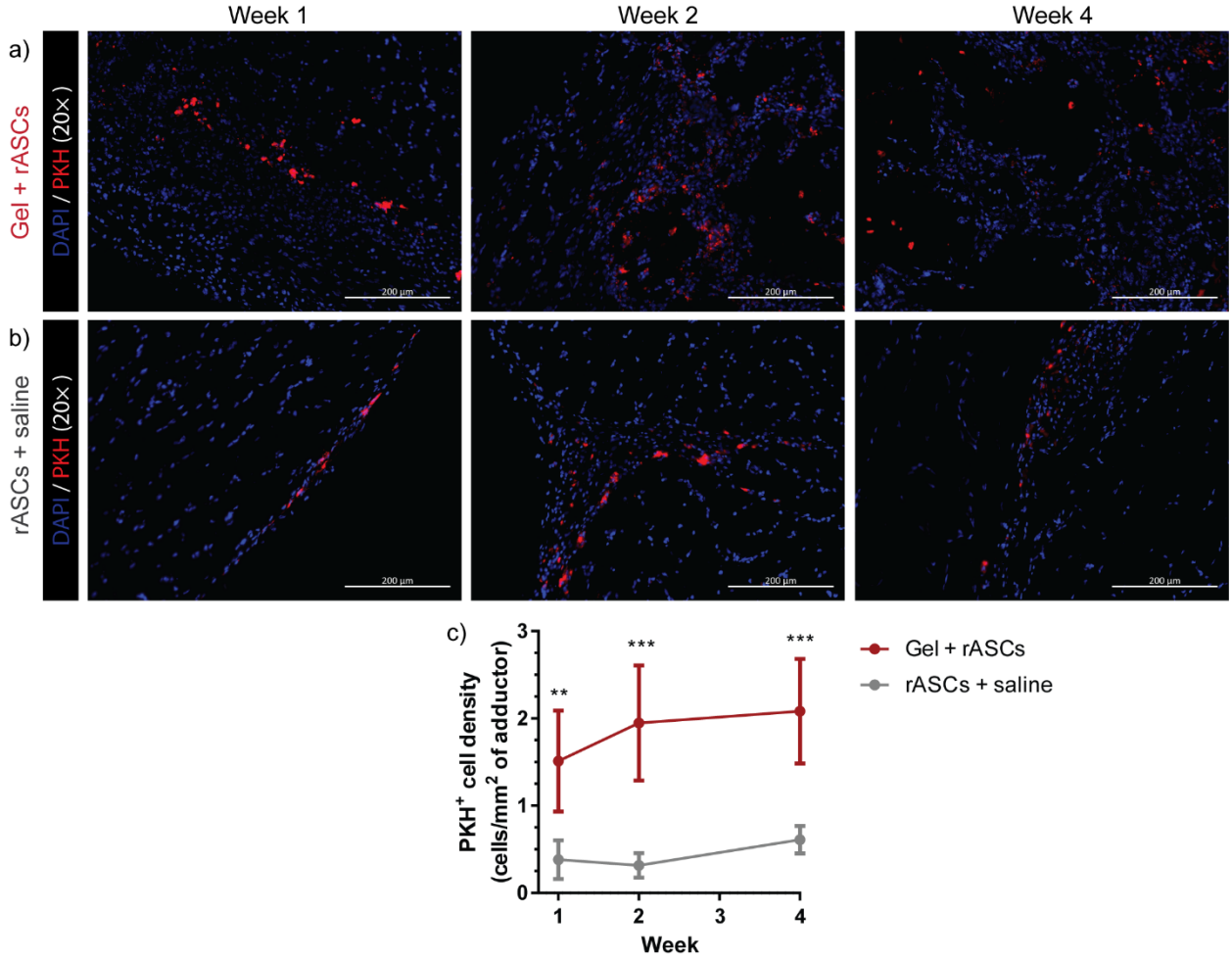

Figure 4-1: rASC retention following intramuscular injection. Representative images from adductor muscle sections showing PKH$^+$ rASCs (red) delivered in the injectable hydrogel (a) and saline (b) at 1, 2, and 4 weeks post-delivery; DAPI counterstain (blue); scale bars = 200 µm (20×). c) Intramuscular PKH$^+$ cell count normalized to total adductor cross sectional area following injection in the hydrogel (red) and saline (grey) at 1, 2, and 4 weeks post-delivery; significant differences between groups at each time point were determined by two-way ANOVA with Sidak's correction for multiple comparisons (** $p < 0.01$; *** $p < 0.001$, N=4).

At all time points, significantly more PKH^+ cells were observed per adductor cross sectional area following delivery in the hydrogel scaffold, compared to saline (Figure 4-1c), supporting that the scaffold improved cell retention. No significant differences in rASC density between time points were found, suggesting that any rASCs that were lost during delivery were lost within the first week.

4.3.2 rASCs promote macrophage recruitment and infiltration into hydrogel scaffolds

CD68 was used as a pan-macrophage marker in assessing the response to the hydrogels with (Figure 4-2a) and without (Figure 4-2b) rASCs. In general, greater $CD68^+$ cell infiltration was observed after 2 weeks in response to the hydrogels with rASCs, compared to those without, in terms of the fractional area of the hydrogel staining $CD68^+$ (Figure 4-2c) and depth of $CD68^+$ cell infiltration (Figure 4-2d). The infiltration depth and fraction did not significantly change over time in the hydrogels without rASCs. In contrast, the infiltration fraction increased significantly from weeks 1 to 2 and the infiltration depth increased significantly from weeks 2 to 4 in hydrogels with rASCs.

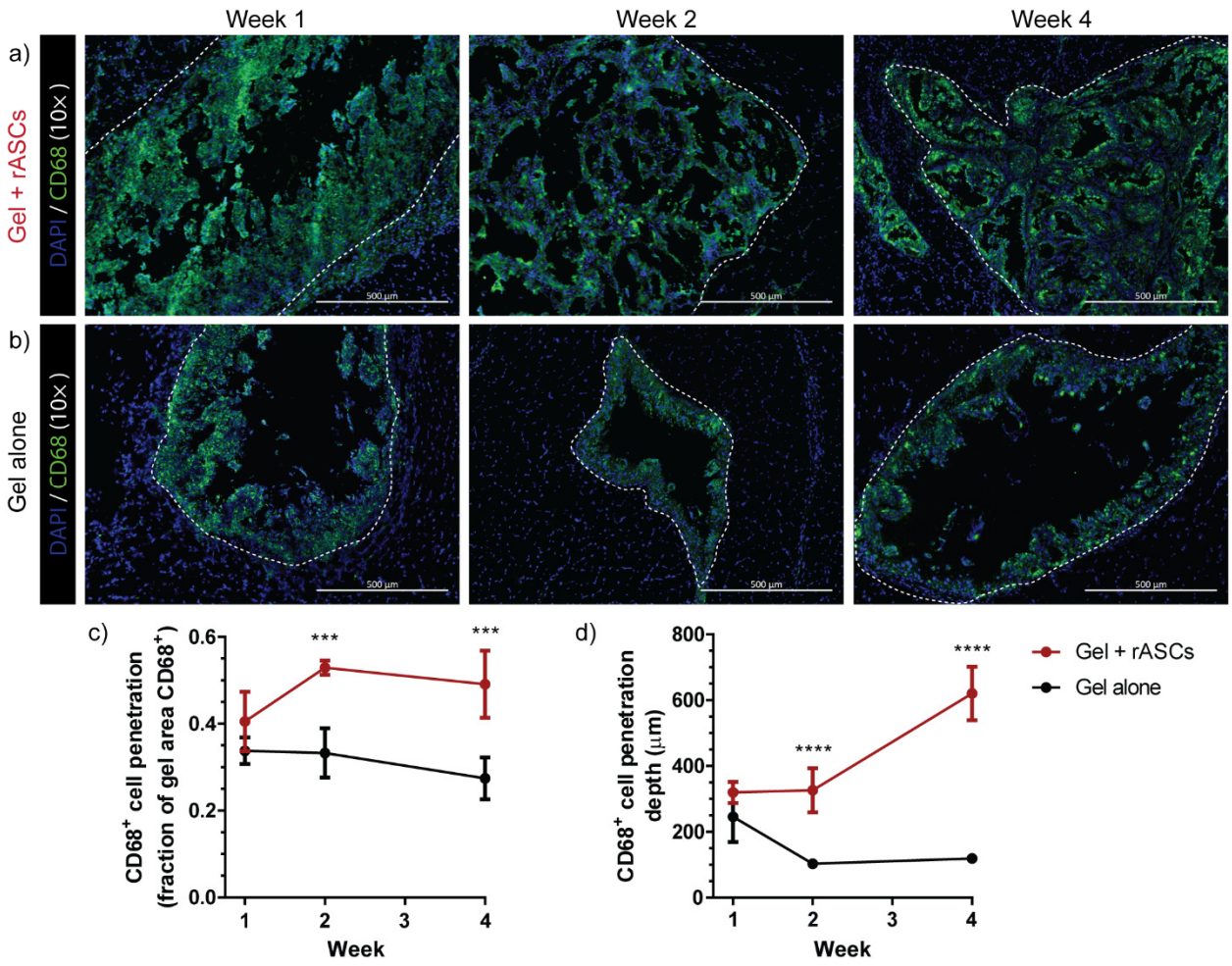

Figure 4-2: Macrophage recruitment and infiltration into intramuscular scaffolds. Representative images of $CD68^+$ cell (green) penetration into the hydrogels with (a) and without (b) rASCs at 1, 2, and 4 weeks post-delivery; DAPI counterstain (blue); gel border indicated in white dashed line; scale bars = 500 µm (10×). Fraction of the gel area positive for CD68 (c) and $CD68^+$ cell penetration depth from the border of the hydrogel (d) in hydrogels with rASCs (red) and without rASCs (black); significant differences between groups at each time point were determined by two-way ANOVA with Sidak's correction for multiple comparisons (*** $p < 0.001$; **** $p < 0.0001$, N=3-4).

4.3.3 rASCs promote an M2c phenotype at the hydrogel periphery and M1 macrophage infiltration

Staining of the scavenger receptor CD163 (Figure 4-3) and the chemokine receptor CCR7 (Figure 4-4) was used to identify M2c macrophages[113,121] and M1 macrophages[113], respectively, at the borders of the hydrogels. In general, $CD163^+$ cells were found at the periphery of the hydrogels, with minimal infiltration into the hydrogel. Infiltrating cells were predominantly $CD68^+$ $CCR7^+$, while few of the $CD68^+$ cells outside of the hydrogel boundary were $CCR7^+$.

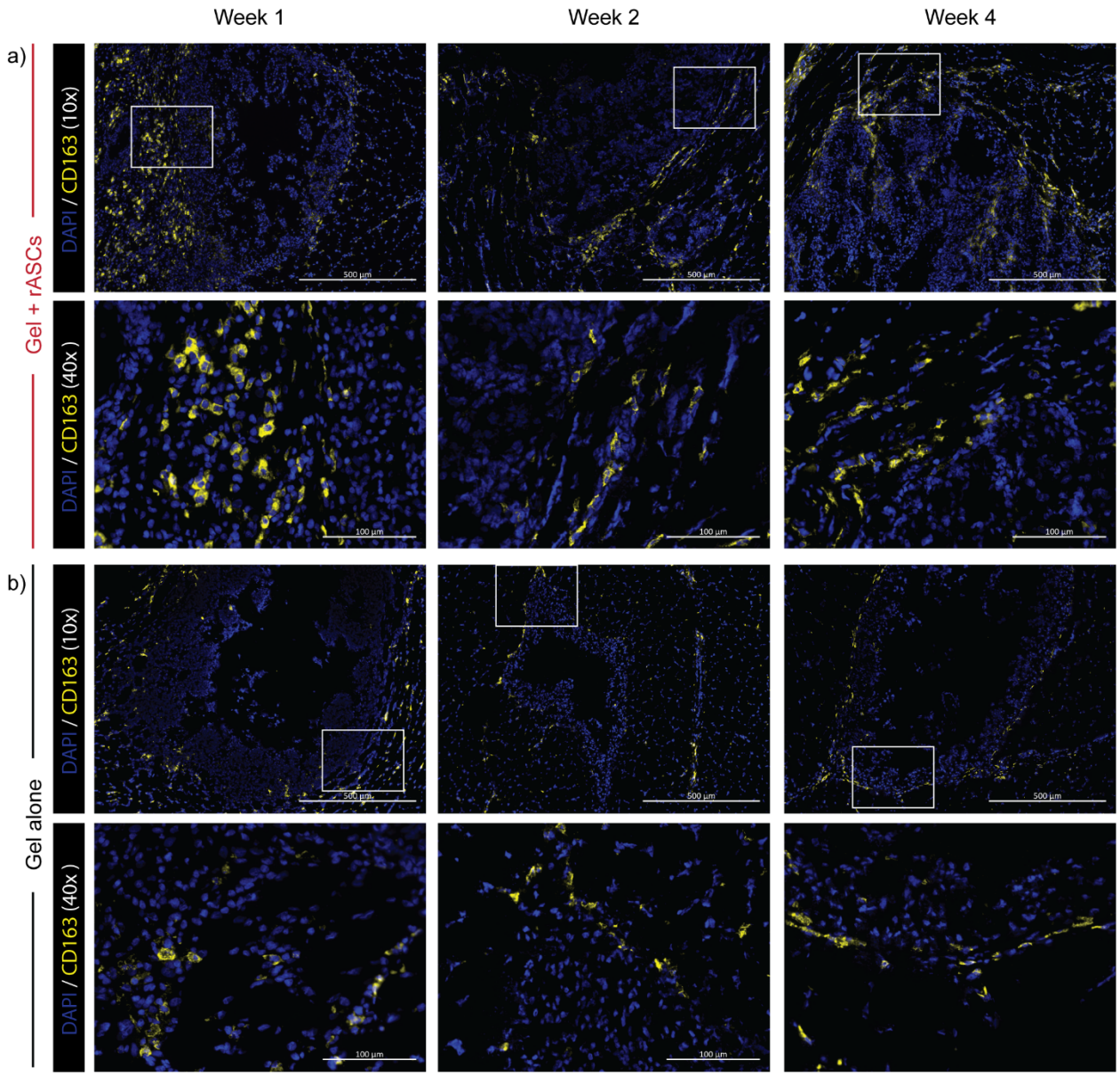

Figure 4-3: M2c macrophages identified by CD163^{+} staining. Representative images CD163^{+} cells (yellow) at hydrogels with (a) and without (b) rASCs at 1, 2, and 4 weeks post-delivery; DAPI counterstain (blue). Scale bars = 500 µm (10×) and 100 µm (40×). White outlines in the 10× images indicate the area of detail in the 40× images.

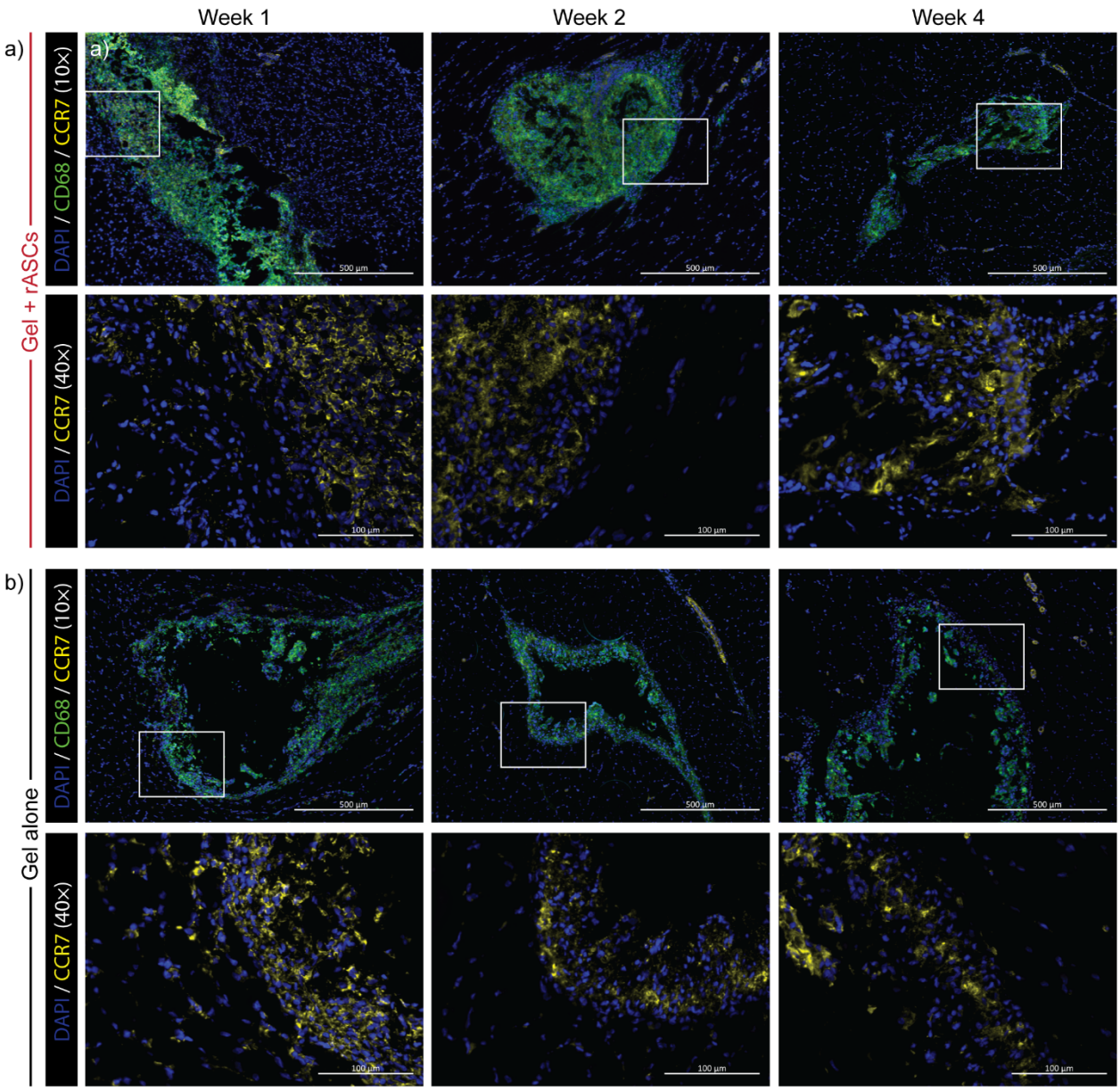

Figure 4-4: M1 macrophages identified by CD68$^+$CCR7$^+$ staining. Representative images of CD68$^+$ cells (green) and CCR7$^+$ cells (yellow) at hydrogels with (a) and without (b) rASCs at 1, 2, and 4 weeks post-delivery; DAPI counterstain (blue). Scale bars = 500 µm (10×) and 100 µm (40×). White outlines in the 10× images indicate the area of detail in the 40× images.

As a fraction of the CD68$^+$ cells, the relative number of CD163$^+$ cells was significantly higher in response to the hydrogels with rASCs (Figure 4-5a), and remained relatively constant over 4 weeks, at approximately 17% and 8% in response to the hydrogels with and without rASCs, respectively. At all time points, the fraction of CD68$^+$ cells that were CCR7$^+$ was not significantly different between the hydrogels

with and without rASCs (Figure 4-5b). However, this ratio reduced significantly ($p = 0.027$) between weeks 1 and 4 in the hydrogels without rASCs, from approximately 78% ± 12% to 44% ± 21%.

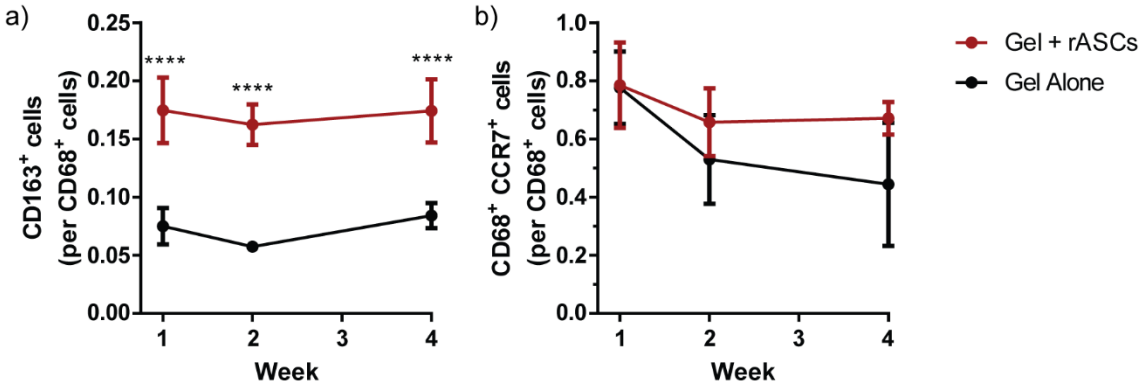

Figure 4-5: M1 and M2c macrophage polarization at hydrogel borders. a) $CD163^+$ cell density and b) $CD68^+$ $CCR7^+$ cell density, normalized to $CD68^+$ cell density for hydrogels with rASCs (red) and without rASCs (black); significant differences between groups at each time point were determined by two-way ANOVA with Sidak's correction for multiple comparisons (**** $p < 0.0001$, N=3-4; note: only N=2 samples were used for $CCR7^+$ in gels without rASCs at week 4 due to limited tissue availability).

4.3.4 rASCs reduce initial iNOS activity and promote Arg-1 activity in infiltrating macrophages

Staining was performed to identify $CD68^+$ cells expressing inducible nitric oxide synthase (iNOS) in the hydrogels with (Figure 4-6a) and without (Figure 4-6b) rASCs. In general, $CD68^+$ $iNOS^+$ cells were predominantly found within the gels, at the advancing edge of the infiltrating $CD68^+$ cells. Staining was also performed to identify $CD68^+$ cells expressing arginase-1 (Arg-1) in the hydrogels with (Figure 4-7a) and without (Figure 4-7b) rASCs. In general, $CD68^+$ $Arg\text{-}1^+$ cells were distributed throughout the infiltrating $CD68^+$ cell population, with no discernable pattern.

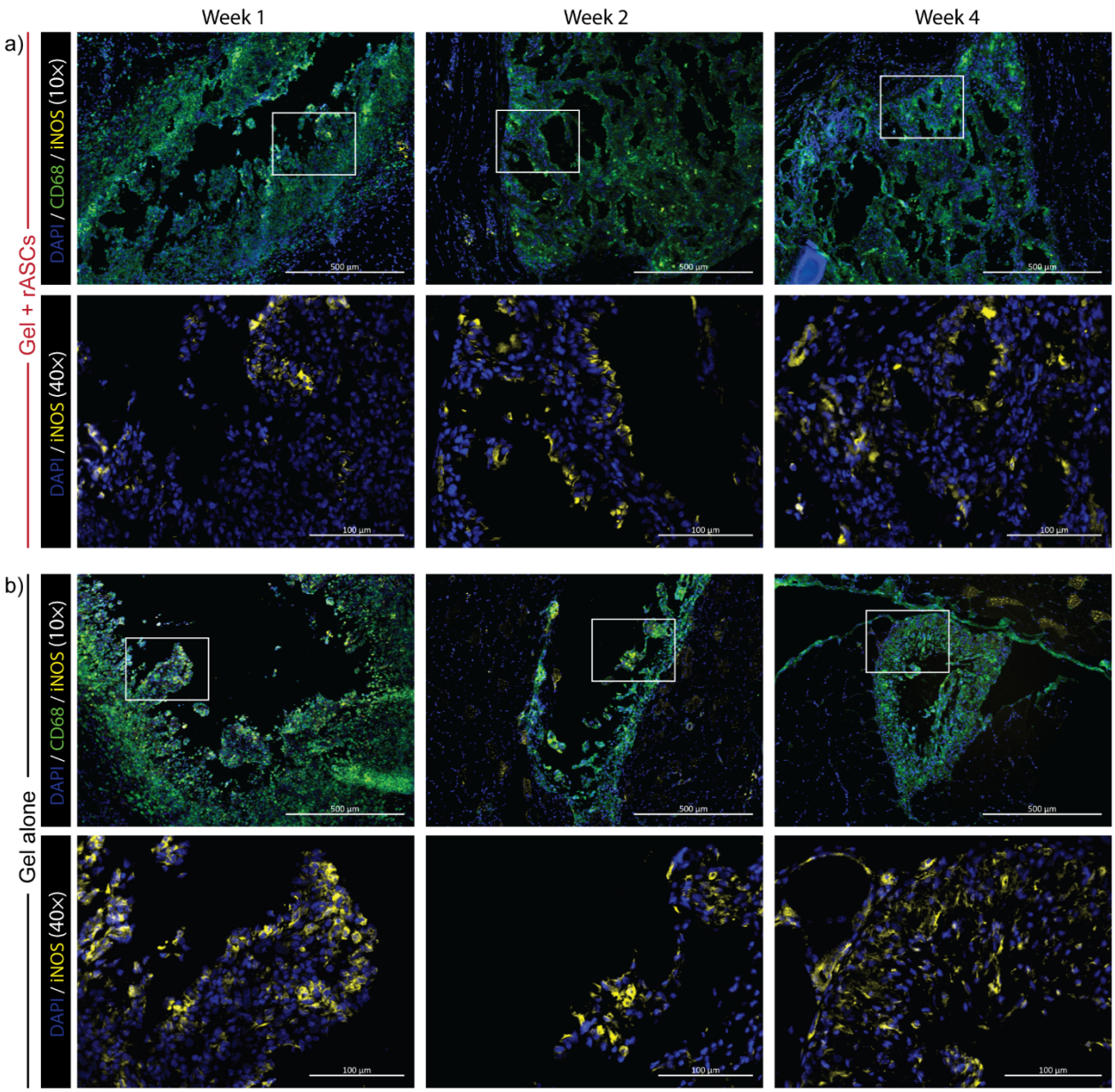

Figure 4-6: iNOS expression in infiltrating macrophages. Representative images of iNOS$^+$ cells (yellow) and CD68$^+$ cells (green) infiltrating the hydrogels with (a) and without (b) rASCs at 1, 2, and 4 weeks post-delivery; DAPI counterstain (blue); scale bars = 500 µm (10×) and 100 µm (40×). White outlines in the 10× images indicate the area of detail in the 40× images.

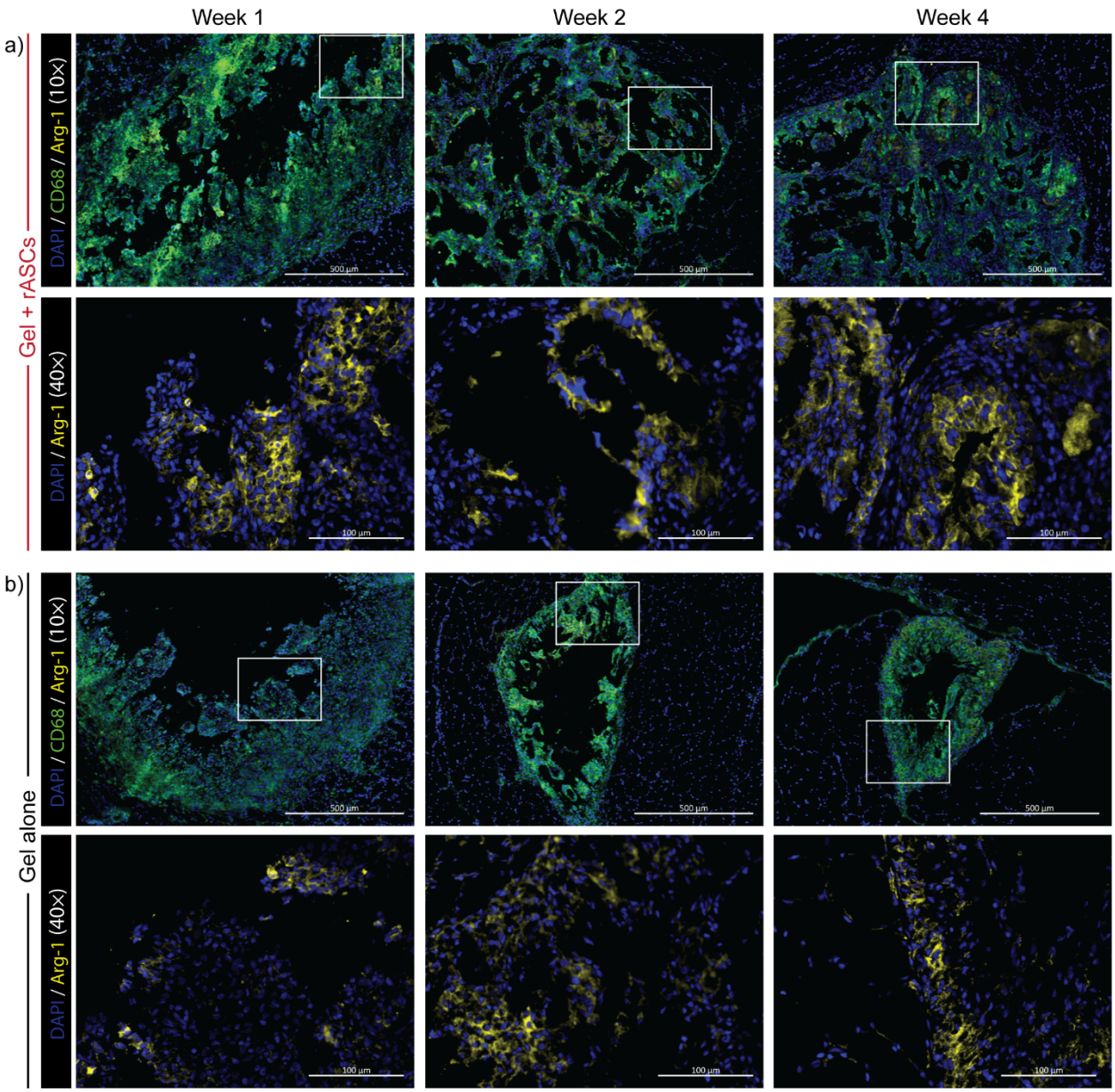

Figure 4-7: Arg-1 expression in infiltrating macrophages. Representative images of Arg-1$^+$ cells (yellow) and CD68$^+$ cells (green) infiltrating the hydrogels with (a) and without (b) rASCs at 1, 2, and 4 weeks post-delivery; DAPI counterstain (blue); scale bars = 500 µm (10×) and 100 µm (40×). White outlines in the 10× images indicate the area of detail in the 40× images.

After 1 week, a significantly higher fraction of CD68$^+$ cells were iNOS$^+$ in the hydrogels with rASCs versus without rASCs (21.6% ± 4.7% vs 10.9% ± 1.9%, p = 0.001) (Figure 4-8a). The fraction of iNOS$^+$ cells in the hydrogels without rASCs was significantly lower at weeks 2 and 4 compared to week 1 (p = 0.027 and p = 0.017, respectively), and not statistically different from hydrogels with rASCs.

At all time points, a significantly higher fraction of $CD68^+$ cells were $Arg\text{-}1^+$ in the hydrogels with rASCs, compared to the hydrogels without rASCs (Figure 4-8b). The fraction of $Arg\text{-}1^+$ cells increased significantly from week 1 to week 4 in the hydrogels with rASCs (20.9% ± 6.5% to 32.7% ± 2.2%, p = 0.037), as well as the hydrogels without rASCs (5.7% ± 1.2% to 20.4% ± 7.7%, p = 0.010).

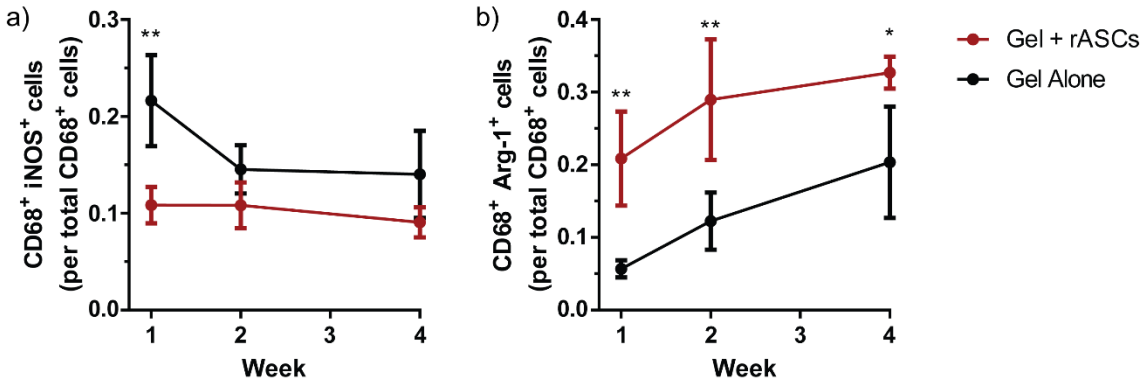

Figure 4-8: Fraction of iNOS+ and Arg-1+ infiltrating macrophages. a) $CD68^+$ $iNOS^+$ and b) $CD68^+$ $Arg\text{-}1^+$ cells as a fraction of $CD68^+$ cells in the hydrogels with rASCs (red) and without rASCs (black) at 1, 2, and 4 weeks post-delivery; significant differences between groups at each time point were determined by two-way ANOVA with Sidak's correction for multiple comparisons (* $p < 0.05$; ** $p < 0.01$, N=3-4).

4.3.5 rASCs enhance angiogenesis when delivered within an *in situ* forming hydrogel

CD31 staining was used to identify capillaries at the border of the hydrogels with and without rASCs, and at the site of rASC localization for saline delivery. At 4 weeks post-delivery, $CD31^+$ vessels were observed at the border and within the hydrogels with rASCs (Figure 4-9a-b), whereas vessels were only observed near, but not within, the hydrogels without rASCs (Figure 4-9c-d). Quantification of $CD31^+$ vessel density normalized to image area (Figure 4-9e) indicated no significant differences in vessel density after 1 week; however, vessel density was significantly greater surrounding the hydrogels with rASCs at 2 and 4 weeks post-delivery as compared to all other groups. The range in the minor vessel diameter was consistent between groups (Figure 4-9f-h), centered at approximately 6 μm, with no statistically significant differences in the mean diameter of each group. However, the mean vessel diameter surrounding the hydrogels with rASCs was significantly lower at weeks 2 and 4, compared to week 1 (p = 0.009 and p = 0.046, respectively), consistent with the formation of new smaller diameter vessels.

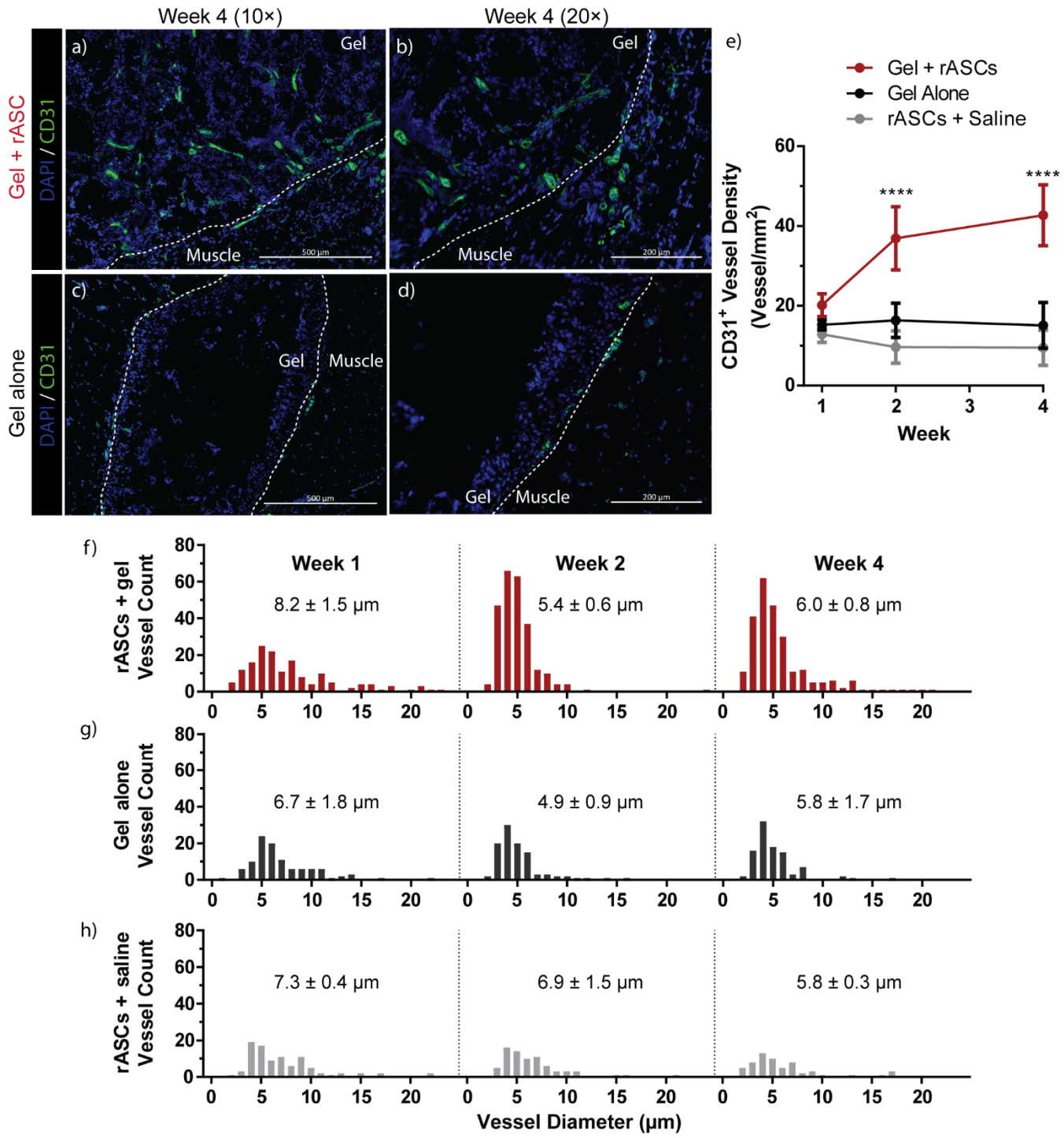

Figure 4-9: Angiogenic response to hydrogels with and without rASCs and rASCs delivered in saline. Representative images of $CD31^+$ vessels (green) surrounding the hydrogels with rASCs (a,b) and without rASCs (c,d), 4 weeks post-delivery; DAPI counterstain (blue); scale bars = 500 µm (10×) and 200 µm (20×). $CD31^+$ vessel density at the hydrogel borders (or the site of rASC localization, when delivered in saline) over time (e); significant differences between groups at each time point were determined by two-way ANOVA with Sidak's correction for multiple comparisons (**** $p < 0.0001$, from all other groups, N=3-4). Histogram of $CD31^+$ lumen diameters at weeks 1, 2, and 4 for hydrogels with rASCs (f), hydrogels without rASCs (g), and rASCs in saline (h). Average vessel diameter ± SD (N = 3-4) listed above each histogram.

4.4 Discussion

Our understanding of the roles that macrophages play in tissue engineering is continually evolving as new evidence refines the definitions of macrophage subtypes and their activities. The field is increasingly interested in modulating this macrophage response as a strategy to promote biomaterial integration, tissue regeneration, and angiogenesis. Evidence of the immunomodulatory nature of MSCs has motivated their use in combination with biomaterial-based therapies to promote such positive outcomes of inflammation.

Chitosan, a natural polysaccharide obtained from the *N*-deacetylation of chitin, was used as the basis for the injectable hydrogel scaffold due to its demonstrated capacity to support encapsulated cell survival and retention *in vitro*.[153,154] The current work extends these findings by demonstrating that chitosan-based hydrogels can effectively retain encapsulated cells intramuscularly, even after 4 weeks of active muscle use. Previous studies have shown that subcutaneously implanted chitosan scaffolds induced significant macrophage recruitment, and that macrophage polarization was dependent on the degree of deacetylation (DOD) of the chitosan used; 85% DOD resulted in a primarily M1 response, whereas 95% DOD was associated predominantly with an M2 phenotype.[194] In the current work, the composite hydrogel containing modified chitosan with a DOD of 85% similarly elicited a strong M1 macrophage response, evident in the extensive recruitment and infiltration of $CD68^+$ $CCR7^+$ cells. Macrophage recruitment is also influenced by the release of chitosan oligosaccharides (COS), the degradation products of chitosan. In a study of implanted chitosan, Zhao *et al.*[195] found that $CD68^+$ macrophage recruitment was significantly enhanced compared to silicone controls at 2 weeks post-implantation, corresponding to the timeline of COS production due to *in vivo* degradation. COS have also been demonstrated to have macrophage immunomodulatory effects, increasing Arg-1 expression in M1 macrophages[196] and reducing the production of inflammatory factors and nitric oxide (NO) in RAW 264.7 macrophages.[197] Thus, in the current work, the enhanced macrophage infiltration observed in hydrogels with rASCs may be contributing to the production of COS by scaffold degradation, subsequently influencing the phenotype of the recruited macrophages.

Previous studies have demonstrated that PEG-(PTMC-A)$_2$ hydrogels were susceptible to macrophage-mediated degradation, where specifically the incorporation of PTMC domains in PEG-based hydrogels permitted macrophage infiltration and enhanced degradation by cholesterol esterase enzymatic activity *in vitro*.[147] While studies of PEG diacrylate hydrogels have indicated that PEG domains are susceptible to oxidative degradation via macrophage generated reactive oxygen species,[198,199] it is expected that the inclusion of carbonate linkages in PEG-(PTMC-A)$_2$ networks increases their susceptibility to macrophage mediated degradation in comparison to purely PEG-based networks. The enzymatic degradation products of the PEG-(PTMC-A)$_2$ copolymer were expected to primarily consist of oligomeric PTMC, 1,3-propane diol, and oligomeric PEG.[63,200,201] While these products are relatively inert, their release during scaffold infiltration may have also contributed to continued macrophage recruitment.

In the current study, the inflammatory and angiogenic responses to intramuscularly injected scaffolds were found to be highly dependent on the encapsulation of rASCs within the scaffolds. The most apparent effect of the allogeneic ASCs was the enhanced recruitment and subsequent scaffold infiltration with CD68$^+$ cells. Although studies with human cells have identified varying levels of CD68 expression in T cells, monocytes, fibroblasts, and fibrocytes,[202–204] it would be expected that macrophages comprise the majority of the CD68$^+$ population in the context and time frame of the current model. The rASC-enhanced recruitment of CD68$^+$ cells was observed at 2 and 4 weeks post-delivery, when both fractional area of infiltration and penetration depth were significantly higher in the hydrogels with rASCs. These infiltrating CD68$^+$ macrophages were predominantly CCR7$^+$, suggesting a primarily M1 infiltrating population. The CCR7$^+$ fraction remained constant over time in hydrogels with rASCs, but decreased in hydrogels without rASCs by week 4, indicating that the rASCs and/or the enhanced total macrophage recruitment may be contributing to the continued M1 activation. While CCR7 is a traditional M1 marker and is most intensely expressed on M1s over other subtypes, it is important to note that not all M1s express CCR7.[121] Thus, it is possible that the infiltrating cells that were not CCR7$^+$ may still have a pro-inflammatory phenotype. M1 inflammatory macrophages are capable of producing high levels of TNF-α.[113] In response to TNF-α, ASCs

have been previously shown to increase production of chemotactic factors responsible for monocyte migration.[138,205] Thus, the rASCs may have responded to TNF-α produced by the early inflammatory M1 macrophages at the scaffolds, secreting chemotactic factors, and recruiting more macrophages into the scaffold. In contrast, this interaction would have been absent at the site of hydrogels without rASCs, consistent with the reduced macrophage infiltration observed.

In addition to enhancing overall macrophage recruitment, our results suggest that rASCs significantly increased the fraction of macrophages polarized towards an M2c phenotype. M2c polarization was assessed based on the CD163 marker,[121] a hemoglobin scavenger receptor associated with scavenging cellular debris and inducing intracellular signaling to secrete anti-inflammatory cytokines.[206] The fraction of M2c polarized cells was constant over 4 weeks for scaffolds both with and without rASCs, and these macrophages were predominantly found at the periphery of the scaffolds. M2c polarization can be stimulated via IL-10,[113,121] and ASCs have previously been shown to produce IL-10,[11] as well as to promote IL-10 production and CD163 expression in macrophages *in vitro*.[134,137,207] Additionally, ASCs delivered *in vivo* have promoted IL-10 production following orthotopic liver transplantation in rats[184] and obese mice.[135] Thus, encapsulated ASCs may be promoting the localized production of IL-10, resulting in the observed enhanced M2c polarization, although further studies would be required to verify this hypothesis.

The rASC-enhanced $CD68^+$ cell infiltration and remodeling of the scaffolds suggests that rASCs not only induce macrophage migration, but also alter macrophage metabolism. This metabolic shift was confirmed by identifying $CD68^+$ cells that were $iNOS^+$ and $Arg\text{-}1^+$. These two subsets represent the two major enzymatic pathways of arginine metabolism, and are commonly used to differentiate M1 and M2 macrophages.[112,208] M1 macrophages express higher levels of iNOS, converting arginine into NO, a precursor to reactive nitrogen species.[209] In contrast, M2 macrophages express higher levels of Arg-1, an enzyme responsible for the hydrolysis of arginine into ornithine (a precursor to polyamines, glutamate, and proline), and an inhibitor of inflammation and fibrosis.[210] At week 1, a higher fraction of $iNOS^+$ macrophages were found in the scaffolds without rASCs, suggesting that rASCs may have reduced the

initial inflammatory action towards the hydrogels. Additionally, the inclusion of rASCs resulted in a higher fraction of Arg-1^+ macrophages at all time points, and the levels increased over time with and without rASCs. In combination with the CD163 staining results, this pattern suggests that the encapsulated rASCs promoted the transition of macrophages from a more pro-inflammatory $iNOS^+$ response to a more pro-regenerative Arg-1^+ response.[122] This causal association is supported by the fact that, *in vitro*, ASCs have been shown to lower iNOS expression and increase Arg-1 expression in M1 activated macrophages,[135] and can induce unactivated macrophages towards a unique immunomodulatory phenotype with low iNOS expression and high Arg-1 expression.[134]

MSC therapy for treating ischemic conditions ultimately relies on stimulating the generation of new, functional blood vessels in the affected tissue. The angiogenic effects observed in the current non-ischemic hindlimb study are a promising sign for subsequent applications in an ischemic model. Compared to the hydrogels without rASCs and the sites of rASCs delivered in saline, the density of $CD31^+$ vessels was significantly increased at the site of hydrogels with rASCs at 2 and 4 weeks post-delivery, and the average vessel diameter was smaller than at week 1, suggesting new vessel formation. These results indicate that the angiogenic effects depend on the sustained, localized concentration of rASCs, and are not simply a response to the scaffold itself.

While the angiogenic effect is likely due in part to the many angiogenic factors produced by ASCs,[9–11] the fact that this process was closely linked to the progress of macrophage recruitment suggests that the macrophages may also be playing a role in the observed angiogenic response. While previous studies proposed that M1 macrophages were anti-angiogenic and that M2 macrophages were responsible for promoting angiogenesis,[127] more recent evidence has revealed that macrophage subtypes function in a coordinated, temporally organized manner to promote vessel growth.[121] Specifically, M1 macrophages are thought to initiate angiogenesis by releasing factors known to promote an endothelial tip cell phenotype and blood vessel sprouting.[121,211,212] Subsequently, M2c macrophages are thought to support vessel growth through the release of matrix remodeling enzymes that facilitate vascular remodeling of the extracellular

matrix.[213] In the current work, the enhanced recruitment of $CD68^+$ $CCR7^+$ cells into the rASC-containing scaffolds observed by week 2 corresponded with the onset of increased vessel density, suggesting that M1 macrophages may have been involved in promoting initial endothelial cell recruitment. Further, rASCs stimulated macrophage polarization towards the M2c phenotype, which may have facilitated the observed migration of endothelial cells and sprouting of vessels towards and into the scaffolds through the secretion of matrix remodeling factors.[213,214] This activity is compared to hydrogels without rASCs, which demonstrated lower $CD68^+$ cell recruitment and infiltration, reduced M2c polarization, and significantly lower $CD31^+$ vessel density. Furthermore, the enhanced vasculature surrounding and penetrating the hydrogels with rASCs may have facilitated the observed migration of macrophages into the hydrogels by providing a network for monocyte migration and extravasation, potentially indicating synergistic effects of macrophage recruitment and angiogenesis.

It is important to note that the immune response observed in the healthy, immunocompetent animal model used in the present study does not represent the inflammatory conditions and activated immune state that would be present in ischemic muscle,[215] which is the intended therapeutic target. While this may affect the rate of macrophage recruitment and the ratio of M1 to M2 subtypes, the current findings that ASCs are immunomodulatory and promote a pro-regenerative M2 phenotype suggests they may be beneficial in treating the chronic inflammation characteristic of ischemic tissue.

4.5 Conclusions

The work of this chapter demonstrates the feasibility of using an *in situ* forming hydrogel to retain therapeutic MSCs in an intramuscular environment. The hydrogel itself, a composite of mechanically robust PEG-$(PTMC\text{-}A)_2$ and cell-supportive MGC-RGD, was easily administered by injection and well retained in the intramuscular space, suggesting that the delivery strategy could be applied to a wide range of mechanically dynamic tissue environments. Compared to delivery in saline, the hydrogel improved the localization and retention of rASCs intramuscularly over 4 weeks *in vivo*. The presence of rASCs enhanced macrophage recruitment into the hydrogel and promoted a more pro-regenerative macrophage phenotype.

The combined rASC and macrophage presence was associated with significantly higher vessel density surrounding, and even within, the hydrogels with rASCs as compared to those without. Together, these results indicate that encapsulated rASCs have a potent immunomodulatory effect on the inflammatory response to implanted biomaterials, and that the combined activities of rASCs and macrophages produce an enhanced angiogenic effect. Thus, this strategy of cell delivery may serve to improve the efficacy of MSC therapies for a variety of ischemic conditions.

Chapter 5

Evaluation of adipose-derived stem cell delivery strategies in a model of peripheral arterial disease

5.1 Introduction

Lower limb peripheral arterial disease (PAD) affects over 200 million individuals worldwide and is the third leading cause of atherosclerotic vascular morbidity after heart disease and stroke.[216] Critical limb ischemia (CLI), an end stage of PAD, is associated with rest pain, non-healing ulcers, and tissue loss, as well as a 30% 1-year amputation rate and 20% 1-year mortality rate.[217,215] The standard treatments to restore limb perfusion include bypass grafting or percutaneous angioplasty. However, for up to 50% of patients with CLI, the severity and distribution of arterial occlusion preclude such interventions.[5] A promising alternative PAD treatment involves the intramuscular (IM) injection of mesenchymal stem cells into the ischemic regions of the affected limb to stimulate revascularization and functional recovery.[5,144] While clinical trials of cell-based treatments have demonstrated improvements to wound healing and reduced amputation rates, the poor extent of cell retention has remained a major challenge.[5]

Preclinical animal models of CLI are an invaluable tool for investigating the safety, efficacy, and limitations of cell-based angiogenic treatment strategies. The most commonly used is a mouse model wherein ligation and excision of the femoral artery produces acute hindlimb ischemia (HI).[144,218] Compared to *in vitro* angiogenic assays, *in vivo* HI models more closely resemble the human CLI condition by incorporating the complexities of skeletal muscle and vasculature architecture, as well as the interactions of multiple cell types involved in angiogenesis, such as endothelial cells, smooth muscle cells, pericytes, and monocytes/macrophages.[81] However, there are several limitations of HI models for studying CLI. The progression and recovery of HI induced by arterial ligation depends on: i) the severity of ligation (length of artery removed, number of collaterals removed, removal of the vein);[219] ii) the strain of mouse;[220] and iii) the age of the mouse.[221] These variabilities make it difficult to compare between studies using different

protocols.[222] Furthermore, the acute induction of HI by femoral ligation does not reproduce the chronic nature of PAD and CLI, nor does it reproduce the comorbidities that reduce angiogenic capacity, such as diabetes, hypertension, and hypercholesterolemia.[215] Therefore, while the progression of perfusion recovery in HI models can be an indication of a treatment's efficacy at stimulating angiogenesis and collateral formation, it does not directly represent the expected progression of perfusion recovery in PAD. Despite these limitations, the HI model has been a valuable tool for determining the efficacy of cell-based treatments of CLI both alone,[12,13,80] and with delivery scaffolds.[104,105,223]

In this chapter, the therapeutic potential of the proposed strategy for delivering human adipose-derived stem/stromal cells (hASCs) in an injectable mixed polymer hydrogel composed of methacrylated glycol chitosan with RGD (MGC-RGD) and poly(trimethylene carbonate)-*b*-poly(ethylene glycol)-*b*-poly(trimethylene carbonate) diacrylate (PEG-(PTMC-A)$_2$) was evaluated in a mouse model of acute HI. To enable testing of the approach with hASCs, an immune deficient non-obese diabetic (NOD)/severe combined immune deficiency (SCID) mouse strain was selected as the xenograft recipient, as it is a well-established model that permits human cell survival and engraftment.[224] In this strain, the NOD genetic background causes deficits in the differentiation and function of macrophages and antigen presenting cells,[225] and the SCID mutation prevents T and B cells from developing to maturity.[226] Furthermore, the NOD/SCID strain has been frequently used as a CLI model to evaluate human cell transplantations,[227–229] thus facilitating comparison of ischemic recovery between the current strategy and previous treatment approaches.

The goal of this work was to determine i) if the hydrogel delivery strategy improved hASC retention in an ischemic environment, and ii) if improved hASC retention was associated with positive outcomes in terms of revascularization and limb function. Following the induction of severe acute hindlimb ischemia by femoral artery and vein ligation, four different treatments were delivered by IM injection: hASCs delivered in the mixed polymer hydrogel, the hydrogel alone, hASCs in saline, and saline alone as a sham treatment. The recovery of limb perfusion was assessed by laser Doppler imaging over 28 days, and limb

function was evaluated by gait analysis at the final 28 day time point. This timeline of assessment was selected to allow observation of the full progression of perfusion recovery, based on previous work using the same mouse model of HI.[228,229] The thigh muscles of the ischemic and contralateral control hindlimbs were analyzed by immunohistochemistry to assess the effects of hydrogel delivery on hASC retention, and to semi-quantitatively measure intramuscular blood vessel density and cell proliferation as markers of a regenerative response.

5.2 Materials and methods

5.2.1 Materials

PEG_{20}-$(PTMC_2$-$A)_2$, referred to as PEG-$(PTMC$-$A)_2$ in this chapter, and MGC-RGD were prepared and characterized as described in Chapter 3. Phosphate buffered saline pH 7.4, the Click-iT® EdU imaging kit, and Cryomatrix frozen embedding resin were obtained from Thermo Fisher Scientific. Mouse anti-human HLA-ABC (cat. 555551) and rat anti-mouse CD31 (cat. 550274) primary antibodies were obtained from BD Biosciences. Goat anti-mouse IgG Alexa Fluor® 488 (cat. ab150113), and goat anti-rat Alexa Fluor® 488 (cat. ab150157) were obtained from Abcam. A mouse-on-mouse blocking kit was obtained from Vectors Labs. Unless specified, all other reagents were obtained from Sigma Aldrich Ltd.

5.2.2 Isolation, culture, and immunophenotyping of hASCs

Human research ethics board approval for this study was obtained from the Health Science Research Ethics Board at The University of Western Ontario (REB#105436, Appendix A.3). Primary hASCs were isolated from freshly excised adipose tissue samples obtained from a female patient (age 47 years; BMI 30.6 kg/m^2) undergoing elective breast reduction surgery. hASCs were expanded on TCPS under standard culture conditions (37 °C, 5% CO_2 in air) in complete medium (DMEM:Ham's F12 medium supplemented with 10% fetal bovine serum, 100 U/mL penicillin, and 0.1 mg/mL streptomycin) replaced every 2-3 days. Upon reaching 80% confluence, hASCs were trypsin-released, washed, counted, and re-

plated at 5000 cells/cm^2. Immediately prior to use, the immunophenotype of passage 2 hASCs was confirmed as previously described in Chapter 3.

5.2.3 Induction of hindlimb ischemia in mice

All animal protocols were approved by the University Animal Care Committee at The University of Western Ontario in accordance with the policies established by the Canadian Council on Animal Care (AUP# 2006-126-12). All animal handling procedures were performed by Stephen Sherman and Tyler Cooper of Dr. David Hess' lab, with my assistance. Ischemia was induced in the right hindlimb of NOD/SCID mice (Jackson Laboratory, Bar Harbor, ME, jax.org). A simplified schematic of the hindlimb arterial anatomy (adapted from Kochi, *et al*.[230]) with the ligation site indicated is presented in Figure 5-1. Initial anesthesia was induced by intraperitoneal injection of ketamine hydrochloride (60-70 mg/kg) and xylazine (2-4 mg/kg), then maintained by inhaled isoflurane for the remainder of the procedure. Anesthetized mice were maintained on a heated pad at 37 °C. A longitudinal incision from the inguinal crease to the midpoint of the thigh was made along the path of the femoral artery. The subcutaneous fat and the superficial caudal epigastric artery were cauterized to expose the femoral neurovascular bundle. The femoral nerve was carefully separated from the artery and vein. Silk sutures were threaded beneath the femoral artery and vein, as indicated in Figure 5-1, and ligated using double surgical knots. Collateral vessels between the ligation points were cauterized, and the ligated segment of the femoral artery and vein was surgically resected. The skin incision was closed with silk sutures, and the mice were monitored during recovery from anesthesia to ensure they retained use of the operated limb.

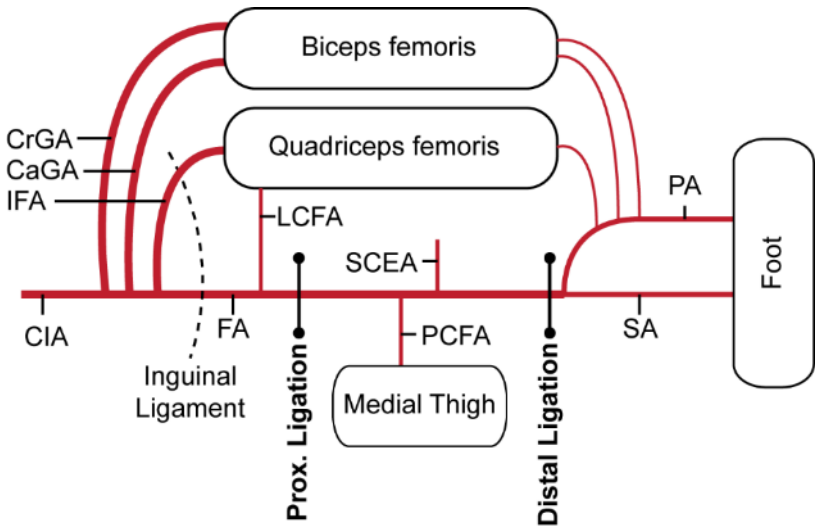

Figure 5-1: Simplified schematic of hindlimb arterial anatomy. Proximal and distal ligation sites of the femoral artery and vein indicated with black lines. CaGA: caudal gluteal artery; CIA: common iliac artery; CrGA: cranial gluteal artery; FA: femoral artery; IFA: internal femoral artery; LCFA: lateral circumflex femoral artery; PA: popliteal artery; PCFA: proximal caudal femoral artery; SA: saphenous artery; SCEA: superficial caudal epigastric artery. Note: For the sake of clarity, only arteries are shown (veins omitted), and not all collateral vessels are illustrated. Adapted from Kochi, *et al*.[230]

5.2.4 Intramuscular delivery of hASCs to an ischemic hindlimb

24 h after surgery, each mouse (N = 8 per treatment group) received one of four treatments:

A) hASCs + gel: 2×10^7 hASCs/mL in mixed polymer (4% w/v PEG-$(PTMC\text{-}A)_2$ + 1% w/v MGC-RGD)

B) Gel alone: Mixed polymer alone

C) hASCs alone: 2×10^7 hASCs/mL in saline

D) Saline

Each mouse, maintained under isoflurane anesthesia, received a single 20 µL intramuscular injection to the adductor muscle at the distal end of the ligation via a Hamilton Gastight syringe with a 25G 5/8” BD needle. Cell and material preparation and crosslinking initiation were performed as described previously for delivery to the rat model (Chapter 4, Section 4.2.4). The mouse was maintained under anesthesia for 10 minutes after injection to prevent dispersal of the cells or polymer.

5.2.5 Laser Doppler perfusion imaging assessment of limb perfusion

Limb perfusion was assessed by laser Doppler perfusion imaging (LDPI) immediately after ligation and at 7, 14, 21, and 28 days post treatment (N = 8 mice per group). Before each measurement, the mice were anesthetized with isoflurane, hair was removed from the hindlimbs using Nair™ hair removal cream, and the mice were warmed at 37 °C on a heated pad for 5 minutes. The mice, maintained under isoflurane anesthesia, were placed in a supine position under a MoorLDI-2 laser Doppler imaging system (Moor Instruments), and flux of moving blood particles was measured in the hindlimbs. The averaged flux in the ischemic and contralateral control limbs was quantified within a region of interest extending from the ankle joint to the distal extremity of the foot (MoorLDI software v6.0). A perfusion ratio (PR) was calculated as a ratio between the average flux in the ischemic and control limbs. The PR measured immediately after ligation was used to confirm the onset of severe limb ischemia.[229]

5.2.6 Gait analysis

Hindlimb function was quantified using a CatWalk™ gait analysis system and software (CatWalk v7.1, Noldus) at 28 days post treatment (N = 4 mice per treatment group). Three traverses of the CatWalk stage were recorded per mouse. Hindlimb function was quantified by calculating the ratio between the ischemic and control hindlimbs of hind paw print area, print intensity, and stand time per step cycle.

5.2.7 Immunohistochemical assessment of hASC retention, endothelial cell recruitment, and cell proliferation

The mice were euthanized at 28 days after treatment. 24 h prior to euthanasia, the mice were given a 100 µL intraperitoneal injection of a 10 mM solution of 5-ethynyl-2'-deoxyuridine (EdU) in saline to label proliferating cells, as previously described.[229] The skin covering the hindlimbs was removed, and the entire thigh muscle was carefully excised, embedded in Cryomatrix, and frozen (N = 6 mice per group). Tissue was cryo-sectioned perpendicular to the muscle fiber orientation at 5 µm thickness. Sections were fixed in 4% paraformaldehyde for 15 min and rinsed with PBS. Negative primary controls were included for each stain, following the exact same staining procedure, but without primary antibodies added to the dilution buffer for incubation (see Appendix A.4). To facilitate assessment of cell retention in the hydrogels, hASCs

were encapsulated in the mixed hydrogel at 2×10^7 hASCs/mL and cultured *in vitro* as previously described (Chapter 3, Section 3.2.12) under normoxic conditions for 7 days. These hydrogels were embedded in Cryomatrix and frozen for immunohistochemical analysis to compare with the hASC density in the hydrogels recovered from the explanted hindlimbs.

For the detection of hASCs, sections were blocked with mouse-on-mouse (MoM) reagent, and stained with primary mouse anti-human HLA-ABC (5 μg/mL in MoM diluent, 30 min at room temperature (RT)) and secondary goat anti-mouse IgG Alexa Fluor® 488 (10 μg/mL in MoM diluent, 30 min at RT). The *in vitro* control hydrogels with hASCs were similarly processed. For the detection of endothelial cells, sections were blocked with 5% goat serum in tris-buffered saline with 0.2% Tween-20 (TBS-T), and stained with primary rat anti-mouse CD31 (1 μg/mL in TBS-T, overnight at 4 °C) and secondary goat anti-rat IgG Alexa Fluor® 488 (8 μg/mL in TBS-T, 1 h at RT). Proliferating EdU^+ cells were labelled on the same sections using a Click-iT® EdU Alexa Fluor® 555 imaging kit according to the manufacturer's instructions.

All sections were imaged on a Zeiss Axio Imager M1 microscope. The density of HLA-ABC^+ hASCs was calculated as cells per hydrogel area from three sections per mouse. The density of hASCs in the *in vitro* cultured hydrogels was similarly assessed. $CD31^+$ cells and EdU^+ cells were counted in at least ten photomicrographic fields (0.710 mm × 0.532 mm) from three sections per mouse, taken at evenly-spaced intervals over the length of each muscle section.

5.2.8 Statistical analysis

All data are presented as the mean ± SD, with the exception of the figure of perfusion ratio (Figure 5-2b), which was expressed as mean ± standard error of mean for the sake of figure clarity. Comparisons made at a single end point (gait and IHC analysis) were made by one-way ANOVA with Tukey's multiple comparisons test to compare all group means. Perfusion ratios over time were compared by two-way ANOVA with Tukey's multiple comparisons test to compare all group means at a single time point. Statistical analysis was performed using GraphPad Prism 7.

5.3 Results

5.3.1 Immunophenotype of hASC used for *in vivo* transplantation

Passage 2 hASCs used for delivery to the ischemic hindlimb exhibited the expected positive and negative expression of surface markers (Table 5-1), confirming that the cells had a stromal cell phenotype.

Table 5-1: Immunophenotype of pooled hASCs used for *in vivo* transplantation. Percent of cells positive for each marker is presented as the average ± SD from n = 3 repeated measurements from passage 2 hASCs from one donor.

Surface Marker	Expected phenotype[163,164]	Percent positive
CD90	>80%	100.00 ± 0.00
CD29	>80%	96.91 ± 0.58
CD44	>80%	99.90 ± 0.04
CD105	>80%	96.93 ± 0.28
CD73	>80%	90.96 ± 0.56
CD34	Variable	1.23 ± 0.15
CD146	Variable	1.48 ± 0.18
CD31	<2%	0.88 ± 0.15
CD45	<2%	1.70 ± 0.09

5.3.2 Hindlimb perfusion determination by laser Doppler perfusion imaging

Hindlimb perfusion was monitored over 28 days by LDPI (Figure 5-2a). The onset of severe acute hindlimb ischemia was confirmed by post-operative PR values of approximately 0.1. No significant differences in average PR between treatment groups were detected until day 28 (Figure 5-2b), at which time the PR of the gel alone group was significantly higher than the ASCs alone group (0.55 ± 0.26 vs. 0.31 ± 0.12, $p = 0.011$; two-way ANOVA with Tukey's correction for multiple comparisons). Notably, the standard deviation in PR measurements at day 28 was higher for the hydrogel treatment groups (±0.216 and ±0.257 for hASC + gel and gel alone, respectively) compared to the groups treated without gels (±0.119 and ±0.102 for hASC alone and saline, respectively).

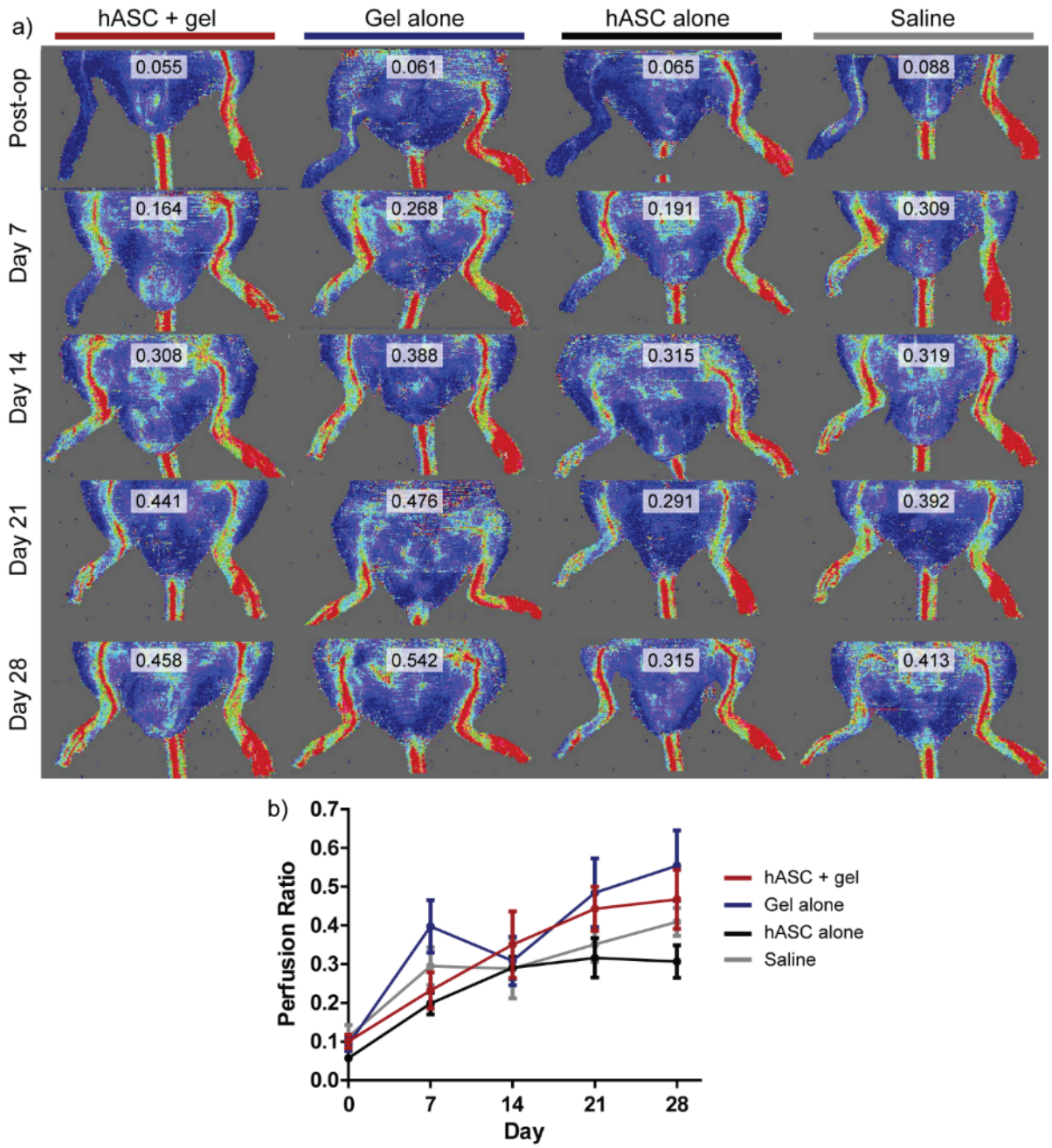

Figure 5-2: Limb perfusion measured by LDPI. a) Representative flux images (ventral view) with PR overlay. Flux is represented by a colour gradient from blue (low flux) to red (high flux). b) Perfusion ratio between the ligated and contralateral control limbs over time (N = 8 mice per group, mean ± SEM).

5.3.3 Hindlimb function determination by gait analysis

The function of the ischemic hindlimb was determined relative to the contralateral control limb using a CatWalk™ gait analysis system. A representative image of the paw prints during a transverse of the stage (left to right) is show in Figure 5-3a. Quantification of the ratio (ischemic/control) of the hind paw

print intensity (an indirect measure of pressure, Figure 5-3b), the hind paw print area (Figure 5-3c), and the hind paw stand time (Figure 5-3d) indicated no significant differences in limb function between the treatment groups. In all three metrics, the ratios were less than 1, indicating reduced ischemic limb function at 28 days post treatment.

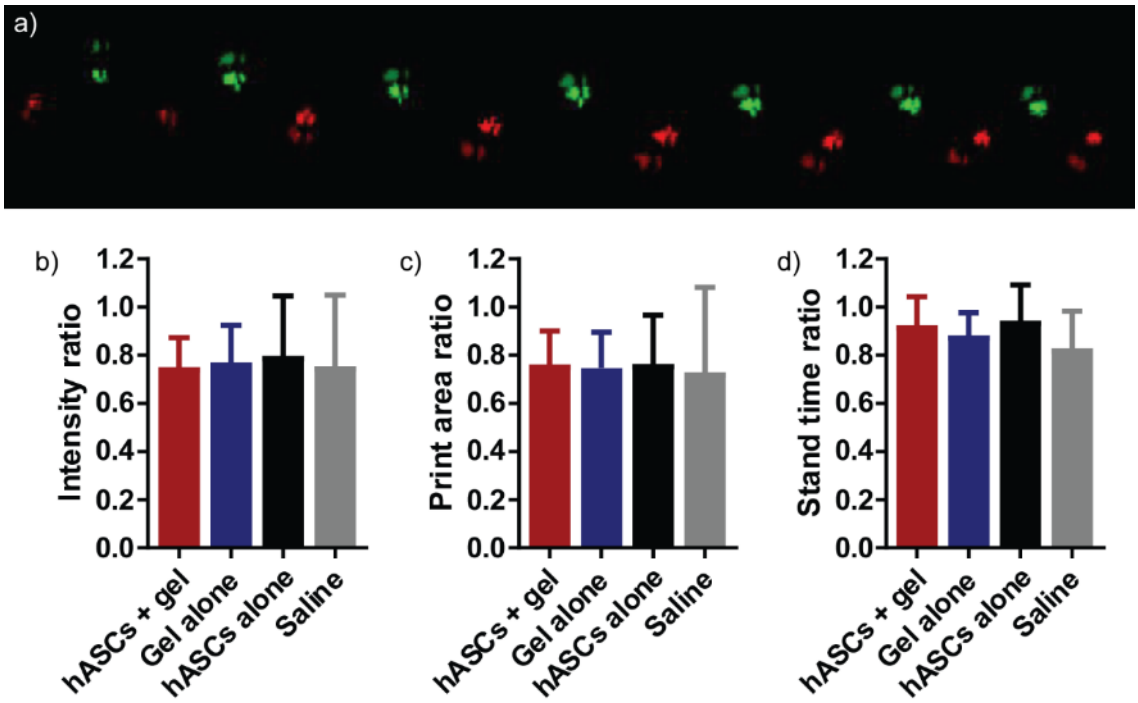

Figure 5-3: Gait analysis of hindlimb function. a) A representative image of paw prints during a transverse (left to right) of the CatWalk™ stage from a mouse treated with hASC + gel (light green: right/front; dark green: right/hind; light red: left/front; dark red: left/hind). The ratio of b) print intensity, c) print area, and d) stand time of the ischemic hind paw relative to the contralateral control hind paw, as determined by CatWalk™ gait analysis (N = 4, mean ± SD).

5.3.4 hASC retention within intramuscular hydrogels

hASCs were identified by HLA-ABC staining only within the hydrogels of the hASCs + gel group (Figure 5-4a), but not in the surrounding tissues or in limbs injected with hASCs in saline (hASCs alone). Further, compared to the control gels cultured *in vitro* (Figure 5-4b), the hASC density in the intramuscular hydrogels was not significantly different (Figure 5-4c), suggesting that the cells were well retained after 28 days of active muscle use *in vivo*.

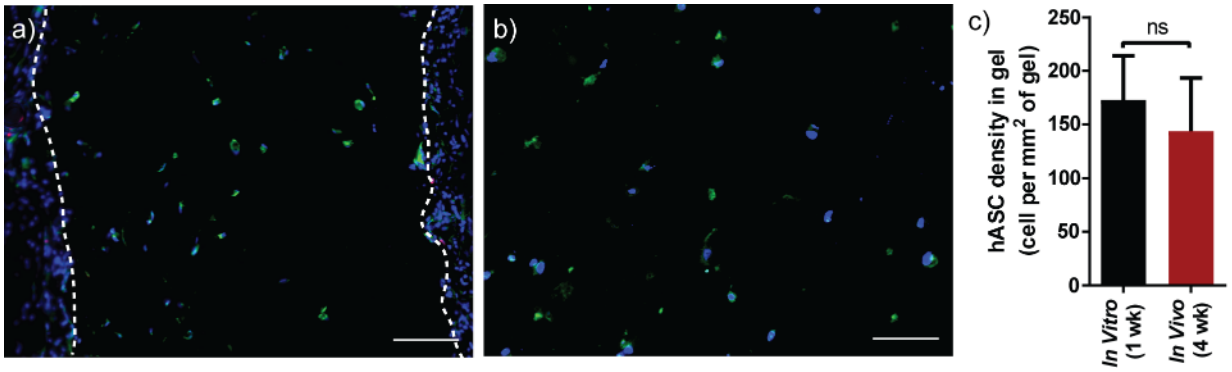

Figure 5-4: hASC retention within intramuscular hydrogels. Representative images of a) hASC + gel explanted 28 days after intramuscular injection into the adductor muscle in an ischemic mouse hindlimb (gel border indicated by dashed lines), and b) control hydrogels with hASCs cultured *in vitro* for 7 days. HLA-ABC$^+$ (green); DAPI$^+$ nuclei (blue). Scale bars = 100 µm. c) Average HLA-ABC$^+$ cell density within the hydrogels (N = 5 hydrogels, mean ± SD); difference between groups was determined by an unpaired t test ($p = 0.53$).

5.3.5 Intramuscular endothelial cell recruitment and cell proliferation

The intramuscular capillary density, as measured by CD31$^+$ cell density, in the hASCs + gel treatment group was significantly higher than all other treatment groups, and not significantly different from the non-ischemic control limbs (Figure 5-5a-f). CD31$^+$ density in the hASCs alone group was intermediate: not significantly lower than the non-ischemic controls and significantly higher than the limbs treated only with saline. In contrast, the CD31$^+$ density in the gel alone and saline groups were both significantly lower than the non-ischemic controls.

The frequency of proliferative cells in the muscle tissue, measured by EdU incorporation, was significantly higher in the limbs treated with hASCs + gel compared to all other treatment types, and was equivalent to the non-ischemic controls (Figure 5-6a-e). While intramuscular CD31$^+$ EdU$^+$ cells were detected in all limbs, a significantly higher density was observed in limbs treated with hASCs + gel compared to those treated with gel alone or saline (Figure 5-6f); however, the fraction of CD31$^+$ cells that were proliferative was equivalent between groups (Figure 5-6g) No HLA-ABC$^+$ EdU$^+$ cells were detected in the intramuscular hydrogels, indicating that the hASCs were not proliferating at the time of explantation.

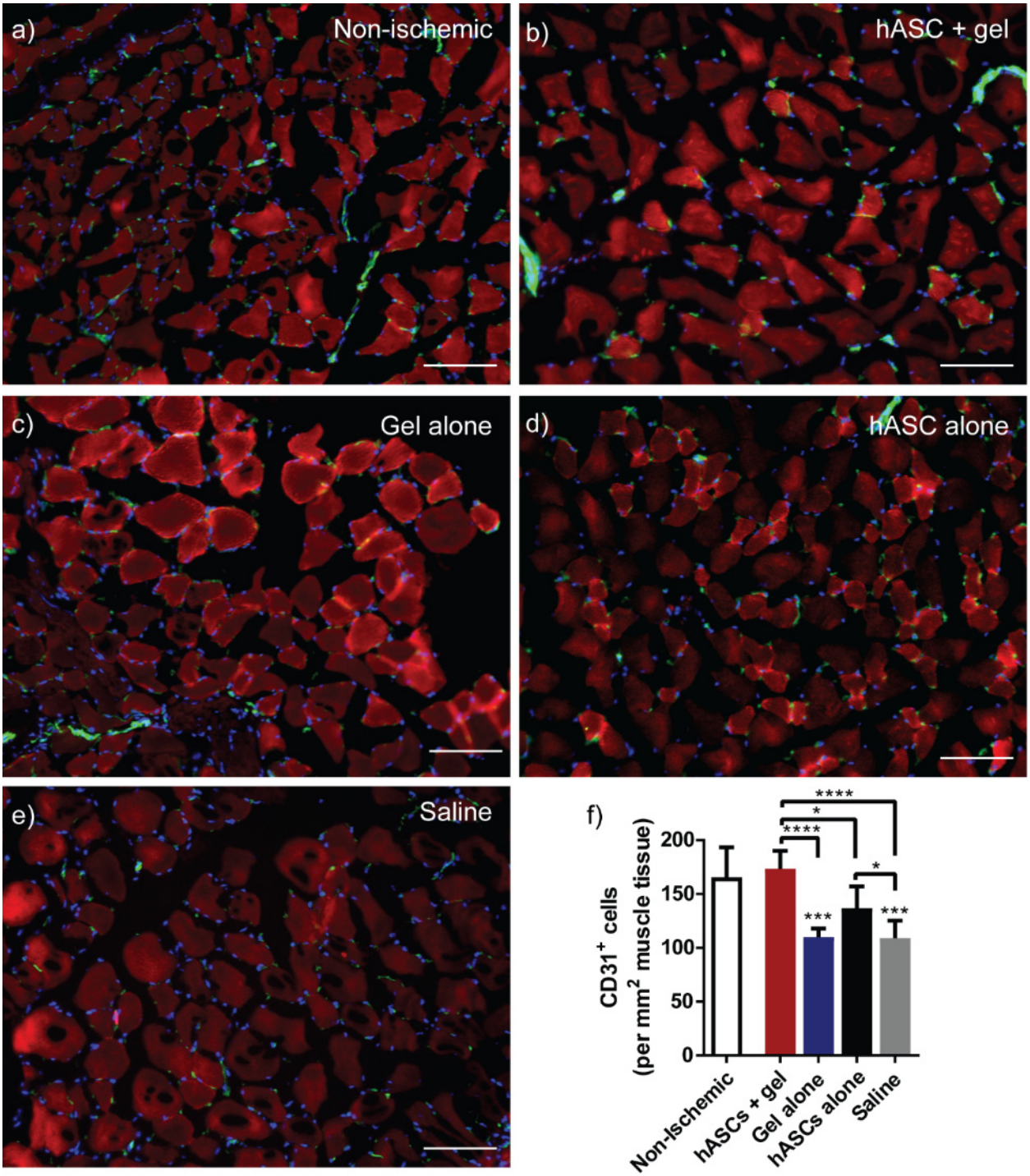

Figure 5-5: Intramuscular CD31$^+$ cell density. Representative images of thigh muscles: CD31$^+$ endothelial cells (green), DAPI$^+$ nuclei (blue), and muscle fascicle autofluorescence (red), from a) non-ischemic, untreated control limb; and ischemic limbs treated with b) hASCs + gel; c) gel alone; d) hASCs alone; e) saline. Scale bars = 100 µm. f) Intramuscular CD31$^+$ cell density (N = 6 mice, mean ± SD). Differences between groups were determined by one-way ANOVA with Tukey's correction for multiple comparisons; differences between treatments and the non-ischemic control are indicated above each treatment group when significant; differences between specific groups are also indicated with bars (* $p<0.05$; *** $p<0.001$; **** $p<0.0001$).

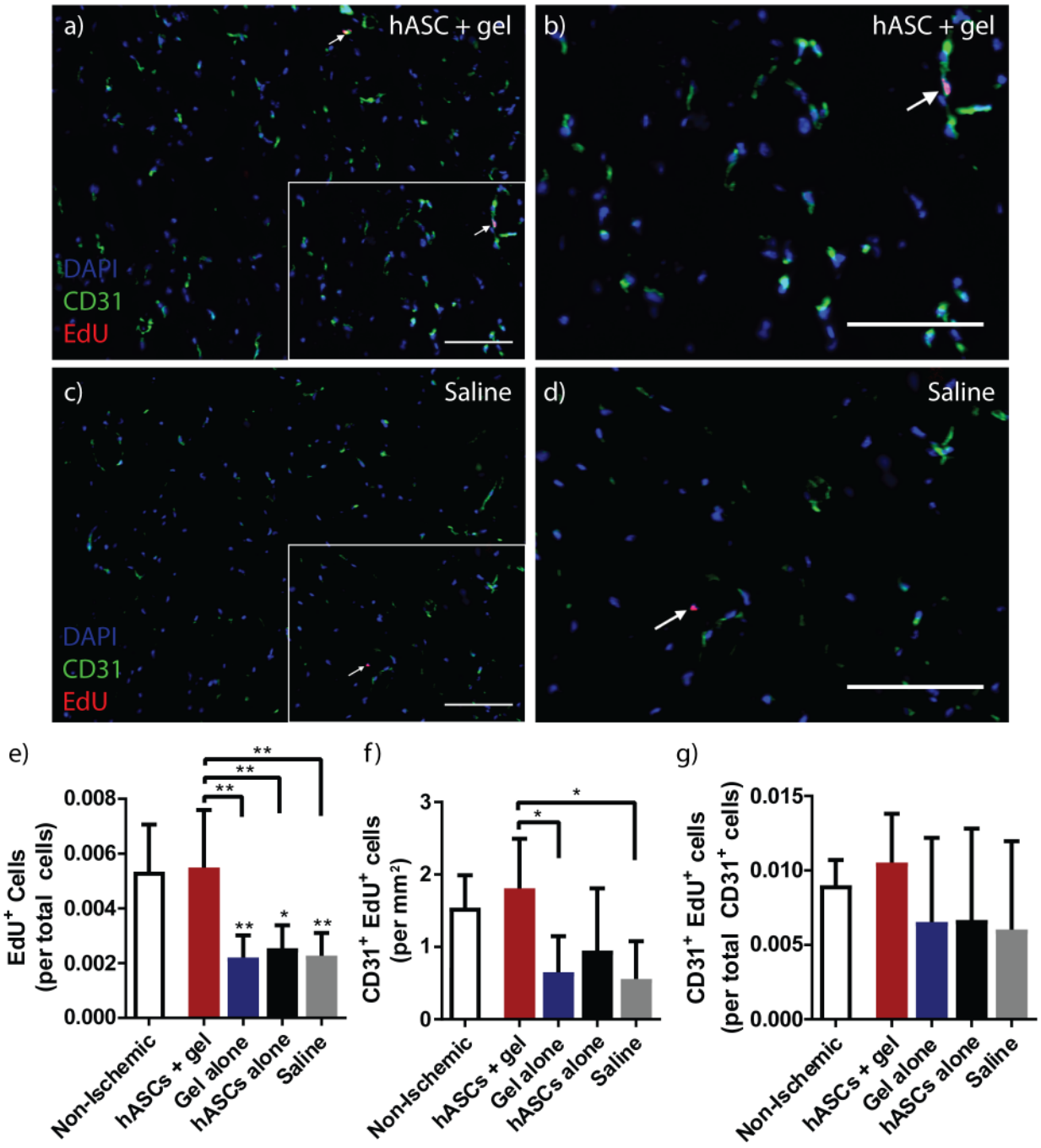

Figure 5-6: Intramuscular EdU$^+$ cell density. Representative images of thigh muscles: CD31$^+$ endothelial cells (green), EdU$^+$ nuclei (red), DAPI$^+$ nuclei (blue) from ischemic limbs treated with a) hASCs + gel (detail in b) and c) saline (detail in d). Scale bars = 100 µm; EdU$^+$ cells indicated with arrows; area of detail indicated with white box. e) EdU$^+$ cell nuclei per total nuclei, f) CD31$^+$ EdU$^+$ cells per mm^2, g) CD31$^+$ EdU$^+$ cells per total CD31$^+$ cells (N = 6 mice, mean ± SD). Differences between groups were determined by one-way ANOVA with Tukey's correction for multiple comparisons; differences between treatments and the non-ischemic control are indicated above each treatment group when significant; differences between specific groups are also indicated with bars (* $p<0.05$; ** $p<0.01$).

5.4 Discussion

Despite the promise of MSC transplantation therapy as a treatment of ischemic cardiovascular disease, maintaining cell retention and survival following injection remains a challenge. In the current work using a NOD/SCID mouse model of hindlimb ischemia, the use of an injectable hydrogel scaffold of MGC-RGD and PEG-$(PTMC\text{-}A)_2$ significantly improved hASC retention, with hASCs detected by IHC after 28 days at a density equivalent to their original seeding density. This level of intramuscular retention marks an improvement over previous delivery strategies, such as MSC-seeded collagen scaffolds implanted in an ischemic hindlimb (3.4% ± 2.7% retention after 8 weeks by IHC)[231]; subcutaneous injections of ASCs in a peptide-based hydrogel (less than 5% of their original density after 14 days by bioluminescent imaging)[232]; and intramuscular injections of MSCs in chitosan- and alginate-based hydrogels to the ischemic heart (50-62% of their original density after 24 h by bioluminescent imaging).[233] Consistent with studies that have demonstrated that less than 10% of cells delivered by IM injection in saline to ischemic muscle remain after 24 h,[20,105,228,233] hASCs delivered in saline were not detected in the ischemic hindlimbs at 28 days.

The improved retention of hydrogel-delivered hASCs corresponded to a significantly increased density of intramuscular capillaries and a higher frequency of proliferative cells compared to all other treatments. In addition, the hydrogel-delivered hASCs resulted in a significantly higher density of proliferative $CD31^+$ cells compared to the gel alone and saline treatments. Together, these results indicate the induction of vascular recovery in the ischemic limbs treated with hASCs + gel. The observation that the frequency of proliferative $CD31^+$ cells per total $CD31^+$ cells was equivalent between groups suggests that enhanced endothelial cell proliferation may have occurred prior to the 28 day end point. This finding supports other studies of HI recovery, which found increases to capillary density occurred within the first 7 days of vascular recovery, with little change in capillary density over the following 21 days.[229] The delivery of the scaffold alone had no effect on endogenous cell proliferation or $CD31^+$ cell density, indicating that the encapsulated hASCs were responsible for the differences in vascular density. Furthermore, few hASCs were observed outside the scaffold after implantation, suggesting that prolonged

localization of the encapsulated hASCs enhanced their ability to increase cell proliferation and support angiogenesis via paracrine factor release. Future work could assess changes in IM capillary density and endothelial cell proliferation at earlier time points to better understand the progression of vascular recovery over time.

While the delivery of hASCs in saline significantly increased capillary density compared to control treatments with saline alone, consistent with the findings of Kondo *et al.*[12] and Miranville *et al.*,[80] the effects were further and significantly enhanced by using the injectable scaffold. This result supports the hindlimb ischemia studies of Suuronen *et al.*,[104] and Tang *et al.*,[105] who found that the improved retention of cells delivered in collagen and hyaluronan, respectively, resulted in enhanced capillary density. However, this work contrasts with the work of Xu *et al.*,[223] who found no significant improvements in capillary density when MSCs were delivered in an injectable poly(*N*-isopropylacrylamide)-based hydrogel, unless basic fibroblast growth factor was co-delivered. This variability in the response suggests that the paracrine effects of injected encapsulated cells may vary depending on the nature of the hydrogel used for delivery.

An important limitation to consider in the interpretation of these results is that the identification of capillaries by CD31 staining does not indicate if the vessels are part of a functional, perfused network. Future work could identify perfused vessels by intravenous injection immediately prior to euthanasia with Evans Blue dye[234] or labeled lectins[235,236] in order to discriminate between nascent, non-perfused vessels and functional vasculature. Furthermore, mature vessels could be identified by co-staining for α-smooth muscle actin.[237]

As measured by LDPI, the recovery of hindlimb perfusion for mice treated with saline followed the expected profile based on previous studies using the same model,[228,229] indicating that the ischemia model was successfully implemented. However, no significant improvements to limb perfusion were achieved with any of the treatments relative to the saline-treated controls. The delivery of 4×10^5 hASCs in saline was expected to result in improvement to the PR, based on previous studies using ASCs. Early work by Moon *et al.*[13] demonstrated that the IM injection of 1×10^5 hASCs to a hindlimb ischemia model in

BALB/c nude mice resulted in significantly improved PR compared to saline (approximately 2-fold greater) after 14 days. Similarly, Kondo *et al*.[12] demonstrated that the IM injection of 1×10^6 allogeneic mouse ASCs to a hindlimb ischemia model in immune competent C57BL/6J mice resulted in significantly improved PR after 14 and 21 days (approximately 1.5- and 1.2-fold improvements, respectively).

By day 28, there was a greater variability in the PR of the groups treated with the hydrogel (with or without hASCs), compared to the groups treated with saline (with or without hASCs). This trend may indicate that the outcome of gel-based treatments was sensitive to factors that would not influence saline-based treatments, such as the location and distribution of the gel in the IM space relative to the site of ligation. In the current work, the gel was administered by a single IM injection near the distal end of the ligation surgery site, thus any discrepancies in that single injection location may have affected the efficacy of the treatment. Future studies could investigate dividing the delivery into multiple smaller injections to reduce the impact of gel placement.

Gait analysis indicated that no statistically significant differences in limb function existed between treatment groups after 28 days, as measured by paw print intensity, area, or stand time. However, previous work with this mouse model by Putman *et al*.[229] found that functional improvements were only detected at earlier time points (7 days post treatment), and that by 28 days, limb use was equivalent even between groups with significantly different recovery of perfusion. In the current study, gait analysis could only be performed at the terminal endpoint due to technical limitations with the CatWalk™ system being only available outside of the barrier suite used to house immunocompromised NOD/SCID mice; however, future studies could be designed to include a time course assessment of limb usage following treatment with ASCs.

Despite the enhanced local intramuscular effects of improved capillary density and cell proliferation detected by IHC for limbs treated with hASCs + gel, these differences were not reflected in improvements to limb perfusion or function. Several factors may have contributed to the lack of recovery of perfusion and limb use observed in the current study. As noted previously, additional staining procedures would be required to confirm if the observed capillaries are part of a functional network. Additionally,

previous work has demonstrated variability in ASC activity due to differences in donor age, gender, body mass index, and insulin sensitivity.[162,238,239] As this work used hASCs derived from one donor, the results are highly dependent on the angiogenic potential of that single source, and may not reflect the potential of ASCs in general. Therefore, it would be recommended that any future studies be extended to include multiple cell donors.

Furthermore, the use of the NOD/SCID mouse is a limitation of the current study, as the NOD mutation causes defects in the development of macrophages from hematopoietic precursors, resulting in weak functional macrophage responses.[240] As macrophages are highly involved in angiogenesis, especially in inflammatory environments and in response to biomaterials,[115,121] the defective macrophages may have influenced the angiogenic response to hASCs and the hydrogel. As demonstrated in Chapter 4 with an immune competent outbred rat model, the intramuscular delivery of the hydrogel elicited a substantial M1 macrophage response, and allogeneic ASCs significantly increased macrophage recruitment and promoted a transition to an alternatively activated M2 phenotype. Both M1 and M2 macrophages are involved in the angiogenic process, particularly in response to biomaterials, by directing endothelial cell migration and vessel anastomosis and stabilization.[115,121] Thus, despite ASCs improving endothelial cell density in the current NOD/SCID model, it is possible that the defective nature of the macrophages may have inhibited the nascent vessels from forming a stable, perfused network capable of significantly improving limb perfusion. This finding suggests that both the inflammatory response to the implanted hydrogel and the modification of that response by encapsulated ASCs may be involved in promoting an angiogenic response.

The failure of ASCs to improve ischemic limb perfusion in the current study is in contrast to previous studies using hASCs in less immunocompromised athymic nude mouse models[13,80,241] or allogeneic ASCs in an immune competent mouse model,[12] which found significant improvements to perfusion. However, the strains used in these studies retain functional macrophages, further suggesting that the immunomodulatory effects of ASCs may be a critical aspect to their therapeutic effects in the ischemic environment. Future studies using a mouse strain that retains normal macrophage numbers and functions

but still permits xenotransplantation, such as a BALB/c SCID or athymic nude mouse strain, may provide a more complete model for studying the immunomodulatory effects of hASCs in an ischemic environment. However, these models would present a risk for the eventual rejection of the xenogeneic hASCs, which may or may not affect their ability to promote angiogenesis via paracrine signaling over 28 days. Ideally, the use of a humanized mouse model in which an immunodeficient mouse strain has been engrafted with, or genetically altered to express, components of a human immune system[242] would allow for the study of the immunomodulatory affects of hASC in a xenotransplantation model. Specifically, a humanized mouse strain that supports the development of functional macrophages[243] would provide insight into the potential for hASCs to modulate the response of human macrophages. Alternatively, the use of allogeneic mouse ASCs in an immunocompetent mouse model could also provide insight into the role of ASCs in the inflammatory ischemic environment; however, the insight into potential clinical applications from this approach would be limited due to the non-human cell source.[244]

5.5 Conclusions

Cell retention following intramuscular injection remains a major hurdle in the implementation of cell-based therapies of peripheral arterial disease. In the current work, the use of an injectable hydrogel scaffold of MGC-RGD and PEG-$(PTMC\text{-}A)_2$ improved the retention of hASCs delivered to a mouse model of hindlimb ischemia. The improved retention of hASCs was associated with local improvements to intramuscular cell proliferation and capillary density; however, these improvements were not associated with changes in limb perfusion or function relative to the controls. The immunocompromised nature of the host NOD/SCID mouse strain may have limited the treatment efficacy, as there is a growing body of evidence to support that the immunomodulatory capacity of ASCs may be an important mechanism in mediating their therapeutic potential. Future studies using hASCs from multiple donors in a less immunocompromised mouse host or allogeneic ASCs in an immune competent mouse host may provide a better model incorporating a more complete host inflammatory response to test the therapeutic efficacy of ASCs and the hydrogel delivery strategy. Overall, however, these findings are a promising indication that

the hydrogel-based delivery strategy can improve cell localization, retention, and survival in an ischemic, mechanically dynamic intramuscular environment. Further, the results support the previous findings that the encapsulated cells can produce local, paracrine-mediated therapeutic benefits.

Chapter 6

Significance and recommendations

6.1 Development of a mechanically robust, injectable hydrogel system for cell delivery

By forming a cell-encapsulating scaffold upon delivery, injectable *in situ*-forming hydrogels have the potential to overcome the poor rates of cell retention and survival that have limited the efficacy of mesenchymal stem/stromal cell (MSC) transplantation therapies. However, the weak, brittle nature of many cell-encapsulating hydrogels limits their utility in load-bearing or mechanically dynamic applications. In the current work, a library of poly(trimethylene carbonate)-*b*-poly(ethylene glycol)-*b*-poly(trimethylene carbonate) diacrylate (PEG-(PTMC-A)$_2$) prepolymers was developed and used to improve the strain resilience and modulate the stiffness of an otherwise-brittle cell-encapsulating *N*-methacrylated glycol chitosan (MGC) network. This strategy of network reinforcement could be applied broadly to a number of cell-encapsulating hydrogels to expand their application to include cell delivery to a variety of load-bearing tissues. Furthermore, the current study demonstrated that the release of paracrine factors from adipose-derived stem/stromal cells (ASCs) encapsulated in the mixed polymer hydrogel was maintained, or even enhanced, in comparison to ASCs cultured on tissue culture polystyrene (TCPS). As paracrine signaling is a critical component of MSC-based therapies, this finding has significant implications for all therapeutic strategies relying on paracrine signaling from encapsulated cells, suggesting that encapsulated MSCs can be employed as "paracrine factories". In addition, the results indicated that encapsulated MSCs may have a different secretory profile than TCPS-cultured MSCs.

Although PEG-(PTMC-A)$_2$ was demonstrated here to reduce the stiffness and brittleness of MGC hydrogels, future work should investigate the specific network structure in the mixed hydrogels that gives rise to these properties. Currently, it is unclear to what extent the two components are co-crosslinked. Several factors may be contributing to the formation of two distinct interpenetrating networks. Acrylate groups have been shown to undergo radical polymerization with a significantly higher propagation rate

constant than methacrylates,[245] suggesting that a PEG-(PTMC-A)$_2$ network may form prior to, and independently from, the MGC network. Furthermore, similar acrylated copolymers of PEG and PTMC have been shown to form nanoparticles when crosslinked in dilute aqueous solution,[246] suggesting the amphiphilic nature of PEG-(PTMC-A)$_2$ results in the aggregation of PTMC blocks in solution. When mixed with MGC, this behavior could promote the formation of a distinct PEG-(PTMC-A)$_2$ network. Future work could investigate the degree co-crosslinking in the combined MGC + PEG-(PTMC-A)$_2$ network by enzymatically degrading one component of the network (*e.g.*: degrade MGC with chitinase[247] or PTMC with cholesterol esterase[248]), and measuring the retention of the non-degraded component.

To better quantify the cytotoxic effects of exposure to APS/TEMED initiation, future work could assay the cytotoxicity of cell culture media used to extract the soluble reactants following crosslinking. This would additionally indicate potential toxicity of the crosslinking process to surrounding tissue when the system is crosslinked *in vivo*. Furthermore, towards optimizing the release of cytokines from hASCs encapsulated within the mixed hydrogel scaffold, future work could investigate the effects of cell density, and more specifically, cell-cell contact on paracrine factor release. Recent work has demonstrated that paracrine factor secretion from mesenchymal stem/stromal cells (MSCs) is enhanced by N-cadherin mediated cell-cell contact.[249] Thus, below a certain seeding density, this contact may be inhibited by the hydrogel network surrounding each individual cell, potentially reducing the paracrine activity of the encapsulated MSCs. Future work could explore the effects on MSC paracrine secretions of increasing the seeding density to promote cell-cell contact or simulating cell-cell contact by grafting an N-cadherin peptide motif to the polymers of the hydrogel. Finally, the effects of the hydrogel dimensions on cell survival and cytokine release could be explored by forming the hydrogels in different shapes *in vitro* (*i.e.* with higher and lower surface area to volume ratios). By affecting the diffusional path length for nutrients, oxygen, waste, and released cytokines, such changes to the hydrogel dimensions could result in significantly different levels of ASC survival and cytokine release. Further, the *in vitro* results from thinner, flatter hydrogels may more accurately represent the *in vivo* IM distribution of the hydrogel. By increasing or

decreasing the crosslinking time by varying the APS/TEMED concentration, it may be possible to respectively increase or decrease the spreading of the hydrogel following IM injection. Increasing the spreading of the hydrogel may have beneficial effects in terms of distributing cells intramuscularly and increasing the region of local cytokine release; however, increasing spreading too much may result in dissemination of the hydrogel and ASCs from the target tissue.

6.2 Immunological and angiogenic response to the intramuscular injection of adipose-derived stem/stromal cells in a hydrogel scaffold

The feasibility of delivering ASCs using the combined PEG-$(PTMC\text{-}A)_2$ MGC-RGD hydrogel and the ammonium persulfate/tetramethylethylenediamine radical initiator system *in vivo* was demonstrated by delivering allogeneic rat ASCs (rASCs) intramuscularly in a healthy rat model. The scaffold itself, and encapsulated rASCs, were well retained in the intramuscular space over 4 weeks of active use, suggesting that the delivery strategy could be more broadly applied to other mechanically dynamic tissues. Furthermore, this work contributed to the understanding of ASCs as modulators of the inflammatory response, demonstrating that encapsulated ASCs can promote the recruitment and regenerative polarization of macrophages responding to a biomaterial implant. These immunomodulatory effects were associated with enhanced angiogenesis, including evidence of scaffold vascularization. These findings have significant implications for tissue regenerative strategies more broadly, indicating that MSCs can be used to alter the host inflammatory response to implanted biomaterials, direct regenerative responses from macrophages, and impact implant remodeling and integration.

In order to translate such a polymer hydrogel into a clinical setting, more rigorous sterilization procedures would be required. While UV exposure used in the current work superficially disinfects the material, future work should explore more rigorous methods such as sterile filtration of the prepolymer solution. To allow for the quantitative assessment of donor cell retention and distribution, future work could use rASCs derived from a transgenic rat donor expressing firefly luciferase. Combined with an *in vivo* bioluminescence imaging system capable of detecting photon flux, this strategy would allow for the semi-

quantitative assessment of donor rASCs at the delivery site over time, as well as the possible distribution of ASCs to other tissues and organs.[250] Future work could also explore the contribution of each hydrogel component, MGC-RGD and PEG-(PTMC-A)$_2$, to the inflammatory response. Specifically, *in vitro* assays could be used to assess each component's susceptibility to enzymes and reactive oxygen species produced by macrophages, and hydrogels of varying compositions could be cultured with macrophages to assess adhesion, activation, and infiltration. Past studies have demonstrated that RGD ligands affect the *in vivo* inflammatory response,[199] and that the presence of PTMC in PEG-based enhances macrophage infiltration.[147] The results of this work may be used to produce hydrogels with controlled rates of macrophage-mediated degradation.

6.3 Evaluation of cell delivery strategies in a model of peripheral arterial disease

In a final evaluation of ASC delivery strategies, the proposed hydrogel delivery system was applied in a mouse hindlimb ischemia model of peripheral arterial disease. Compared to the delivery of the hydrogel alone, hASCs in saline, and saline alone, hASCs delivered in the hydrogel were retained in the ischemic hindlimb and significantly improved the intramuscular capillary density and frequency of proliferative cells. Importantly, this study indicated that the release of pro-angiogenic paracrine factors from encapsulated hASCs observed *in vitro* could be translated to an *in vivo* setting, and that the improved retention of hASCs by hydrogel delivery resulted in an enhanced therapeutic effect.

However, despite the immunohistochemical (IHC) evidence of local paracrine effects from hASCs delivered in the hydrogel, these effects were not reflected in improvements to limb perfusion or function. A possible explanation for this failure is the immunocompromised nature of the host NOD/SCID mouse model, specifically the defective macrophage component. As a major role of ASCs in ischemic recovery may be the modulation of inflammation and macrophage activity, this function may not be represented in studies using NOD/SCID hosts. In order to capture the immunomodulatory effects of ASCs, future work should consider using either i) hASCs in a less immunocompromised host (i.e. an athymic nude mouse or a humanized mouse model), or ii) using allogeneic mouse-derived ASCs in an immunocompetent mouse

model. Furthermore, ASCs should be derived from multiple donors to assess the potential effects of inter-donor variability.

The discrepancy between the increased capillary density (by IHC) and the unaffected limb perfusion (by laser Doppler imaging) suggests that the capillaries may not represent a mature, functional, perfused vascular network. This may be further evidence of a deficit in macrophage activities, as macrophages are involved in blood vessel maturation and anastomosis. Future work should consider assays to discriminate between non-perfused and perfused vessels, such as labeling perfused vessels with the intravenous delivery of a marker such as Evans Blue dye[234] or labeled lectins.[235] Additionally, micro computed tomography (micro-CT) could be used to generate 3-D representations of a perfused vascular contrast agent, allowing for the quantification of vascular architecture and limb perfusion at the terminal endpoint.[251] Finally, as both IHC and micro-CT are terminal endpoint assessments of vascular recovery, future studies may benefit from running multiple cohorts of mice with early endpoint (1-2 weeks) and late endpoints (4-5 weeks) to assess the progression of recovery.

References

(1) Townsend, N.; Wilson, L.; Bhatnagar, P.; Wickramasinghe, K.; Rayner, M.; Nichols, M. Cardiovascular disease in Europe: Epidemiological update 2016. *Eur. Heart J.* **2016**, *37* (42), 3232–3245 DOI: 10.1093/eurheartj/ehw334.

(2) Mukherjee, D.; Bhatt, D. L.; Roe, M. T.; Patel, V.; Ellis, S. G. Direct myocardial revascularization and angiogenesis--how many patients might be eligible? *Am. J. Cardiol.* **1999**, *84* (5), 598–600, A8.

(3) Adam, D. J.; Beard, J. D.; Cleveland, T.; Bell, J.; Bradbury, a W.; Forbes, J. F.; Fowkes, F. G. R.; Gillepsie, I.; Ruckley, C. V; Raab, G.; et al. Bypass versus angioplasty in severe ischaemia of the leg (BASIL): multicentre, randomised controlled trial. *Lancet* **2005**, *366* (9501), 1925–1934 DOI: 10.1016/S0140-6736(05)67704-5.

(4) Golomb, B. A.; Dang, T. T.; Criqui, M. H. Peripheral arterial disease: Morbidity and mortality implications. *Circulation*. August 15, 2006, pp 688–699.

(5) Rigato, M.; Monami, M.; Fadini, G. P. Autologous Cell Therapy for Peripheral Arterial Disease: Systematic Review and Meta-Analysis of Randomized, Nonrandomized, and Noncontrolled Studies. *Circ. Res.* **2017**, *120* (8), 1326–1340 DOI: 10.1161/CIRCRESAHA.116.309045.

(6) Lawall, H.; Bramlage, P.; Amann, B. Treatment of peripheral arterial disease using stem and progenitor cell therapy. *J. Vasc. Surg.* **2011**, *53* (2), 445–453 DOI: 10.1016/j.jvs.2010.08.060.

(7) de Jong, R.; Houtgraaf, J. H.; Samiei, S.; Boersma, E.; Duckers, H. J. Intracoronary Stem Cell Infusion After Acute Myocardial Infarction: A Meta-Analysis and Update on Clinical Trials. *Circ. Cardiovasc. Interv.* **2014**, *7* (2), 156–167 DOI: 10.1161/CIRCINTERVENTIONS.113.001009.

(8) Kwon, H. M.; Hur, S. M.; Park, K. Y.; Kim, C. K.; Kim, Y. M.; Kim, H. S.; Shin, H. C.; Won, M. H.; Ha, K. S.; Kwon, Y. G.; et al. Multiple paracrine factors secreted by mesenchymal stem cells contribute to angiogenesis. *Vascul. Pharmacol.* **2014**, *63* (1), 19–28 DOI: 10.1016/j.vph.2014.06.004.

(9) Amable, P. R.; Teixeira, M. V. T.; Carias, R. B. V.; Granjeiro, J. M.; Borojevic, R. Protein synthesis and secretion in human mesenchymal cells derived from bone marrow, adipose tissue and Wharton's jelly. *Stem Cell Res. Ther.* **2014**, *5* (2), 53 DOI: 10.1186/scrt442.

(10) Rehman, J.; Traktuev, D.; Li, J.; Merfeld-Clauss, S.; Temm-Grove, C. J.; Bovenkerk, J. E.; Pell, C. L.; Johnstone, B. H.; Considine, R. V; March, K. L. Secretion of Angiogenic and Antiapoptotic Factors by Human Adipose Stromal Cells. *Circulation* **2004**, *109* (10), 1292–1298 DOI: 10.1161/01.CIR.0000121425.42966.F1.

(11) Blaber, S. P.; Webster, R. A.; Hill, C. J.; Breen, E. J.; Kuah, D.; Vesey, G.; Herbert, B. R. Analysis of in vitro secretion profiles from adipose-derived cell populations. *J. Transl. Med.* **2012**, *10* (1), 172 DOI: 10.1186/1479-5876-10-172.

(12) Kondo, K.; Shintani, S.; Shibata, R.; Murakami, H.; Murakami, R.; Imaizumi, M.; Kitagawa, Y.; Murohara, T. Implantation of adipose-derived regenerative cells enhances ischemia-induced angiogenesis. *Arterioscler. Thromb. Vasc. Biol.* **2009**, *29* (1), 61–66 DOI: 10.1161/ATVBAHA.108.166496.

(13) Moon, M. H.; Kim, S. Y.; Kim, Y. J.; Kim, S. J.; Lee, J. B.; Bae, Y. C.; Sung, S. M.; Jung, J. S. Human adipose tissue-derived mesenchymal stem cells improve postnatal neovascularization in a mouse model of hindlimb ischemia. *Cell. Physiol. Biochem.* **2006**, *17* (5–6), 279–290 DOI: 10.1159/000094140.

(14) Perin, E. C.; Murphy, M. P.; March, K. L.; Bolli, R.; Loughran, J.; Yang, P. C.; Leeper, N. J.; Dalman, R. L.; Alexander, J.; Henry, T. D.; et al. Evaluation of Cell Therapy on Exercise Performance and Limb Perfusion in Peripheral Artery Disease: The CCTRN PACE Trial (Patients with Intermittent Claudication Injected with ALDH Bright Cells). *Circulation* **2017**, *135* (15), 1417–1428 DOI: 10.1161/CIRCULATIONAHA.116.025707.

(15) Henry, T. D.; Moyé, L.; Traverse, J. H. Consistently Inconsistent-Bone Marrow Mononuclear Stem Cell Therapy Following Acute Myocardial Infarction: A Decade Later. *Circ. Res.* **2016**, *119*

(3), 404–406 DOI: 10.1161/CIRCRESAHA.116.309231.

(16) Prasad, K.; Sharma, A.; Garg, A.; Mohanty, S.; Bhatnagar, S.; Johri, S.; Singh, K. K.; Nair, V.; Sarkar, R. S.; Gorthi, S. P.; et al. Intravenous autologous bone marrow mononuclear stem cell therapy for ischemic stroke: A multicentric, randomized trial. *Stroke* **2014**, *45* (12), 3618–3624 DOI: 10.1161/STROKEAHA.114.007028.

(17) Pons, J.; Huang, Y.; Takagawa, J.; Arakawa-Hoyt, J.; Ye, J.; Grossman, W.; Kan, Y. W.; Su, H. Combining angiogenic gene and stem cell therapies for myocardial infarction. *J. Gene Med.* **2009**, *11* (9), 743–753 DOI: 10.1002/jgm.1362.

(18) Gyongyosi, M.; Blanco, J.; Marian, T.; Tron, L.; Petnehazy, O.; Petrasi, Z.; Hemetsberger, R.; Rodriguez, J.; Font, G.; Pavo, I. J.; et al. Serial Noninvasive In Vivo Positron Emission Tomographic Tracking of Percutaneously Intramyocardially Injected Autologous Porcine Mesenchymal Stem Cells Modified for Transgene Reporter Gene Expression. *Circ. Cardiovasc. Imaging* **2008**, *1* (2), 94–103 DOI: 10.1161/CIRCIMAGING.108.797449.

(19) Hou, D.; Youssef, E. A.-S.; Brinton, T. J.; Zhang, P.; Rogers, P.; Price, E. T.; Yeung, A. C.; Johnstone, B. H.; Yock, P. G.; March, K. L. Radiolabeled cell distribution after intramyocardial, intracoronary, and interstitial retrograde coronary venous delivery: implications for current clinical trials. *Circulation* **2005**, *112* (9 Suppl), I150-6 DOI: 10.1161/CIRCULATIONAHA.104.526749.

(20) Laurila, J. P.; Laatikainen, L.; Castellone, M. D.; Trivedi, P.; Heikkila, J.; Hinkkanen, A.; Hematti, P.; Laukkanen, M. O. Human embryonic stem cell-derived mesenchymal stromal cell transplantation in a rat hind limb injury model. *Cytotherapy* **2009**, *11* (6), 726–737 DOI: 10.3109/14653240903067299.

(21) Radhakrishnan, J.; Krishnan, U. M.; Sethuraman, S. Hydrogel based injectable scaffolds for cardiac tissue regeneration. *Biotechnol. Adv.* **2014**, *32* (2), 449–461 DOI: 10.1016/j.biotechadv.2013.12.010.

(22) Ungerleider, J. L.; Christman, K. L. Concise Review: Injectable Biomaterials for the Treatment of

Myocardial Infarction and Peripheral Artery Disease: Translational Challenges and Progress. *Stem Cells Transl. Med.* **2014**, *3* (9), 1090–1099 DOI: 10.5966/sctm.2014-0049.

(23) Sart, S.; Ma, T.; Li, Y. Preconditioning Stem Cells for *In Vivo* Delivery. *Biores. Open Access* **2014**, *3* (4), 137–149 DOI: 10.1089/biores.2014.0012.

(24) Madonna, R.; De Caterina, R. Stem cells and growth factor delivery systems for cardiovascular disease. *J. Biotechnol.* **2011**, *154* (4), 291–297 DOI: 10.1016/j.jbiotec.2011.05.014.

(25) Gimble, J. M.; Bunnell, B. A.; Chiu, E. S.; Guilak, F. Concise review: Adipose-derived stromal vascular fraction cells and stem cells: let's not get lost in translation. *Stem Cells* **2011**, *29* (5), 749–754 DOI: 10.1002/stem.629.

(26) Murohara, T. Autologous adipose tissue as a new source of progenitor cells for therapeutic angiogenesis. *J. Cardiol.* **2009**, *53* (2), 155–163 DOI: 10.1016/j.jjcc.2009.01.003.

(27) Cai, L.; Johnstone, B. H.; Cook, T. G.; Tan, J.; Fishbein, M. C.; Chen, P.-S.; March, K. L. IFATS collection: Human adipose tissue-derived stem cells induce angiogenesis and nerve sprouting following myocardial infarction, in conjunction with potent preservation of cardiac function. *Stem Cells* **2009**, *27* (1), 230–237 DOI: 10.1634/stemcells.2008-0273.

(28) Zvonic, S.; Lefevre, M.; Kilroy, G.; Floyd, Z. E.; DeLany, J. P.; Kheterpal, I.; Gravois, A.; Dow, R.; White, A.; Wu, X.; et al. Secretome of primary cultures of human adipose-derived stem cells: modulation of serpins by adipogenesis. *Mol. Cell. Proteomics* **2007**, *6* (1), 18–28 DOI: 10.1074/mcp.M600217-MCP200.

(29) Nuttelman, C. R.; Rice, M. A.; Rydholm, A. E.; Salinas, C. N.; Shah, D. N.; Anseth, K. S. Macromolecular Monomers for the Synthesis of Hydrogel Niches and Their Application in Cell Encapsulation and Tissue Engineering. *Prog. Polym. Sci.* **2008**, *33* (2), 167–179 DOI: 10.1016/j.progpolymsci.2007.09.006.

(30) Burdick, J. A.; Mauck, R. L.; Gerecht, S. To Serve and Protect: Hydrogels to Improve Stem Cell-Based Therapies. *Cell Stem Cell* **2016**, *18* (1), 13–15 DOI: 10.1016/j.stem.2015.12.004.

(31) Russo, V.; Young, S.; Hamilton, A.; Amsden, B. G.; Flynn, L. E. Mesenchymal stem cell delivery strategies to promote cardiac regeneration following ischemic injury. *Biomaterials* **2014**, *35* (13), 3956–3974 DOI: 10.1016/j.biomaterials.2014.01.075.

(32) Li, Z.; Guan, J. Hydrogels for Cardiac Tissue Engineering. *Polymers (Basel).* **2011**, *3* (2), 740–761 DOI: 10.3390/polym3020740.

(33) Nuttelman, C. R.; Tripodi, M. C.; Anseth, K. S. Synthetic hydrogel niches that promote hMSC viability. *Matrix Biol.* **2005**, *24* (3), 208–218 DOI: 10.1016/j.matbio.2005.03.004.

(34) Yu, Y.; Deng, C.; Meng, F.; Shi, Q.; Feijen, J.; Zhong, Z. Novel injectable biodegradable glycol chitosan-based hydrogels crosslinked by Michael-type addition reaction with oligo(acryloyl carbonate)-b-poly(ethylene glycol)-b-oligo(acryloyl carbonate) copolymers. *J. Biomed. Mater. Res. A* **2011**, 316–326 DOI: 10.1002/jbm.a.33199.

(35) Jin, R.; Moreira Teixeira, L. S.; Krouwels, a; Dijkstra, P. J.; van Blitterswijk, C. a; Karperien, M.; Feijen, J. Synthesis and characterization of hyaluronic acid-poly(ethylene glycol) hydrogels via Michael addition: An injectable biomaterial for cartilage repair. *Acta Biomater.* **2010**, *6* (6), 1968–1977 DOI: 10.1016/j.actbio.2009.12.024.

(36) Daniele, M. A.; Adams, A. A.; Naciri, J.; North, S. H.; Ligler, F. S. Interpenetrating networks based on gelatin methacrylamide and PEG formed using concurrent thiol click chemistries for hydrogel tissue engineering scaffolds. *Biomaterials* **2014**, *35* (6), 1845–1856 DOI: 10.1016/j.biomaterials.2013.11.009.

(37) Naficy, S.; Brown, H. R.; Razal, J. M.; Spinks, G. M.; Whitten, P. G. Progress toward robust polymer hydrogels. *Aust. J. Chem.* **2011**, *64* (8), 1007–1025 DOI: 10.1071/CH11156.

(38) Balakrishnan, B.; Banerjee, R. Biopolymer-based hydrogels for cartilage tissue engineering. *Chem. Rev.* **2011**, *111* (8), 4453–4474 DOI: 10.1021/cr100123h.

(39) Markeson, D.; Pleat, J. M.; Sharpe, J. R.; Harris, A. L.; Seifalian, A. M.; Watt, S. M. Scarring, stem cells, scaffolds and skin repair. *J. Tissue Eng. Regen. Med.* **2015**, *9* (6), 649–668 DOI:

10.1002/term.1841.

(40) Shinohara, M.; Sabra, K.; Gennisson, J.-L.; Fink, M.; Tanter, M. Real-time visualization of muscle stiffness distribution with ultrasound shear wave imaging during muscle contraction. *Muscle Nerve* **2010**, *42* (3), 438–441 DOI: 10.1002/mus.21723.

(41) Bergmann, G.; Graichen, F.; Rohlmann, A.; Bender, A.; Heinlein, B.; Duda, G. N.; Heller, M. O.; Morlock, M. M. Realistic loads for testing hip implants. *Biomed. Mater. Eng.* **2010**, *20* (2), 65–75 DOI: 10.3233/BME-2010-0616.

(42) Anseth, K. S.; Bowman, C. N.; Brannon-Peppas, L. Mechanical properties of hydrogels and their experimental determination. *Biomaterials* **1996**, *17* (17), 1647–1657 DOI: 10.1016/0142-9612(96)87644-7.

(43) Treloar, L. R. G. *The Physics of Rubber Elasticity (Third Edition)*, 3rd ed.; Clarendon Press: Oxford.

(44) Lake, G. J.; Thomas, A. G. The Strength of Highly Elastic Materials. *Proc. R. Soc. A Math. Phys. Eng. Sci.* **1967**, *300* (1460), 108–119 DOI: 10.1098/rspa.1967.0160.

(45) Furukawa, H.; Horie, K.; Nozaki, R.; Okada, M. Swelling-induced modulation of static and dynamic fluctuations in polyacrylamide gels observed by scanning microscopic light scattering. *Phys. Rev. E* **2003**, *68* (3), 31406 DOI: 10.1103/PhysRevE.68.031406.

(46) Webber, R. E.; Creton, C.; Brown, H. R.; Gong, J. P. Large Strain Hysteresis and Mullins Rffect of Tough Double Network Hydrogels. *Macromolecules* **2007**, *40*, 2919–2927 DOI: 10.1021/ma062924y.

(47) Richtering, W.; Saunders, B. R. Gel architectures and their complexity. *Soft Matter* **2014**, *10* (21), 3695–3702 DOI: 10.1039/c4sm00208c.

(48) Rodell, C. B.; Dusaj, N. N.; Highley, C. B.; Burdick, J. A. Injectable and Cytocompatible Tough Double-Network Hydrogels through Tandem Supramolecular and Covalent Crosslinking. *Adv. Mater.* **2016**, 8419–8424 DOI: 10.1002/adma.201602268.

(49) Gong, J. P.; Katsuyama, Y.; Kurokawa, T.; Osada, Y. Double-Network Hydrogels with Extremely High Mechanical Strength. *Adv. Mater.* **2003**, *15* (14), 1155–1158 DOI: 10.1002/adma.200304907.

(50) Brown, H. R. A model of the fracture of double network gels. *Macromolecules* **2007**, *40* (10), 3815–3818 DOI: 10.1021/ma062642y.

(51) Gong, J. P. Why are double network hydrogels so tough? *Soft Matter* **2010**, *6* (12), 2583 DOI: 10.1039/b924290b.

(52) Nakajima, T.; Furukawa, H.; Tanaka, Y.; Kurokawa, T.; Osada, Y.; Gong, J. P. True chemical structure of double network hydrogels. *Macromolecules* **2009**, *42* (6), 2184–2189 DOI: 10.1021/ma802148p.

(53) Costa, A. M. S.; Mano, J. F. Highly robust hydrogels via a fast, simple and cytocompatible dual crosslinking-based process. *Chem. Commun.* **2015**, *51*, 15673–15676 DOI: 10.1039/C5CC05564D.

(54) Guo, M.; Pitet, L. M.; Wyss, H. M.; Vos, M.; Dankers, P. Y. W.; Meijer, E. W. Tough stimuli-responsive supramolecular hydrogels with hydrogen-bonding network junctions. *J. Am. Chem. Soc.* **2014**, *136* (19), 6969–6977 DOI: 10.1021/ja500205v.

(55) Truong, V. X.; Ablett, M. P.; Richardson, S. M.; Hoyland, J. A.; Dove, A. P. Simultaneous orthogonal dual-click approach to tough, in-situ -forming hydrogels for cell encapsulation. *J. Am. Chem. Soc.* **2015**, *137* (4), 1618–1622 DOI: 10.1021/ja511681s.

(56) Haraguchi, K.; Takehisa, T. Nanocomposite Hydrogels: A Unique Organic–Inorganic Network Structure with Extraordinary Mechanical, Optical, and Swelling/De-swelling Properties. *Adv. Mater.* **2002**, *14* (16), 1120 DOI: 10.1002/1521-4095(20020816)14:16<1120::AID-ADMA1120>3.0.CO;2-9.

(57) Haraguchi, K. Nanocomposite hydrogels. *Curr. Opin. Solid State Mater. Sci.* **2007**, *11* (3–4), 47–54 DOI: 10.1016/j.cossms.2008.05.001.

(58) Abdurrahmanoglu, S.; Okay, O. Rheological behavior of polymer-clay nanocomposite hydrogels: Effect of nanoscale interactions. *J. Appl. Polym. Sci.* **2010**, *116* (4), 2328–2335 DOI: 10.1002/app.31705.

(59) Gaharwar, A. K.; Dammu, S. A.; Canter, J. M.; Wu, C. J.; Schmidt, G. Highly extensible, tough, and elastomeric nanocomposite hydrogels from poly(ethylene glycol) and hydroxyapatite nanoparticles. *Biomacromolecules* **2011**, *12* (5), 1641–1650 DOI: 10.1021/bm200027z.

(60) Jaiswal, M. K.; Xavier, J. R.; Carrow, J. K.; Desai, P.; Alge, D.; Gaharwar, A. K. Mechanically stiff nanocomposite hydrogels at ultralow nanoparticle content. *ACS Nano* **2016**, *10* (1), 246–256 DOI: 10.1021/acsnano.5b03918.

(61) Meenach, S. A.; Anderson, K. W.; Hilt, J. Z. Safety of Nanoparticles; Webster, T. J., Ed.; Nanostructure Science and Technology; Springer New York: New York, NY, 2009; pp 131–157.

(62) Zhang, C.; Aung, A.; Liao, L.; Varghese, S. A novel single precursor-based biodegradable hydrogel with enhanced mechanical properties. *Soft Matter* **2009**, *5* (20), 3831 DOI: 10.1039/b912102a.

(63) Zhang, C.; Sangaj, N.; Hwang, Y.; Phadke, A.; Chang, C.-W.; Varghese, S. Oligo(trimethylene carbonate)-poly(ethylene glycol)-oligo(trimethylene carbonate) triblock-based hydrogels for cartilage tissue engineering. *Acta Biomater.* **2011**, *7* (9), 3362–3369 DOI: 10.1016/j.actbio.2011.05.024.

(64) Madonna, R.; Geng, Y.-J.; De Caterina, R. Adipose tissue-derived stem cells: characterization and potential for cardiovascular repair. *Arterioscler. Thromb. Vasc. Biol.* **2009**, *29* (11), 1723–1729 DOI: 10.1161/ATVBAHA.109.187179.

(65) Sultan, S.; Hynes, N. Critical appraisal of stem cell therapy in peripheral arterial disease: Do current scientific breakthroughs offer true promise or false hope? *J. Biomed. Sci. Eng.* **2014**, *7* (2), 75–85 DOI: 10.4236/jbise.2014.72011.

(66) Liang, X.; Ding, Y.; Zhang, Y.; Tse, H. F.; Lian, Q. Paracrine mechanisms of mesenchymal stem

cell-based therapy: Current status and perspectives. *Cell Transplant.* **2014**, *23* (9), 1045–1059 DOI: 10.3727/096368913X667709.

(67) Wang, Y.; Chen, X.; Cao, W.; Shi, Y. Plasticity of mesenchymal stem cells in immunomodulation: pathological and therapeutic implications. *Nat. Immunol.* **2014**, *15* (11), 1009–1016 DOI: 10.1038/ni.3002.

(68) Friedenstein, A. J.; Piatetzky-Shapiro, I. I.; Petrakova, K. V. Osteogenesis in transplants of bone marrow cells. *J. Embryol. Exp. Morphol.* **1966**, *16* (3), 381–390.

(69) Zuk, P. A.; Zhu, M.; Ashjian, P.; De Ugarte, D. A.; Huang, J. I.; Mizuno, H.; Alfonso, Z. C.; Fraser, J. K.; Benhaim, P.; Hedrick, M. H. Human adipose tissue is a source of multipotent stem cells. *Mol. Biol. Cell* **2002**, *13* (12), 4279–4295 DOI: 10.1091/mbc.E02-02-0105.

(70) Chong, P. P.; Selvaratnam, L.; Abbas, A. A.; Kamarul, T. Human peripheral blood derived mesenchymal stem cells demonstrate similar characteristics and chondrogenic differentiation potential to bone marrow derived mesenchymal stem cells. *J Orthop Res* **2012**, *30* (4), 634–642 DOI: 10.1002/jor.21556.

(71) Chamberlain, G.; Fox, J.; Ashton, B.; Middleton, J. Concise review: mesenchymal stem cells: their phenotype, differentiation capacity, immunological features, and potential for homing. *Stem Cells* **2007**, *25* (11), 2739–2749 DOI: 10.1634/stemcells.2007-0197.

(72) Wexler, S. A.; Donaldson, C.; Denning-Kendall, P.; Rice, C.; Bradley, B.; Hows, J. M. Adult bone marrow is a rich source of human mesenchymal “stem” cells but umbilical cord and mobilized adult blood are not. *Br. J. Haematol.* **2003**, *121* (2), 368–374 DOI: 10.1046/j.1365-2141.2003.04284.x.

(73) Bonab, M. M.; Alimoghaddam, K.; Talebian, F.; Ghaffari, S. H.; Ghavamzadeh, A.; Nikbin, B. Aging of mesenchymal stem cell in vitro. *BMC Cell Biol.* **2006**, *7*, 14 DOI: 10.1186/1471-2121-7-14.

(74) Gimble, J. M.; Katz, A. J.; Bunnell, B. A. Adipose-derived stem cells for regenerative medicine.

Circ. Res. **2007**, *100* (9), 1249–1260 DOI: 10.1161/01.RES.0000265074.83288.09.

(75) Strem, B. M.; Hicok, K. C.; Zhu, M.; Wulur, I.; Alfonso, Z.; Schreiber, R. E.; Fraser, J. K.; Hedrick, M. H. Multipotential differentiation of adipose tissue-derived stem cells. *Keio J.Med.* **2005**, *54* (0022–9717 (Print)), 132–141 DOI: 10.2302/kjm.54.132.

(76) Nakanishi, C.; Nagaya, N.; Ohnishi, S.; Yamahara, K.; Takabatake, S.; Konno, T.; Hayashi, K.; Kawashiri, M. a; Tsubokawa, T.; Yamagishi, M. Gene and Protein Expression Analysis of Mesenchymal Stem Cells Derived From Rat Adipose Tissue and Bone Marrow. *Circ. J.* **2011**, *75* (1347–4820 (Electronic)), 2260–2268 DOI: 10.1253/circj.CJ-11-0246.

(77) Meyerrose, T. E.; De Ugarte, D. a; Hofling, a A.; Herrbrich, P. E.; Cordonnier, T. D.; Shultz, L. D.; Eagon, J. C.; Wirthlin, L.; Sands, M. S.; Hedrick, M. a; et al. In Vivo Distribution of Human Adipose-Derived Mesenchymal Stem Cells in Novel Xenotransplantation Models. *Stem Cells* **2007**, *25* (1), 220–227 DOI: 10.1634/stemcells.2006-0243.

(78) Hu, X.; Wei, L.; Taylor, T. M.; Wei, J.; Zhou, X.; Wang, J.; Yu, S. P. Hypoxic preconditioning enhances bone marrow mesenchymal stem cell migration via Kv2 . 1 channel and FAK activation. *Am J Physiol Cell Physiol* **2011**, *301* (51), 362–372 DOI: 10.1152/ajpcell.00013.2010.

(79) Kim, Y. J.; Kim, H. K.; Cho, H. H.; Bae, Y. C.; Suh, K. T.; Jung, J. S. Direct Comparison of Human Mesenchymal Stem Cells Derived from Adipose Tissues and Bone Marrow in Mediating Neovascularization in Response to Vascular Ischemia. *Cell. Physiol. Biochem.* **2007**, *20* (6), 867–876 DOI: 10.1159/000110447.

(80) Miranville, A.; Heeschen, C.; Sengenès, C.; Curat, C. a; Busse, R.; Bouloumié, A. Improvement of postnatal neovascularization by human adipose tissue-derived stem cells. *Circulation* **2004**, *110* (3), 349–355 DOI: 10.1161/01.CIR.0000135466.16823.D0.

(81) Lotfi, S.; Patel, A. S.; Mattock, K.; Egginton, S.; Smith, A.; Modarai, B. Towards a more relevant hind limb model of muscle ischaemia. *Atherosclerosis* **2013**, *227* (1), 1–8 DOI: 10.1016/j.atherosclerosis.2012.10.060.

(82) Caplan, A. I.; Dennis, J. E. Mesenchymal stem cells as trophic mediators. *J. Cell. Biochem.* **2006**, *98* (5), 1076–1084 DOI: 10.1002/jcb.20886.

(83) Noiseux, N.; Gnecchi, M.; Lopez-Ilasaca, M.; Zhang, L.; Solomon, S. D.; Deb, A.; Dzau, V. J.; Pratt, R. E. Mesenchymal stem cells overexpressing Akt dramatically repair infarcted myocardium and improve cardiac function despite infrequent cellular fusion or differentiation. *Mol. Ther.* **2006**, *14* (6), 840–850 DOI: 10.1016/j.ymthe.2006.05.016.

(84) Gnecchi, M.; Zhang, Z.; Ni, A.; Dzau, V. J. Paracrine mechanisms in adult stem cell signaling and therapy. *Circ. Res.* **2008**, *103* (11), 1204–1219 DOI: 10.1161/CIRCRESAHA.108.176826.

(85) Gnecchi, M.; He, H.; Noiseux, N.; Liang, O. D.; Zhang, L.; Morello, F.; Mu, H.; Melo, L. G.; Pratt, R. E.; Ingwall, J. S.; et al. Evidence supporting paracrine hypothesis for Akt-modified mesenchymal stem cell-mediated cardiac protection and functional improvement. *FASEB J.* **2006**, *20* (6), 661–669 DOI: 10.1096/fj.05-5211com.

(86) Mirotsou, M.; Jayawardena, T. M.; Schmeckpeper, J.; Gnecchi, M.; Dzau, V. J. Paracrine mechanisms of stem cell reparative and regenerative actions in the heart. *J. Mol. Cell. Cardiol.* **2011**, *50* (2), 280–289 DOI: 10.1016/j.yjmcc.2010.08.005.

(87) Song, S.-Y.; Chung, H.-M.; Sung, J.-H. The pivotal role of VEGF in adipose-derived-stem-cell-mediated regeneration. *Expert Opin. Biol. Ther.* **2010**, *10* (11), 1529–1537 DOI: 10.1517/14712598.2010.522987.

(88) Bell, L. N.; Cai, L.; Johnstone, B. H.; Traktuev, D. O.; March, K. L.; Considine, R. V. A central role for hepatocyte growth factor in adipose tissue angiogenesis. *AJP Endocrinol. Metab.* **2007**, *294* (2), E336–E344 DOI: 10.1152/ajpendo.00272.2007.

(89) Bhang, S. H.; Lee, S.; Shin, J.-Y.; Lee, T.-J.; Jang, H.-K.; Kim, B.-S. Efficacious and clinically relevant conditioned medium of human adipose-derived stem cells for therapeutic angiogenesis. *Mol. Ther.* **2014**, *22* (4), 862–872 DOI: 10.1038/mt.2013.301.

(90) Hung, S.-C.; Pochampally, R. R.; Chen, S.-C.; Hsu, S.-C.; Prockop, D. J. Angiogenic effects of

human multipotent stromal cell conditioned medium activate the PI3K-Akt pathway in hypoxic endothelial cells to inhibit apoptosis, increase survival, and stimulate angiogenesis. *Stem Cells* **2007**, *25* (9), 2363–2370 DOI: 10.1634/stemcells.2006-0686.

(91) Suga, H.; Glotzbach, J. P.; Sorkin, M.; Longaker, M. T.; Gurtner, G. C. Paracrine mechanism of angiogenesis in adipose-derived stem cell transplantation. *Ann. Plast. Surg.* **2014**, *72* (2), 234–241 DOI: 10.1097/SAP.0b013e318264fd6a.

(92) Hsiao, S. T.; Lokmic, Z.; Peshavariya, H.; Abberton, K. M.; Dusting, G. J.; Lim, S. Y.; Dilley, R. J. Hypoxic conditioning enhances the angiogenic paracrine activity of human adipose-derived stem cells. *Stem Cells Dev.* **2013**, *22* (10), 1614–1623 DOI: 10.1089/scd.2012.0602.

(93) Kinnaird, T.; Stabile, E.; Burnett, M. S.; Epstein, S. E. Bone-marrow-derived cells for enhancing collateral development: mechanisms, animal data, and initial clinical experiences. *Circ. Res.* **2004**, *95* (4), 354–363 DOI: 10.1161/01.RES.0000137878.26174.66.

(94) da Silva Meirelles, L.; Fontes, A. M.; Covas, D. T.; Caplan, A. I. Mechanisms involved in the therapeutic properties of mesenchymal stem cells. *Cytokine Growth Factor Rev.* **2009**, *20* (5–6), 419–427 DOI: 10.1016/j.cytogfr.2009.10.002.

(95) Nakagami, H.; Maeda, K.; Morishita, R.; Iguchi, S.; Nishikawa, T.; Takami, Y.; Kikuchi, Y.; Saito, Y.; Tamai, K.; Ogihara, T.; et al. Novel autologous cell therapy in ischemic limb disease through growth factor secretion by cultured adipose tissue-derived stromal cells. *Arterioscler. Thromb. Vasc. Biol.* **2005**, *25* (12), 2542–2547 DOI: 10.1161/01.ATV.0000190701.92007.6d.

(96) Kubo, M.; Li, T.-S.; Suzuki, R.; Shirasawa, B.; Morikage, N.; Ohshima, M.; Qin, S.-L.; Hamano, K. Hypoxic preconditioning increases survival and angiogenic potency of peripheral blood mononuclear cells via oxidative stress resistance. *Am. J. Physiol. Heart Circ. Physiol.* **2008**, *294* (2), H590-5 DOI: 10.1152/ajpheart.00856.2007.

(97) Rosová, I.; Dao, M.; Capoccia, B.; Link, D.; Nolta, J. a. Hypoxic preconditioning results in increased motility and improved therapeutic potential of human mesenchymal stem cells. *Stem*

Cells **2008**, *26* (8), 2173–2182 DOI: 10.1634/stemcells.2007-1104.

(98) Chacko, S. M.; Ahmed, S.; Selvendiran, K.; Kuppusamy, M. L.; Khan, M.; Kuppusamy, P. Hypoxic preconditioning induces the expression of prosurvival and proangiogenic markers in mesenchymal stem cells. *Am. J. Physiol. Cell Physiol.* **2010**, *299* (6), C1562-70 DOI: 10.1152/ajpcell.00221.2010.

(99) Zhang, M.; Mal, N.; Kiedrowski, M.; Chacko, M.; Askari, A. T.; Popovic, Z. B.; Koc, O. N.; Penn, M. S. SDF-1 expression by mesenchymal stem cells results in trophic support of cardiac myocytes after myocardial infarction. *FASEB J.* **2007**, *21* (12), 3197–3207 DOI: 10.1096/fj.06-6558com.

(100) Lee, S.; Choi, E.; Cha, M. J.; Hwang, K. C. Cell adhesion and long-term survival of transplanted mesenchymal stem cells: A prerequisite for cell therapy. *Oxid. Med. Cell. Longev.* **2015**, *2015* DOI: 10.1155/2015/632902.

(101) Fan, Y.; Maley, M.; Beilharz, M.; Grounds, M. Rapid death of injected myoblasts in myoblast transfer therapy. *Muscle Nerve* **1996**, *19* (7), 853–860 DOI: 10.1002/(SICI)1097-4598(199607)19:7<853::AID-MUS7>3.0.CO;2-8.

(102) Wobma, H. M.; Liu, D.; Vunjak-novakovic, G. Paracrine Effects of Mesenchymal Stromal Cells Cultured in Three-Dimensional Settings on Tissue Repair. **2017** DOI: 10.1021/acsbiomaterials.7b00005.

(103) Collins, M. C.; Moore, J. L.; Burrows, B. J.; Kypson, A. P.; Muller-Borer, B. J. Early Cell Loss Associated with Mesenchymal Stem Cell Cardiomyoplasty. *Open Tissue* **2012**, *3*, 17–24.

(104) Suuronen, E. J.; Veinot, J. P.; Wong, S.; Kapila, V.; Price, J.; Griffith, M.; Mesana, T. G.; Ruel, M. Tissue-engineered injectable collagen-based matrices for improved cell delivery and vascularization of ischemic tissue using CD133+ progenitors expanded from the peripheral blood. *Circulation* **2006**, *114* (1 Suppl), I138-44 DOI: 10.1161/CIRCULATIONAHA.105.001081.

(105) Tang, Z. C. W.; Liao, W.-Y.; Tang, A. C. L.; Tsai, S.-J.; Hsieh, P. C. H. The enhancement of endothelial cell therapy for angiogenesis in hindlimb ischemia using hyaluronan. *Biomaterials*

2011, *32* (1), 75–86 DOI: 10.1016/j.biomaterials.2010.08.085.

(106) Landázuri, N.; Levit, R. D.; Joseph, G.; Ortega-Legaspi, J. M.; Flores, C. A.; Weiss, D.; Sambanis, A.; Weber, C. J.; Safley, S. A.; Taylor, W. R. Alginate microencapsulation of human mesenchymal stem cells as a strategy to enhance paracrine-mediated vascular recovery after hindlimb ischaemia. *J. Tissue Eng. Regen. Med.* **2016**, *10* (3), 222–232 DOI: 10.1002/term.1680.

(107) Follin, B.; Juhl, M.; Cohen, S.; Pedersen, A. E.; Gad, M.; Kastrup, J.; Ekblond, A. Human adipose-derived stromal cells in a clinically applicable injectable alginate hydrogel: Phenotypic and immunomodulatory evaluation. *Cytotherapy* **2015**, *17* (8), 1104–1118 DOI: 10.1016/j.jcyt.2015.04.008.

(108) Anderson, J. M.; Rodriguez, A.; Chang, D. T. Foreign body reaction to biomaterials. *Semin. Immunol.* **2008**, *20* (2), 86–100 DOI: 10.1016/j.smim.2007.11.004.

(109) Babensee, J. E.; Anderson, J. M.; McIntire, L. V.; Mikos, A. G. Host response to tissue engineered devices. *Adv. Drug Deliv. Rev.* **1998**, *33* (1–2), 111–139 DOI: 10.1016/S0169-409X(98)00023-4.

(110) Brown, B. N.; Sicari, B. M.; Badylak, S. F. Rethinking regenerative medicine: A macrophage-centered approach. *Front. Immunol.* **2014**, *5* (NOV), 1–11 DOI: 10.3389/fimmu.2014.00510.

(111) Mosser, D. M.; Edwards, J. P. Exploring the full spectrum of macrophage activation. *Nat. Rev. Immunol.* **2008**, *8* (12), 958–969 DOI: 10.1038/nri2448.

(112) Martinez, F. O.; Gordon, S. The M1 and M2 paradigm of macrophage activation: time for reassessment. *F1000Prime Rep.* **2014**, *6* (March), 13 DOI: 10.12703/P6-13.

(113) Mantovani, A.; Sica, A.; Sozzani, S.; Allavena, P.; Vecchi, A.; Locati, M. The chemokine system in diverse forms of macrophage activation and polarization. *Trends Immunol.* **2004**, *25* (12), 677–686 DOI: 10.1016/j.it.2004.09.015.

(114) Murray, P. J.; Allen, J. E.; Biswas, S. K.; Fisher, E. A.; Gilroy, D. W.; Goerdt, S.; Gordon, S.; Hamilton, J. A.; Ivashkiv, L. B.; Lawrence, T.; et al. Macrophage Activation and Polarization: Nomenclature and Experimental Guidelines. *Immunity* **2014**, *41* (1), 14–20 DOI:

10.1016/j.immuni.2014.06.008.

(115) Spiller, K. L.; Freytes, D. O.; Vunjak-Novakovic, G. Macrophages Modulate Engineered Human Tissues for Enhanced Vascularization and Healing. *Ann. Biomed. Eng.* **2015**, *43* (3), 616–627 DOI: 10.1007/s10439-014-1156-8.

(116) Stout, R. D. Functional plasticity of macrophages: reversible adaptation to changing microenvironments. *J. Leukoc. Biol.* **2004**, *76* (3), 509–513 DOI: 10.1189/jlb.0504272.

(117) Arnold, L.; Henry, A.; Poron, F.; Baba-Amer, Y.; van Rooijen, N.; Plonquet, A.; Gherardi, R. K.; Chazaud, B. Inflammatory monocytes recruited after skeletal muscle injury switch into antiinflammatory macrophages to support myogenesis. *J. Exp. Med.* **2007**, *204* (5), 1057–1069 DOI: 10.1084/jem.20070075.

(118) Sridharan, R.; Cameron, A. R.; Kelly, D. J.; Kearney, C. J.; O'Brien, F. J. Biomaterial based modulation of macrophage polarization: A review and suggested design principles. *Mater. Today* **2015**, *18* (6), 313–325 DOI: 10.1016/j.mattod.2015.01.019.

(119) Brown, B. N.; Valentin, J. E.; Stewart-Akers, A. M.; McCabe, G. P.; Badylak, S. F. Macrophage phenotype and remodeling outcomes in response to biologic scaffolds with and without a cellular component. *Biomaterials* **2009**, *30* (8), 1482–1491 DOI: 10.1016/j.biomaterials.2008.11.040.

(120) Brown, B. N.; Londono, R.; Tottey, S.; Zhang, L.; Kukla, K. A.; Wolf, M. T.; Daly, K. A.; Reing, J. E.; Badylak, S. F. Macrophage phenotype as a predictor of constructive remodeling following the implantation of biologically derived surgical mesh materials. *Acta Biomater.* **2012**, *8* (3), 978–987 DOI: 10.1016/j.actbio.2011.11.031.

(121) Spiller, K. L.; Anfang, R. R.; Spiller, K. J.; Ng, J.; Nakazawa, K. R.; Daulton, J. W.; Vunjak-Novakovic, G. The role of macrophage phenotype in vascularization of tissue engineering scaffolds. *Biomaterials* **2014**, *35* (15), 4477–4488 DOI: 10.1016/j.biomaterials.2014.02.012.

(122) Satriano, J. Arginine pathways and the inflammatory response: interregulation of nitric oxide and polyamines: review article. *Amino Acids* **2004**, *26* (4), 321–329 DOI: 10.1007/s00726-004-0078-4.

(123) Brown, B. N.; Ratner, B. D.; Goodman, S. B.; Amar, S.; Badylak, S. F. Macrophage polarization: An opportunity for improved outcomes in biomaterials and regenerative medicine. *Biomaterials* **2012**, *33* (15), 3792–3802 DOI: 10.1016/j.biomaterials.2012.02.034.

(124) Blakney, A. K.; Swartzlander, M. D.; Bryant, S. J. The effects of substrate stiffness on the in vitro activation of macrophages and in vivo host response to poly(ethylene glycol)-based hydrogels. *J. Biomed. Mater. Res. Part A* **2012**, *100A* (6), 1375–1386 DOI: 10.1002/jbm.a.34104.

(125) DeFalco, T.; Bhattacharya, I.; Williams, A. V.; Sams, D. M.; Capel, B. Yolk-sac-derived macrophages regulate fetal testis vascularization and morphogenesis. *Proc. Natl. Acad. Sci.* **2014**, *111* (23), E2384–E2393 DOI: 10.1073/pnas.1400057111.

(126) Willenborg, S.; Lucas, T.; van Loo, G.; Knipper, J. A.; Krieg, T.; Haase, I.; Brachvogel, B.; Hammerschmidt, M.; Nagy, A.; Ferrara, N.; et al. CCR2 recruits an inflammatory macrophage subpopulation critical for angiogenesis in tissue repair. *Blood* **2012**, *120* (3), 613–625 DOI: 10.1182/blood-2012-01-403386.

(127) Jetten, N.; Verbruggen, S.; Gijbels, M. J.; Post, M. J.; De Winther, M. P. J.; Donners, M. M. P. C. Anti-inflammatory M2, but not pro-inflammatory M1 macrophages promote angiogenesis in vivo. *Angiogenesis* **2014**, *17* (1), 109–118 DOI: 10.1007/s10456-013-9381-6.

(128) Zajac, E.; Schweighofer, B.; Kupriyanova, T. A.; Juncker-Jensen, A.; Minder, P.; Quigley, J. P.; Deryugina, E. I. Angiogenic capacity of M1- and M2-polarized macrophages is determined by the levels of TIMP-1 complexed with their secreted proMMP-9. *Blood* **2013**, *122* (25), 4054–4067 DOI: 10.1182/blood-2013-05-501494.

(129) Lolmede, K.; Campana, L.; Vezzoli, M.; Bosurgi, L.; Tonlorenzi, R.; Clementi, E.; Bianchi, M. E.; Cossu, G.; Manfredi, A. a; Brunelli, S.; et al. Inflammatory and alternatively activated human macrophages attract vessel-associated stem cells, relying on separate HMGB1- and MMP-9-dependent pathways. *J. Leukoc. Biol.* **2009**, *85* (5), 779–787 DOI: 10.1189/jlb.0908579.

(130) Spiller, K. L.; Nassiri, S.; Witherel, C. E.; Anfang, R. R.; Ng, J.; Nakazawa, K. R.; Yu, T.;

Vunjak-Novakovic, G. Sequential delivery of immunomodulatory cytokines to facilitate the M1-to-M2 transition of macrophages and enhance vascularization of bone scaffolds. *Biomaterials* **2015**, *37*, 194–207 DOI: 10.1016/j.biomaterials.2014.10.017.

(131) Zheng, G.; Ge, M.; Qiu, G.; Shu, Q.; Xu, J. Mesenchymal Stromal Cells Affect Disease Outcomes via Macrophage Polarization. *Stem Cells Int.* **2015**, *2015* DOI: 10.1155/2015/989473.

(132) Waterman, R. S.; Tomchuck, S. L.; Henkle, S. L.; Betancourt, A. M. A new mesenchymal stem cell (MSC) paradigm: Polarization into a pro-inflammatory MSC1 or an immunosuppressive MSC2 phenotype. *PLoS One* **2010**, *5* (4) DOI: 10.1371/journal.pone.0010088.

(133) Bernardo, M. E.; Fibbe, W. E. Mesenchymal stromal cells: Sensors and switchers of inflammation. *Cell Stem Cell* **2013**, *13* (4), 392–402 DOI: 10.1016/j.stem.2013.09.006.

(134) Anderson, P.; Souza-Moreira, L.; Morell, M.; Caro, M.; O'Valle, F.; Gonzalez-Rey, E.; Delgado, M. Adipose-derived mesenchymal stromal cells induce immunomodulatory macrophages which protect from experimental colitis and sepsis. *Gut* **2013**, *62* (8), 1131–1141 DOI: 10.1136/gutjnl-2012-302152.

(135) Shang, Q.; Bai, Y.; Wang, G.; Song, Q.; Guo, C.; Zhang, L.; Wang, Q. Delivery of Adipose-Derived Stem Cells Attenuates Adipose Tissue Inflammation and Insulin Resistance in Obese Mice Through Remodeling Macrophage Phenotypes. *Stem Cells Dev.* **2015**, *24* (17), 2052–2064 DOI: 10.1089/scd.2014.0557.

(136) Kim, J.; Hematti, P. Mesenchymal stem cell-educated macrophages: A novel type of alternatively activated macrophages. *Exp. Hematol.* **2009**, *37* (12), 1445–1453 DOI: 10.1016/j.exphem.2009.09.004.

(137) Melief, S. M.; Zwaginga, J. J.; Fibbe, W. E.; Roelofs, H. Adipose tissue-derived multipotent stromal cells have a higher immunomodulatory capacity than their bone marrow-derived counterparts. *Stem Cells Transl. Med.* **2013**, *2* (6), 455–463 DOI: 10.5966/sctm.2012-0184.

(138) Lee, M. J.; Kim, J.; Kim, M. Y.; Bae, Y.-S.; Ryu, S. H.; Lee, T. G.; Kim, J. H. Proteomic analysis

of tumor necrosis factor-alpha-induced secretome of human adipose tissue-derived mesenchymal stem cells. *J. Proteome Res.* **2010**, *9* (4), 1754–1762 DOI: 10.1021/pr900898n.

(139) Cantu, D. A.; Hematti, P.; Kao, W. J. Cell Encapsulating Biomaterial Regulates Mesenchymal Stromal/Stem Cell Differentiation and Macrophage Immunophenotype. *Stem Cells Transl. Med.* **2012**, *1* (10), 740–749 DOI: 10.5966/sctm.2012-0061.

(140) King, S. N.; Hanson, S. E.; Chen, X.; Kim, J.; Hematti, P.; Thibeault, S. L. In vitro characterization of macrophage interaction with mesenchymal stromal cell-hyaluronan hydrogel constructs. *J. Biomed. Mater. Res. - Part A* **2014**, *102* (3), 890–902 DOI: 10.1002/jbm.a.34746.

(141) Seebach, E.; Freischmidt, H.; Holschbach, J.; Fellenberg, J.; Richter, W. Mesenchymal stroma cells trigger early attraction of M1 macrophages and endothelial cells into fibrin hydrogels, stimulating long bone healing without long-term engraftment. *Acta Biomater.* **2014**, *10* (11), 4730–4741 DOI: 10.1016/j.actbio.2014.07.017.

(142) Lyons, F. G.; Al-Munajjed, A. A.; Kieran, S. M.; Toner, M. E.; Murphy, C. M.; Duffy, G. P.; O'Brien, F. J. The healing of bony defects by cell-free collagen-based scaffolds compared to stem cell-seeded tissue engineered constructs. *Biomaterials* **2010**, *31* (35), 9232–9243 DOI: 10.1016/j.biomaterials.2010.08.056.

(143) Han, T. T. Y.; Toutounji, S.; Amsden, B. G.; Flynn, L. E. Adipose-derived stromal cells mediate in vivo adipogenesis, angiogenesis and inflammation in decellularized adipose tissue bioscaffolds. *Biomaterials* **2015**, *72*, 125–137 DOI: 10.1016/j.biomaterials.2015.08.053.

(144) Cooke, J. P.; Losordo, D. W. Modulating the Vascular Response to Limb Ischemia: Angiogenic and Cell Therapies. *Circ. Res.* **2015**, *116* (9), 1561–1578 DOI: 10.1161/CIRCRESAHA.115.303565.

(145) Segers, V. F. M.; Lee, R. T. Biomaterials to enhance stem cell function in the heart. *Circ. Res.* **2011**, *109* (8), 910–922 DOI: 10.1161/CIRCRESAHA.111.249052.

(146) Silva, E. A.; Kim, E. S.; Kong, H. J.; Mooney, D. J. Material-based deployment enhances efficacy

of endothelial progenitor cells. *Proc. Natl. Acad. Sci. U. S. A.* **2008**, *105* (38), 14347–14352 DOI: 10.1073/pnas.0803873105.

(147) Sharifi, S.; Blanquer, S. B. G.; van Kooten, T. G.; Grijpma, D. W. Biodegradable nanocomposite hydrogel structures with enhanced mechanical properties prepared by photo-crosslinking solutions of poly(trimethylene carbonate)–poly(ethylene glycol)–poly(trimethylene carbonate) macromonomers and nanoclay particles. *Acta Biomater.* **2012**, *8* (12), 4233–4243 DOI: 10.1016/j.actbio.2012.09.014.

(148) Cao, Z.; Yang, Q.; Fan, C.; Liu, L.; Liao, L. Biocompatible, ionic-strength-sensitive, double-network hydrogel based on chitosan and an oligo(trimethylene carbonate)-poly(ethylene glycol)-oligo(trimethylene carbonate) triblock copolymer. *J. Appl. Polym. Sci.* **2015**, *132* (35) DOI: 10.1002/app.42459.

(149) Anjum, F.; Carroll, A.; Young, S. A.; Flynn, L. E.; Amsden, B. G. Tough, Semisynthetic Hydrogels for Adipose Derived Stem Cell Delivery for Chondral Defect Repair. *Macromol. Biosci.* **2017**, *17* (5), 1600373 DOI: 10.1002/mabi.201600373.

(150) Hyun, H.; Kim, M. S.; Khang, G.; Lee, H. B. Ring-opening polymerization of trimethylene carbonate by poly(ethylene glycol) in the presence of HCl·Et2O as a monomer activator. *J. Polym. Sci. Part A Polym. Chem.* **2006**, *44* (13), 4235–4241 DOI: 10.1002/pola.21504.

(151) Cho, J. S.; Kim, B. S.; Hyun, H.; Youn, J. Y.; Kim, M. S.; Ko, J. H.; Park, Y. H.; Khang, G.; Lee, H. B. Precise preparation of four-arm-poly(ethylene glycol)-block-poly(trimethylene carbonate) star block copolymers via activated monomer mechanism and examination of their solution properties. *Polymer (Guildf).* **2008**, *49* (7), 1777–1782 DOI: 10.1016/j.polymer.2008.02.030.

(152) Kim, B. S.; Oh, J. M.; Cho, J. S.; Lee, S. H.; Lee, B.; Khang, G.; Lee, H. B.; Kim, M. S. Comparison of micelles formed by amphiphilic poly(ethylene glycol)- b -poly(trimethylene carbonate) star block copolymers. *J. Appl. Polym. Sci.* **2009**, *111* (4), 1706–1712 DOI: 10.1002/app.29179.

(153) Amsden, B. G.; Sukarto, A.; Knight, D. K.; Shapka, S. N. Methacrylated glycol chitosan as a photopolymerizable biomaterial. *Biomacromolecules* **2007**, *8* (12), 3758–3766 DOI: 10.1021/bm700691e.

(154) Sukarto, A.; Yu, C.; Flynn, L. E.; Amsden, B. G. Co-delivery of Adipose-Derived Stem Cells and Growth Factor-Loaded Microspheres in RGD-Grafted N-Methacrylate Glycol Chitosan Gels for Focal Chondral Repair. *Biomacromolecules* **2012**, *13* (8), 2490–2502 DOI: 10.1021/bm300733n.

(155) Liu, H.-T.; Li, W.-M.; Xu, G.; Li, X.-Y.; Bai, X.-F.; Wei, P.; Yu, C.; Du, Y.-G. Chitosan oligosaccharides attenuate hydrogen peroxide-induced stress injury in human umbilical vein endothelial cells. *Pharmacol. Res.* **2009**, *59* (3), 167–175 DOI: 10.1016/j.phrs.2008.12.001.

(156) Qiao, Y.; Bai, X.-F.; Du, Y.-G. Chitosan oligosaccharides protect mice from LPS challenge by attenuation of inflammation and oxidative stress. *Int. Immunopharmacol.* **2011**, *11* (1), 121–127 DOI: 10.1016/j.intimp.2010.10.016.

(157) Alvarado-Velez, M.; Pai, S. B.; Bellamkonda, R. V. Hydrogels as Carriers for Stem Cell Transplantation. *IEEE Trans. Biomed. Eng.* **2014**, *61* (5), 1474–1481 DOI: 10.1109/TBME.2014.2305753.

(158) Kharkar, P. M.; Kiick, K. L.; Kloxin, A. M. Designing degradable hydrogels for orthogonal control of cell microenvironments. *Chem. Soc. Rev.* **2013**, *42* (17), 7335–7372 DOI: 10.1039/c3cs60040h.

(159) Huang, Y.; Chen, B.; Zhang, J. Oxygen Tension Variation in Ischemic Gastrocnemius Muscle, Marrow, and different Hypoxic Conditions In Vitro. *Med. Sci. Monit.* **2014**, *20*, 2171–2176 DOI: 10.12659/MSM.892354.

(160) Hayami, J. W. S.; Waldman, S. D.; Amsden, B. G. Photo-cross-linked methacrylated polysaccharide solution blends with high chondrocyte viability, minimal swelling, and moduli similar to load bearing soft tissues. *Eur. Polym. J.* **2015**, 1–11 DOI: 10.1016/j.eurpolymj.2015.01.038.

(161) Flynn, L.; Semple, J. L.; Woodhouse, K. A. Decellularized placental matrices for adipose tissue engineering. *J. Biomed. Mater. Res. A* **2006**, *79* (2), 359–369 DOI: 10.1002/jbm.a.30762.

(162) Russo, V.; Yu, C.; Belliveau, P.; Hamilton, A.; Flynn, L. E. Comparison of Human Adipose-Derived Stem Cells Isolated from Subcutaneous, Omental, and Intrathoracic Adipose Tissue Depots for Regenerative Applications. *Stem Cells Transl. Med.* **2014**, *3* (2), 206–217 DOI: 10.5966/sctm.2013-0125.

(163) Bourin, P.; Bunnell, B. A.; Casteilla, L.; Dominici, M.; Katz, A. J.; March, K. L.; Redl, H.; Rubin, J. P.; Yoshimura, K.; Gimble, J. M. Stromal cells from the adipose tissue-derived stromal vascular fraction and culture expanded adipose tissue-derived stromal/stem cells: A joint statement of the International Federation for Adipose Therapeutics and Science (IFATS) and the International So. *Cytotherapy* **2013**, *15* (6), 641–648 DOI: 10.1016/j.jcyt.2013.02.006.

(164) Gronthos, S.; Franklin, D. M.; Leddy, H. a; Robey, P. G.; Storms, R. W.; Gimble, J. M. Surface protein characterization of human adipose tissue-derived stromal cells. *J. Cell. Physiol.* **2001**, *189* (1), 54–63 DOI: 10.1002/jcp.1138.

(165) Jurgens, W. J. F. M.; Lu, Z.; Zandieh-Doulabi, B.; Kuik, D. J.; Ritt, M. J. P. F.; Helder, M. N. Hyperosmolarity and hypoxia induce chondrogenesis of adipose-derived stem cells in a collagen type 2 hydrogel. *J. Tissue Eng. Regen. Med.* **2012**, *6* (7), 570–578 DOI: 10.1002/term.464.

(166) Amsden, B. Solute Diffusion within Hydrogels. Mechanisms and Models. *Macromolecules* **1998**, *31* (23), 8382–8395 DOI: 10.1021/ma980765f.

(167) Shin, H.; Temenoff, J. S.; Mikos, A. G. In Vitro Cytotoxicity of Unsaturated Oligo[poly(ethylene glycol) fumarate] Macromers and Their Cross-Linked Hydrogels. *Biomacromolecules* **2003**, *4* (3), 552–560 DOI: 10.1021/bm020121m.

(168) Winter, H. H.; Chambon, F. Analysis of Linear Viscoelasticity of a Crosslinking Polymer at the Gel Point. *J. Rheol. (N. Y. N. Y).* **1986**, *30* (2), 367–382 DOI: 10.1122/1.549853.

(169) Shibayama, M. Structure-mechanical property relationship of tough hydrogels. *Soft Matter* **2012**, *8*

(31), 8030 DOI: 10.1039/c2sm25325a.

(170) Haque, M. A.; Kurokawa, T.; Gong, J. P. Super tough double network hydrogels and their application as biomaterials. *Polymer (Guildf).* **2012**, *53* (9), 1805–1822 DOI: 10.1016/j.polymer.2012.03.013.

(171) Henderson, K. J.; Zhou, T. C.; Otim, K. J.; Shull, K. R. Ionically Cross-Linked Triblock Copolymer Hydrogels with High Strength. *Macromolecules* **2010**, *43* (14), 6193–6201 DOI: 10.1021/ma100963m.

(172) Nachtergael, A.; Coulembier, O.; Dubois, P.; Helvenstein, M.; Duez, P.; Blankert, B.; Mespouille, L. Organocatalysis Paradigm Revisited: Are Metal-Free Catalysts Really Harmless? *Biomacromolecules* **2015**, *16* (2), 507–514 DOI: 10.1021/bm5015443.

(173) Temenoff, J. S.; Park, H.; Jabbari, E.; Conway, D. E.; Sheffield, T. L.; Ambrose, C. G.; Mikos, A. G. Thermally cross-linked oligo(poly(ethylene glycol) fumarate) hydrogels support osteogenic differentiation of encapsulated marrow stromal cells in vitro. *Biomacromolecules* **2004**, *5* (1), 5–10 DOI: 10.1021/bm030067p.

(174) Klouda, L.; Perkins, K. R.; Watson, B. M.; Hacker, M. C.; Bryant, S. J.; Raphael, R. M.; Kasper, F. K.; Mikos, A. G. Thermoresponsive, in situ cross-linkable hydrogels based on N-isopropylacrylamide: fabrication, characterization and mesenchymal stem cell encapsulation. *Acta Biomater.* **2011**, *7* (4), 1460–1467 DOI: 10.1016/j.actbio.2010.12.027.

(175) Saxena, V.; Kim, M.; Keah, N. M.; Neuwirth, A. L.; Stoeckl, B. D.; Bickard, K.; Restle, D. J.; Salowe, R.; Wang, M. Y.; Steinberg, D. R.; et al. Anatomic Mesenchymal Stem Cell-Based Engineered Cartilage Constructs for Biologic Total Joint Replacement. *Tissue Eng. Part A* **2016**, *22* (3–4), 386–395 DOI: 10.1089/ten.tea.2015.0384.

(176) Hong, Y.; Mao, Z.; Wang, H.; Gao, C.; Shen, J. Covalently crosslinked chitosan hydrogel formed at neutral pH and body temperature. *J. Biomed. Mater. Res. Part A* **2006**, *79A* (4), 913–922 DOI: 10.1002/jbm.a.30837.

(177) Hong, Y.; Song, H.; Gong, Y.; Mao, Z.; Gao, C.; Shen, J. Covalently crosslinked chitosan hydrogel: properties of in vitro degradation and chondrocyte encapsulation. *Acta Biomater.* **2007**, *3* (1), 23–31 DOI: 10.1016/j.actbio.2006.06.007.

(178) Guo, Y.; Yuan, T.; Xiao, Z.; Tang, P.; Xiao, Y.; Fan, Y.; Zhang, X. Hydrogels of collagen/chondroitin sulfate/hyaluronan interpenetrating polymer network for cartilage tissue engineering. *J. Mater. Sci. Mater. Med.* **2012**, *23* (9), 2267–2279 DOI: 10.1007/s10856-012-4684-5.

(179) Ifkovits, J. L.; Tous, E.; Minakawa, M.; Morita, M.; Robb, J. D.; Koomalsingh, K. J.; Gorman, J. H.; Gorman, R. C.; Burdick, J. A. Injectable hydrogel properties influence infarct expansion and extent of postinfarction left ventricular remodeling in an ovine model. *Proc. Natl. Acad. Sci.* **2010**, *107* (25), 11507–11512 DOI: 10.1073/pnas.1004097107.

(180) Tous, E.; Ifkovits, J. L.; Koomalsingh, K. J.; Shuto, T.; Soeda, T.; Kondo, N.; Gorman, J. H.; Gorman, R. C.; Burdick, J. A. Influence of Injectable Hyaluronic Acid Hydrogel Degradation Behavior on Infarction-Induced Ventricular Remodeling. *Biomacromolecules* **2011**, *12* (11), 4127–4135 DOI: 10.1021/bm201198x.

(181) Mironi-Harpaz, I.; Wang, D. Y.; Venkatraman, S.; Seliktar, D. Photopolymerization of cell-encapsulating hydrogels: crosslinking efficiency versus cytotoxicity. *Acta Biomater.* **2012**, *8* (5), 1838–1848 DOI: 10.1016/j.actbio.2011.12.034.

(182) Stubbs, S. L.; Hsiao, S. T.-F.; Peshavariya, H. M.; Lim, S. Y.; Dusting, G. J.; Dilley, R. J. Hypoxic Preconditioning Enhances Survival of Human Adipose-Derived Stem Cells and Conditions Endothelial Cells In Vitro. *Stem Cells Dev.* **2012**, *21* (11), 1887–1896 DOI: 10.1089/scd.2011.0289.

(183) Abdeen, A. A.; Weiss, J. B.; Lee, J.; Kilian, K. A. Matrix Composition and Mechanics Direct Proangiogenic Signaling from Mesenchymal Stem Cells. *Tissue Eng. Part A* **2014**, *20* (19–20), 2737–2745 DOI: 10.1089/ten.tea.2013.0661.

(184) Wan, C.-D.; Cheng, R.; Wang, H.-B.; Liu, T. Immunomodulatory effects of mesenchymal stem cells derived from adipose tissues in a rat orthotopic liver transplantation model. *Hepatobiliary Pancreat. Dis. Int* **2008**, *7* (1), 29–33 DOI: 1055 [pii].

(185) Gonzalez-Simon, A. L.; Eniola-Adefeso, O. Host Response to Biomaterials. In *Engineering Biomaterials for Regenerative Medicine*; Springer New York: New York, NY, 2012; pp 143–159.

(186) Granger, D.; E, S. *Inflammation and the Microcirculation*; Morgan & Claypool Life Sciences: San Rafael (CA), 2010.

(187) Holladay, C.; Power, K.; Sefton, M.; O'Brien, T.; Gallagher, W. M.; Pandit, A. Functionalized scaffold-mediated interleukin 10 gene delivery significantly improves survival rates of stem cells in vivo. *Mol. Ther.* **2011**, *19* (5), 969–978 DOI: 10.1038/mt.2010.311.

(188) Jay, S. M.; Shepherd, B. R.; Andrejecsk, J. W.; Kyriakides, T. R.; Pober, J. S.; Saltzman, W. M. Dual delivery of VEGF and MCP-1 to support endothelial cell transplantation for therapeutic vascularization. *Biomaterials* **2010**, *31* (11), 3054–3062 DOI: 10.1016/j.biomaterials.2010.01.014.

(189) Hsu, C. W.; Poché, R. A.; Saik, J. E.; Ali, S.; Wang, S.; Yosef, N.; Calderon, G. A.; Scott, L.; Vadakkan, T. J.; Larina, I. V.; et al. Improved angiogenesis in response to localized delivery of macrophage-recruiting molecules. *PLoS One* **2015**, *10* (7), 1–27 DOI: 10.1371/journal.pone.0131643.

(190) Feng, Y.; Li, Q.; Wu, D.; Niu, Y.; Yang, C.; Dong, L.; Wang, C. A macrophage-activating, injectable hydrogel to sequester endogenous growth factors for in situ angiogenesis. *Biomaterials* **2017**, *134*, 128–142 DOI: 10.1016/j.biomaterials.2017.04.042.

(191) Tous, E.; Weber, H. M.; Lee, M. H.; Koomalsingh, K. J.; Shuto, T.; Kondo, N.; Gorman, J. H.; Lee, D.; Gorman, R. C.; Burdick, J. A. Tunable hydrogel-microsphere composites that modulate local inflammation and collagen bulking. *Acta Biomater.* **2012**, *8* (9), 3218–3227 DOI: 10.1016/j.actbio.2012.05.027.

(192) Reeves, A. R. D.; Spiller, K. L.; Freytes, D. O.; Vunjak-Novakovic, G.; Kaplan, D. L. Controlled

release of cytokines using silk-biomaterials for macrophage polarization. *Biomaterials* **2015**, *73*, 272–283 DOI: 10.1016/j.biomaterials.2015.09.027.

(193) Sukarto, A. Co-delivery of Growth Factor-Loaded Microspheres and Adipose- Derived Stem Cells In A Gel Matrix for Cartilage Repair Thesis submitted to the Department of Chemical Engineering, Queen's University, 2011.

(194) Vasconcelos, D. P.; Fonseca, A. C.; Costa, M.; Amaral, I. F.; Barbosa, M. A.; Águas, A. P.; Barbosa, J. N. Macrophage polarization following chitosan implantation. *Biomaterials* **2013**, *34* (38), 9952–9959 DOI: 10.1016/j.biomaterials.2013.09.012.

(195) Zhao, Y.; Wang, Y.; Gong, J.; Yang, L.; Niu, C.; Ni, X.; Wang, Y.; Peng, S.; Gu, X.; Sun, C.; et al. Chitosan degradation products facilitates peripheral nerve regeneration by improving macrophage-constructed microenvironments. *Biomaterials* **2017**, *134*, 64–77 DOI: 10.1016/j.biomaterials.2017.02.026.

(196) Porporatto, C.; Bianco, I. D.; Riera, C. M.; Correa, S. G. Chitosan induces different L-arginine metabolic pathways in resting and inflammatory macrophages. *Biochem. Biophys. Res. Commun.* **2003**, *304* (2), 266–272 DOI: 10.1016/S0006-291X(03)00579-5.

(197) Yoon, H. J.; Moon, M. E.; Park, H. S.; Im, S. Y.; Kim, Y. H. Chitosan oligosaccharide (COS) inhibits LPS-induced inflammatory effects in RAW 264.7 macrophage cells. *Biochem. Biophys. Res. Commun.* **2007**, *358* (3), 954–959 DOI: 10.1016/j.bbrc.2007.05.042.

(198) Reid, B.; Gibson, M.; Singh, A.; Taube, J.; Furlong, C.; Murcia, M.; Elisseeff, J. PEG hydrogel degradation and the role of the surrounding tissue environment. *J. Tissue Eng. Regen. Med.* **2015**, *9* (3), 315–318 DOI: 10.1002/term.1688.

(199) Lynn, A. D.; Kyriakides, T. R.; Bryant, S. J. Characterization of the in vitro macrophage response and in vivo host response to poly(ethylene glycol)-based hydrogels. *J. Biomed. Mater. Res. - Part A* **2010**, *93* (3), 941–953 DOI: 10.1002/jbm.a.32595.

(200) Zhang, Z.; Kuijer, R.; Bulstra, S. K.; Grijpma, D. W.; Feijen, J. The in vivo and in vitro

degradation behavior of poly(trimethylene carbonate). *Biomaterials* **2006**, *27* (9), 1741–1748 DOI: 10.1016/j.biomaterials.2005.09.017.

(201) Fukushima, K. Poly(trimethylene carbonate)-based polymers engineered for biodegradable functional biomaterials. *Biomater. Sci.* **2015**, *4*, 9–24 DOI: 10.1039/C5BM00123D.

(202) Gottfried, E.; Kunz-Schughart, L. A.; Weber, A.; Rehli, M.; Peuker, A.; Müller, A.; Kastenberger, M.; Brockhoff, G.; Andreesen, R.; Kreutz, M. Expression of CD68 in non-myeloid cell types. *Scand. J. Immunol.* **2008**, *67* (5), 453–463 DOI: 10.1111/j.1365-3083.2008.02091.x.

(203) Pilling, D.; Fan, T.; Huang, D.; Kaul, B.; Gomer, R. H. Identification of markers that distinguish monocyte-derived fibrocytes from monocytes, macrophages, and fibroblasts. *PLoS One* **2009**, *4* (10), 31–33 DOI: 10.1371/journal.pone.0007475.

(204) Hameed, a; Hruban, R. H.; Gage, W.; Pettis, G.; Fox, W. M. Immunohistochemical expression of CD68 antigen in human peripheral blood T cells. *Hum. Pathol.* **1994**, *25* (9), 872–876.

(205) Heo, S. C.; Jeon, E. S.; Lee, I. H.; Kim, H. S.; Kim, M. B.; Kim, J. H. Tumor Necrosis Factor-α-Activated Human Adipose Tissue–Derived Mesenchymal Stem Cells Accelerate Cutaneous Wound Healing through Paracrine Mechanisms. *J. Invest. Dermatol.* **2011**, *131* (7), 1559–1567 DOI: 10.1038/jid.2011.64.

(206) Moestrup, S.; Møller, H. CD163: a regulated hemoglobin scavenger receptor with a role in the anti-inflammatory response. *Ann. Med.* **2004**, *36* (5), 347–354 DOI: 10.1080/07853890410033171.

(207) Adutler-Lieber, S.; Ben-Mordechai, T.; Naftali-Shani, N.; Asher, E.; Loberman, D.; Raanani, E.; Leor, J. Human Macrophage Regulation Via Interaction With Cardiac Adipose Tissue-Derived Mesenchymal Stromal Cells. *J. Cardiovasc. Pharmacol. Ther.* **2012**, *18* (1), 78–86 DOI: 10.1177/1074248412453875.

(208) Brown, B. N.; Badylak, S. F. Expanded applications, shifting paradigms and an improved understanding of host-biomaterial interactions. *Acta Biomater.* **2013**, *9* (2), 4948–4955 DOI:

10.1016/j.actbio.2012.10.025.

(209) Rath, M.; Müller, I.; Kropf, P.; Closs, E. I.; Munder, M. Metabolism via arginase or nitric oxide synthase: Two competing arginine pathways in macrophages. *Front. Immunol.* **2014**, *5* (OCT), 1–10 DOI: 10.3389/fimmu.2014.00532.

(210) Pesce, J. T.; Ramalingam, T. R.; Mentink-Kane, M. M.; Wilson, M. S.; Kasmi, K. C. E.; Smith, A. M.; Thompson, R. W.; Cheever, A. W.; Murray, P. J.; Wynn, T. A. Arginase-1-expressing macrophages suppress Th2 cytokine-driven inflammation and fibrosis. *PLoS Pathog.* **2009**, *5* (4) DOI: 10.1371/journal.ppat.1000371.

(211) Sainson, R. C. A.; Johnston, D. A.; Chu, H. C.; Holderfield, M. T.; Nakatsu, M. N.; Crampton, S. P.; Davis, J.; Conn, E.; Hughes, C. C. W. TNF primes endothelial cells for angiogenic sprouting by inducing a tip cell phenotype. *Blood* **2008**, *111* (10), 4997–5007 DOI: 10.1182/blood-2007-08-108597.

(212) Fantin, A.; Vieira, J. M.; Gestri, G.; Denti, L.; Schwarz, Q.; Prykhozhij, S.; Peri, F.; Wilson, S. W.; Ruhrberg, C. Tissue macrophages act as cellular chaperones for vascular anastomosis downstream of VEGF-mediated endothelial tip cell induction. *Blood* **2010**, *116* (5), 829–840 DOI: 10.1182/blood-2009-12-257832.

(213) Jadhav, U.; Chigurupati, S.; Lakka, S. S.; Mohanam, S. Inhibition of matrix metalloproteinase-9 reduces in vitro invasion and angiogenesis in human microvascular endothelial cells. *Int. J. Oncol.* **2004**, *25* (5), 1407–1414.

(214) Ardi, V. C.; Kupriyanova, T. A.; Deryugina, E. I.; Quigley, J. P. Human neutrophils uniquely release TIMP-free MMP-9 to provide a potent catalytic stimulator of angiogenesis. *Proc. Natl. Acad. Sci.* **2007**, *104* (51), 20262–20267 DOI: 10.1073/pnas.0706438104.

(215) Norgren, L.; Hiatt, W. R.; Dormandy, J. A.; Nehler, M. R.; Harris, K. A.; Fowkes, F. G. R. Inter-Society Consensus for the Management of Peripheral Arterial Disease (TASC II). *J. Vasc. Surg.* **2007**, *45* (1), S5–S67 DOI: 10.1016/j.jvs.2006.12.037.

(216) Fowkes, F. G. R.; Rudan, D.; Rudan, I.; Aboyans, V.; Denenberg, J. O.; McDermott, M. M.; Norman, P. E.; Sampson, U. K.; Williams, L. J.; Mensah, G. A.; et al. Comparison of global estimates of prevalence and risk factors for peripheral artery disease in 2000 and 2010: a systematic review and analysis. *Lancet* **2013**, *382* (9901), 1329–1340 DOI: 10.1016/S0140-6736(13)61249-0.

(217) Raval, Z.; Losordo, D. W. Cell Therapy of Peripheral Arterial Disease: From Experimental Findings to Clinical Trials. *Circ. Res.* **2013**, *112* (9), 1288–1302 DOI: 10.1161/CIRCRESAHA.113.300565.

(218) Brenes, R. A.; Jadlowiec, C. C.; Bear, M.; Hashim, P.; Protack, C. D.; Li, X.; Lv, W.; Collins, M. J.; Dardik, A. Toward a mouse model of hind limb ischemia to test therapeutic angiogenesis. *J. Vasc. Surg.* **2012**, *56* (6), 1669–1679 DOI: 10.1016/j.jvs.2012.04.067.

(219) Hellingman, A. A.; Bastiaansen, A. J. N. M.; De Vries, M. R.; Seghers, L.; Lijkwan, M. A.; Löwik, C. W.; Hamming, J. F.; Quax, P. H. A. Variations in surgical procedures for hind limb ischaemia mouse models result in differences in collateral formation. *Eur. J. Vasc. Endovasc. Surg.* **2010**, *40* (6), 796–803 DOI: 10.1016/j.ejvs.2010.07.009.

(220) Chalothorn, D.; Faber, J. E. Strain-dependent variation in collateral circulatory function in mouse hindlimb. *Physiol. Genomics* **2010**, *42* (3), 469–479 DOI: 10.1152/physiolgenomics.00070.2010.

(221) Westvik, T. S.; Fitzgerald, T. N.; Muto, A.; Maloney, S. P.; Pimiento, J. M.; Fancher, T. T.; Magri, D.; Westvik, H. H.; Nishibe, T.; Velazquez, O. C.; et al. Limb ischemia after iliac ligation in aged mice stimulates angiogenesis without arteriogenesis. *J. Vasc. Surg.* **2009**, *49* (2), 464–473 DOI: 10.1016/j.jvs.2008.08.077.

(222) Limbourg, A.; Korff, T.; Napp, L. C.; Schaper, W.; Drexler, H.; Limbourg, F. P. Evaluation of postnatal arteriogenesis and angiogenesis in a mouse model of hind-limb ischemia. *Nat. Protoc.* **2009**, *4* (12), 1737–1746 DOI: 10.1038/nprot.2009.185.

(223) Xu, Y.; Fu, M.; Li, Z.; Fan, Z.; Li, X.; Liu, Y.; Anderson, P. M.; Xie, X.; Liu, Z.; Guan, J. A

prosurvival and proangiogenic stem cell delivery system to promote ischemic limb regeneration. *Acta Biomater.* **2016**, *31*, 99–113 DOI: 10.1016/j.actbio.2015.12.021.

(224) Greiner, D. L.; Hesselton, R. a; Shultz, L. D.; a Hesselton, R.; Shultz, L. D.; Hesselton, R. a; Shultz, L. D. SCID mouse models of human stem cell engraftment. *Stem Cells* **1998**, *16* (3), 166–177 DOI: 10.1002/stem.160166.

(225) Shultz, L. D.; Schweitzer, P. A.; Christianson, S. W.; Gott, B.; Tennent, B.; Mckenna, S.; Mobraaten, L.; Shultz, L. D.; Schweitzer, P. A.; Christianson, S. W.; et al. Multiple defects in innate and adaptive immunologic function in NOD / LtSz-scid mice. *J. Immunol.* **2010**, *154* (15), 180–191.

(226) Market, E.; Papavasiliou, F. N. V(D)J recombination and the evolution of the adaptive immune system. *PLoS Biol.* **2003**, *1* (1), 24–27 DOI: 10.1371/journal.pbio.0000016.

(227) Capoccia, B. J.; Robson, D. L.; Levac, K. D.; Maxwell, D. J.; Hohm, S. A.; Neelamkavil, M. J.; Bell, G. I.; Xenocostas, A.; Link, D. C.; Piwnica-Worms, D.; et al. Revascularization of ischemic limbs after transplantation of human bone marrow cells with high aldehyde dehydrogenase activity. *Blood* **2009**, *113* (21), 5340–5351 DOI: 10.1182/blood-2008-04-154567.

(228) Putman, D. M.; Liu, K. Y.; Broughton, H. C.; Bell, G. I.; Hess, D. a. Umbilical cord blood-derived aldehyde dehydrogenase-expressing progenitor cells promote recovery from acute ischemic injury. *Stem Cells* **2012**, *30* (10), 2248–2260 DOI: 10.1002/stem.1206.

(229) Putman, D. M.; Cooper, T. T.; Sherman, S. E.; Seneviratne, A. K.; Hewitt, M.; Bell, G. I.; Hess, D. A. Expansion of Umbilical Cord Blood Aldehyde Dehydrogenase Expressing Cells Generates Myeloid Progenitor Cells that Stimulate Limb Revascularization. *Stem Cells Transl. Med.* **2017**, *6* (7), 1607–1619 DOI: 10.1002/sctm.16-0472.

(230) Kochi, T.; Imai, Y.; Takeda, A.; Watanabe, Y.; Mori, S.; Tachi, M.; Kodama, T. Characterization of the arterial anatomy of the murine hindlimb: Functional role in the design and understanding of ischemia models. *PLoS One* **2013**, *8* (12) DOI: 10.1371/journal.pone.0084047.

(231) Wang, J.; Cui, W.; Ye, J.; Ji, S.; Zhao, X.; Zhan, L.; Feng, J.; Zhang, Z.; Zhao, Y. A cellular delivery system fabricated with autologous BMSCs and collagen scaffold enhances angiogenesis and perfusion in ischemic hind limb. *J. Biomed. Mater. Res. - Part A* **2012**, *100 A* (6), 1438–1447 DOI: 10.1002/jbm.a.34081.

(232) Parisi-Amon, A.; Mulyasasmita, W.; Chung, C.; Heilshorn, S. C. Protein-Engineered Injectable Hydrogel to Improve Retention of Transplanted Adipose-Derived Stem Cells. *Adv. Healthc. Mater.* **2013**, *2* (3), 428–432 DOI: 10.1002/adhm.201200293.

(233) Roche, E. T.; Hastings, C. L.; Lewin, S. A.; Shvartsman, D. E.; Brudno, Y.; Vasilyev, N. V.; O'Brien, F. J.; Walsh, C. J.; Duffy, G. P.; Mooney, D. J. Comparison of biomaterial delivery vehicles for improving acute retention of stem cells in the infarcted heart. *Biomaterials* **2014**, *35* (25), 6850–6858 DOI: 10.1016/j.biomaterials.2014.04.114.

(234) Wälchli, T.; Mateos, J. M.; Weinman, O.; Babic, D.; Regli, L.; Hoerstrup, S. P.; Gerhardt, H.; Schwab, M. E.; Vogel, J. Quantitative assessment of angiogenesis, perfused blood vessels and endothelial tip cells in the postnatal mouse brain. *Nat. Protoc.* **2014**, *10* (1), 53–74 DOI: 10.1038/nprot.2015.002.

(235) Robertson, R. T.; Levine, S. T.; Haynes, S. M.; Gutierrez, P.; Baratta, J. L.; Tan, Z.; Longmuir, K. J. Use of labeled tomato lectin for imaging vasculature structures. *Histochem. Cell Biol.* **2014**, *143* (2), 225–234 DOI: 10.1007/s00418-014-1301-3.

(236) Bryson, J. L.; Coles, M. C.; Manley, N. R. A Method for Labeling Vasculature in Embryonic Mice. *J. Vis. Exp.* **2011**, No. 56 DOI: 10.3791/3267.

(237) Helfrich, I.; Schadendorf, D. Blood vessel maturation, vascular phenotype and angiogenic potential in malignant melanoma: One step forward for overcoming anti-angiogenic drug resistance? *Mol. Oncol.* **2011**, *5* (2), 137–149 DOI: 10.1016/j.molonc.2011.01.003.

(238) Van Harmelen, V.; Skurk, T.; Röhrig, K.; Lee, Y.-M.; Halbleib, M.; Aprath-Husmann, I.; Hauner, H. Effect of BMI and age on adipose tissue cellularity and differentiation capacity in women. *Int.*

J. Obes. **2003**, *27*, 889–895 DOI: 10.1038/sj.ijo.0802314.

(239) Flynn, L. E. The use of decellularized adipose tissue to provide an inductive microenvironment for the adipogenic differentiation of human adipose-derived stem cells. *Biomaterials* **2010**, *31* (17), 4715–4724 DOI: 10.1016/j.biomaterials.2010.02.046.

(240) Serreze, D. V; Gaedeke, J. W.; Leiter, E. H. Hematopoietic stem-cell defects underlying abnormal macrophage development and maturation in NOD/Lt mice: defective regulation of cytokine receptors and protein kinase C. *Proc. Natl. Acad. Sci. U. S. A.* **1993**, *90* (20), 9625–9629 DOI: 10.1073/pnas.90.20.9625.

(241) Cao, Y.; Sun, Z.; Liao, L.; Meng, Y.; Han, Q.; Zhao, R. C. Human adipose tissue-derived stem cells differentiate into endothelial cells in vitro and improve postnatal neovascularization in vivo. *Biochem. Biophys. Res. Commun.* **2005**, *332* (2), 370–379 DOI: 10.1016/j.bbrc.2005.04.135.

(242) Ito, R.; Takahashi, T.; Katano, I.; Ito, M. Current advances in humanized mouse models. *Cell. Mol. Immunol.* **2012**, *9* (3), 208–214 DOI: 10.1038/cmi.2012.2.

(243) Willinger, T.; Rongvaux, A.; Takizawa, H.; Yancopoulos, G. D.; Valenzuela, D. M.; Murphy, A. J.; Auerbach, W.; Eynon, E. E.; Stevens, S.; Manz, M. G.; et al. Human IL-3/GM-CSF knock-in mice support human alveolar macrophage development and human immune responses in the lung. *Proc. Natl. Acad. Sci.* **2011**, *108* (6), 2390–2395 DOI: 10.1073/pnas.1019682108.

(244) Li, J.; Ezzelarab, M. B.; Cooper, D. K. C. Do mesenchymal stem cells function across species barriers? Relevance for xenotransplantation. *Xenotransplantation* **2012**, *19* (5), 273–285 DOI: 10.1111/xen.12000.

(245) Anseth, K. S.; Wang, C. M.; Bowman, C. N. Reaction behaviour and kinetic constants for photopolymerizations of multi(meth)acrylate monomers. *Polymer (Guildf).* **1994**, *35* (15), 3243–3250 DOI: 10.1016/0032-3861(94)90129-5.

(246) Buwalda, S. J.; Perez, L. B.; Teixeira, S.; Calucci, L.; Forte, C.; Feijen, J.; Dijkstra, P. J. Self-assembly and photo-cross-linking of eight-armed PEG-PTMC star block copolymers.

Biomacromolecules **2011**, *12* (7), 2746–2754 DOI: 10.1021/bm200515h.

(247) Hirano, S.; Tsuchida, H.; Nagao, N. N-acetylation in chitosan and the rate of its enzymic hydrolysis. *Biomaterials* **1989**, *10* (8), 574–576.

(248) Bat, E.; van Kooten, T. G.; Feijen, J.; Grijpma, D. W. Resorbable elastomeric networks prepared by photocrosslinking of high-molecular-weight poly(trimethylene carbonate) with photoinitiators and poly(trimethylene carbonate) macromers as crosslinking aids. *Acta Biomater.* **2011**, *7* (5), 1939–1948 DOI: 10.1016/j.actbio.2011.01.010.

(249) Qazi, T. H.; Mooney, D. J.; Duda, G. N.; Geissler, S. Biomaterials that promote cell-cell interactions enhance the paracrine function of MSCs. *Biomaterials* **2017**, *140*, 103–114 DOI: 10.1016/j.biomaterials.2017.06.019.

(250) Hakamata, Y.; Murakami, T.; Kobayashi, E. "Firefly rats" as an organ/cellular source for long-term in vivo bioluminescent imaging. *Transplantation* **2006**, *81* (8), 1179–1184 DOI: 10.1097/01.tp.0000203137.06587.4a.

(251) Zagorchev, L.; Oses, P.; Zhuang, Z. W.; Moodie, K.; Mulligan-Kehoe, M.; Simons, M.; Couffinhal, T. Micro computed tomography for vascular exploration. *J. Angiogenes. Res.* **2010**, *2* (1), 7 DOI: 10.1186/2040-2384-2-7.

Appendix A

Supplemental Information

A.1 ^{1}H NMR Spectra of PEG-(PTMC-A)$_2$ copolymers and mechanical properties

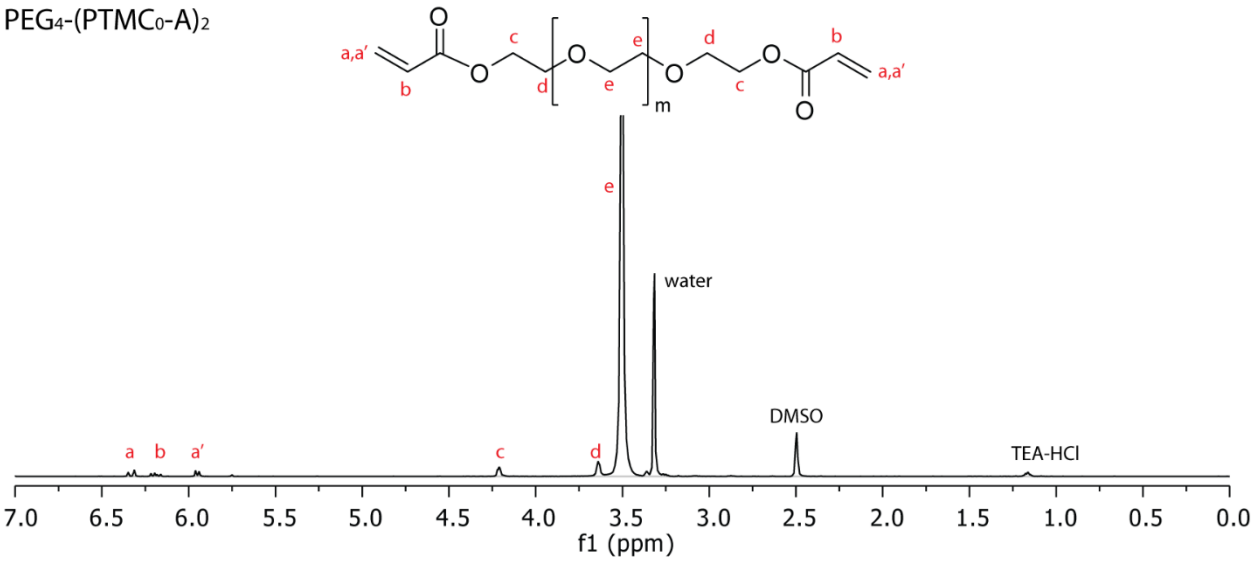

Figure A-1: Chemical structure and ^{1}H NMR spectrum of PEG$_4$-(PTMC$_0$-A)$_2$. Spectrum recorded from sample dissolved in DMSO-d$_6$, 25 °C, 400 MHz.

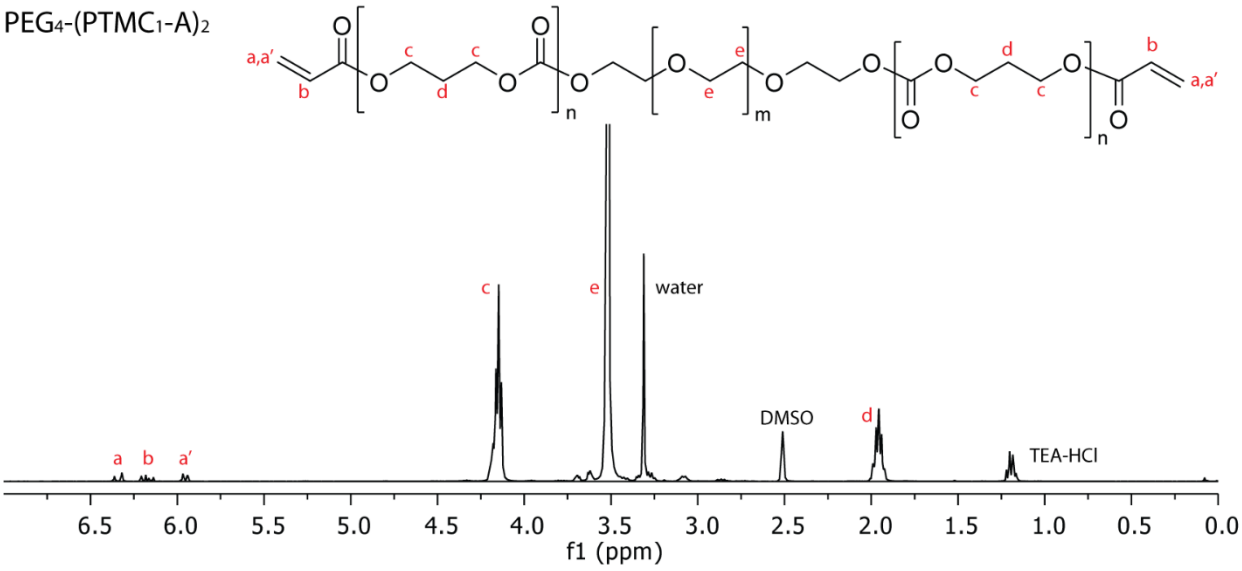

Figure A-2: Chemical structure and ^{1}H NMR spectrum of PEG$_4$-(PTMC$_1$-A)$_2$. Spectrum recorded from sample dissolved in DMSO-d$_6$, 25 °C, 400 MHz.

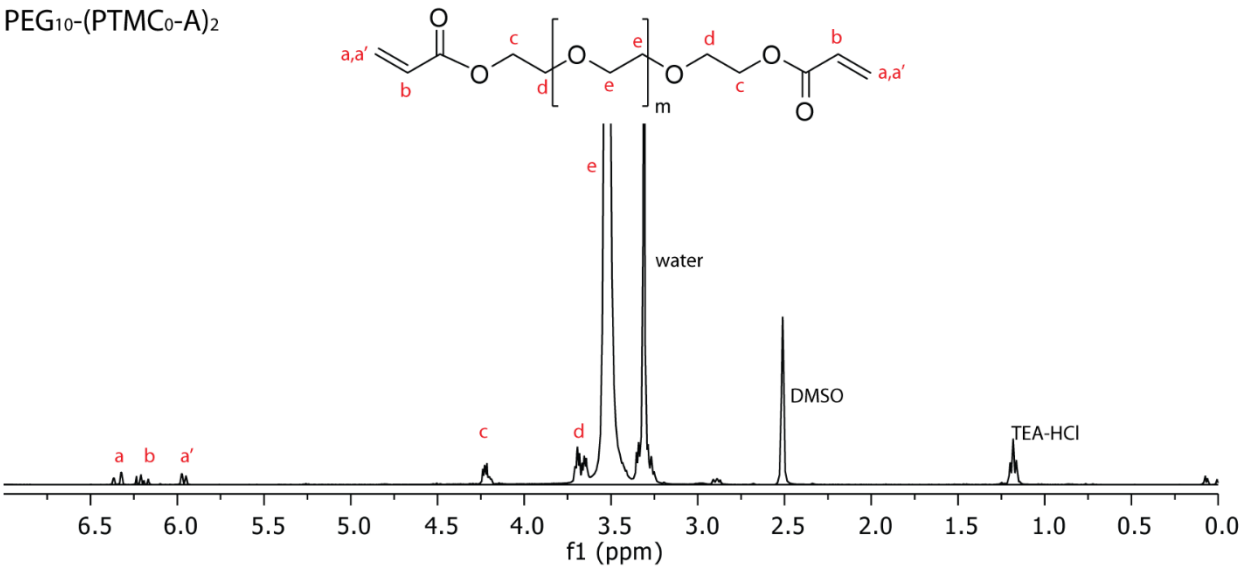

Figure A-3: Chemical structure and ^{1}H NMR spectrum of PEG$_{10}$-(PTMC$_{0}$-A)$_{2}$. Spectrum recorded from sample dissolved in DMSO-d$_6$, 25 °C, 400 MHz.

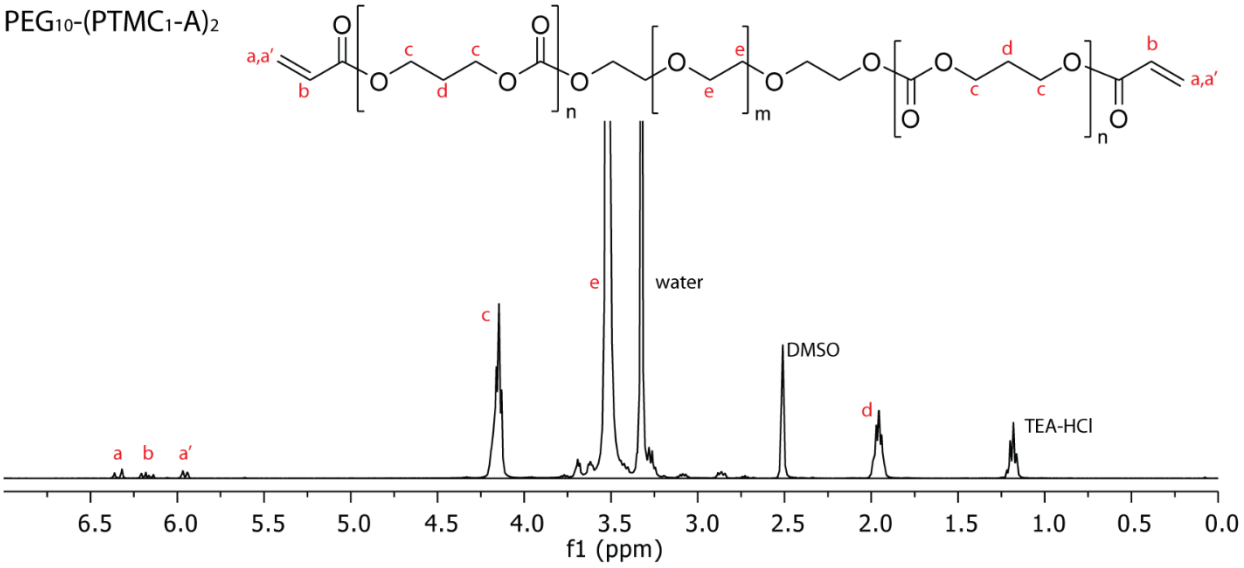

Figure A-4: Chemical structure and ^{1}H NMR spectrum of PEG$_{10}$-(PTMC$_{1}$-A)$_{2}$. Spectrum recorded from sample dissolved in DMSO-d$_6$, 25 °C, 400 MHz.

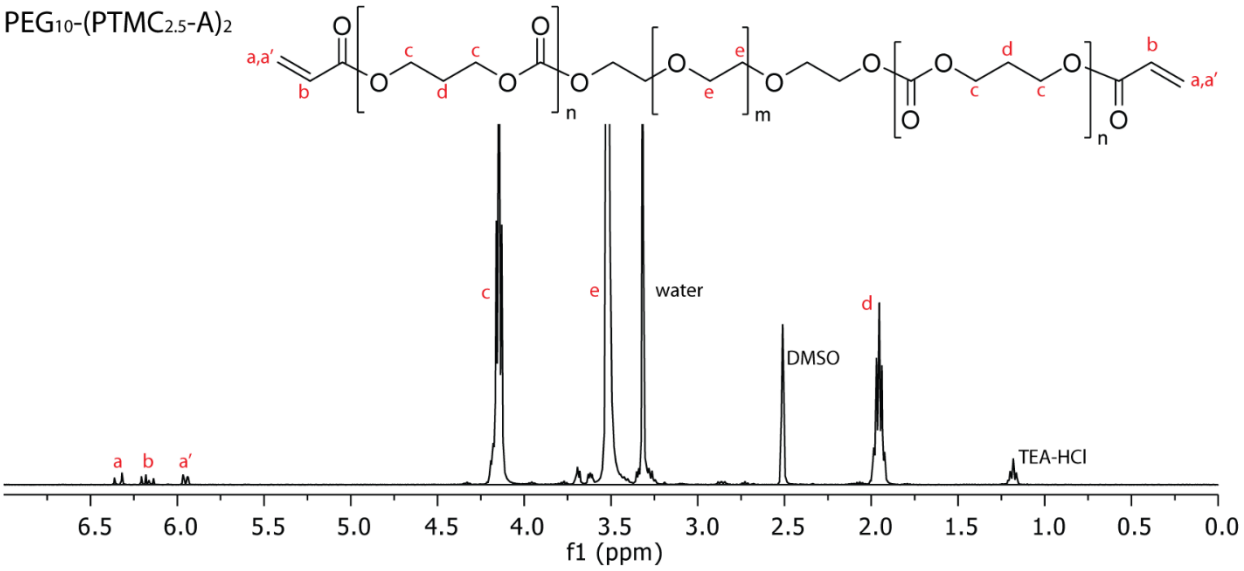

Figure A-5: Chemical structure and ^{1}H NMR spectrum of PEG$_{10}$-(PTMC$_{2.5}$-A)$_2$. Spectrum recorded from sample dissolved in DMSO-d$_6$, 25 °C, 400 MHz.

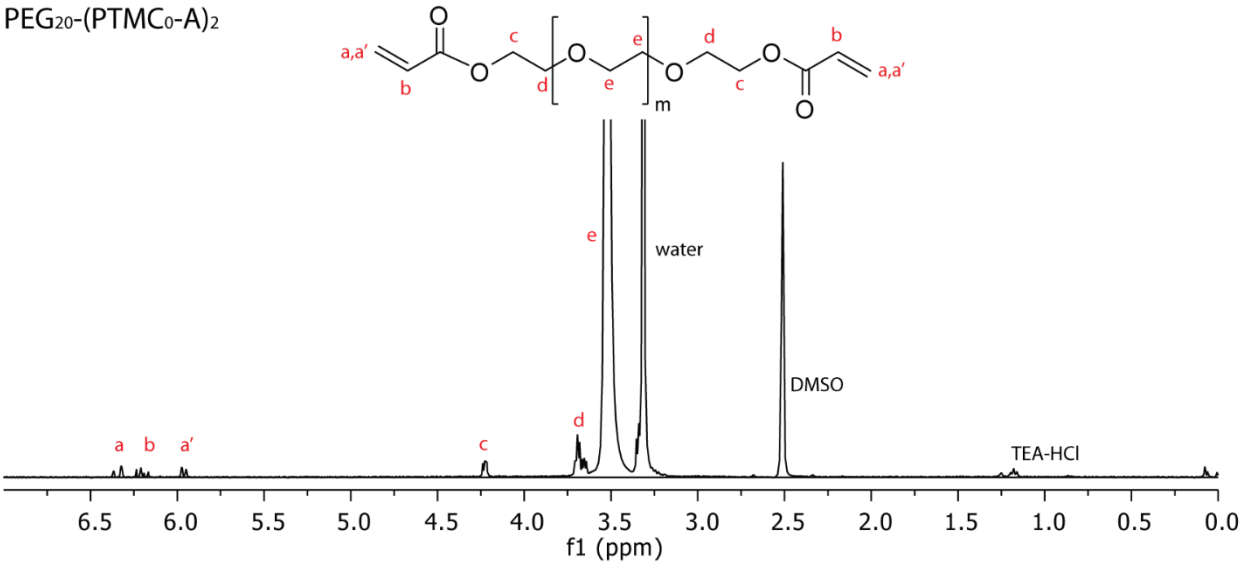

Figure A-6: Chemical structure and ^{1}H NMR spectrum of PEG$_{20}$-(PTMC$_{0}$-A)$_2$. Spectrum recorded from sample dissolved in DMSO-d$_6$, 25 °C, 400 MHz.

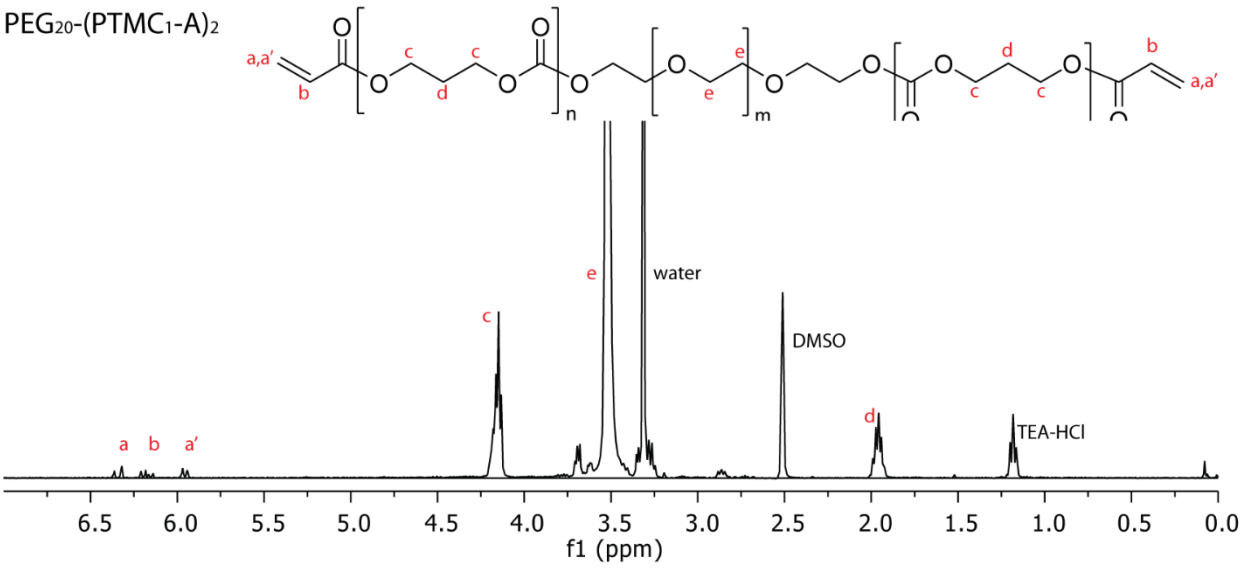

Figure A-7: Chemical structure and ^{1}H NMR spectrum of PEG$_{20}$-(PTMC$_{1}$-A)$_{2}$. Spectrum recorded from sample dissolved in DMSO-d$_6$, 25 °C, 400 MHz.

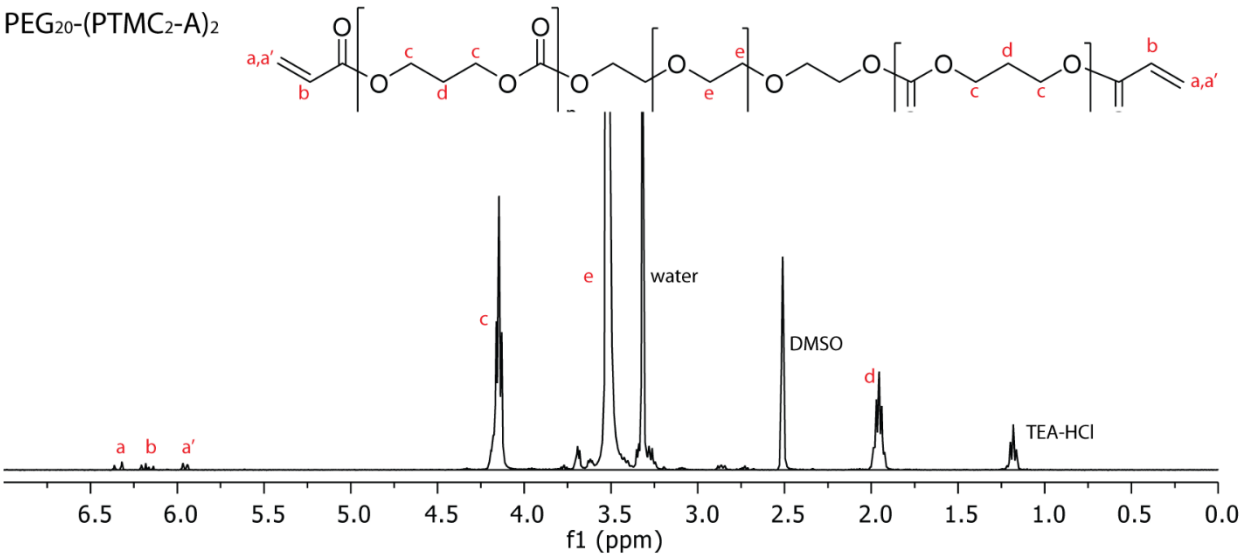

Figure A-8: Chemical structure and ^{1}H NMR spectrum of PEG$_{20}$-(PTMC$_{2}$-A)$_{2}$. Spectrum recorded from sample dissolved in DMSO-d$_6$, 25 °C, 400 MHz.

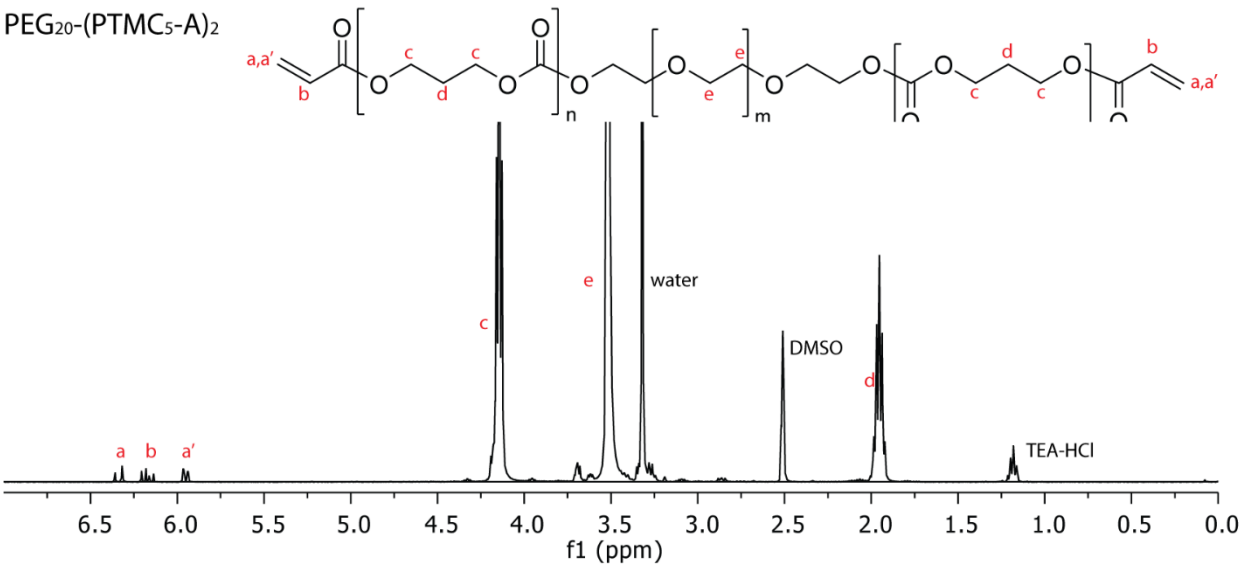

Figure A-9: Chemical structure and ^{1}H NMR spectrum of PEG$_{20}$-(PTMC$_5$-A)$_2$. Spectrum recorded from sample dissolved in DMSO-d$_6$, 25 °C, 400 MHz.

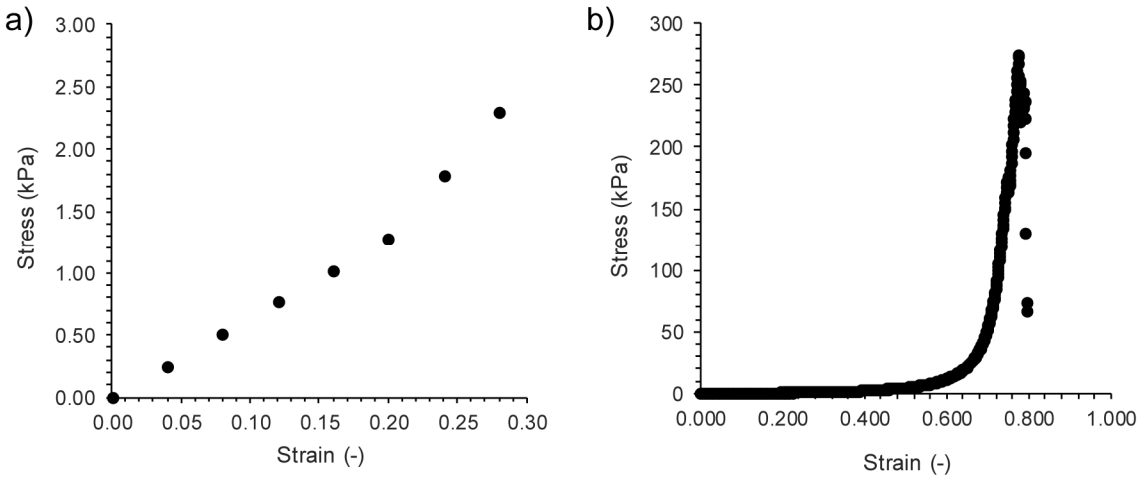

Figure A-10: Representative plots from the mechanical testing of mixed 1% w/v MGC + 4% w/v PEG$_{10}$-(PTMC$_1$-A)$_2$ hydrogels. a) Equilibrium stress versus strain, and b) Stress versus strain during compressive failure testing.

A.2 Queen's University research ethics board approval

QUEEN'S UNIVERSITY HEALTH SCIENCES & AFFILIATED TEACHING HOSPITALS RESEARCH ETHICS BOARD (HSREB)

HSREB Renewal of Ethics Clearance

June 01, 2016

Dr. Lauren Flynn
Department of Chemical Engineering
Dupuis Hall, Queen's University

ROMEO/TRAQ #: 6004616
Department Code: CHEM-002-07
Study Title: Tissue Engineering with Adipose-Derived Stem Cells
Review Type: Delegated
Date Ethics Clearance Effective: June 24, 2016
Ethics Clearance Expiry Date: June 24, 2017

Dear Dr. Flynn,

The Queen's University Health Sciences & Affiliated Teaching Hospitals Research Ethics Board (HSREB) has reviewed the application. This study, including all currently approved documentation has been granted ethical clearance until the expiry date noted above.

Prior to the expiration of your ethics clearance, you will be reminded to submit your renewal report through ROMEO. Any lapses in ethical clearance will be documented below.

Yours sincerely,

Albert J. Clark.

Chair, Health Sciences Research Ethics Board

The HSREB operates in compliance with, and is constituted in accordance with, the requirements of the Tri-Council Policy Statement: Ethical Conduct for Research Involving Humans (TCPS 2); the International Conference on Harmonisation Good Clinical Practice Consolidated Guideline (ICH GCP); Part C, Division 5 of the Food and Drug Regulations; Part 4 of the Natural Health Products Regulations; Part 3 of the Medical Devices Regulations, Canadian General Standards Board, and the provisions of the Ontario Personal Health Information Protection Act (PHIPA 2004) and its applicable regulations. The HSREB is qualified through the CTO REB Qualification Program and is registered with the U.S. Department of Health and Human Services (DHHS) Office for Human Research Protection (OHRP). Federalwide Assurance Number: FWA#:00004184, IRB#:00001173

HSREB members involved in the research project do not participate in the review, discussion, or decision.

A.3 University of Western Ontario research ethics board approval

Western Research

Research Ethics

Western University Health Science Research Ethics Board
HSREB Delegated Initial Approval Notice

Principal Investigator: Dr. Lauren Flynn
Department & Institution: Schulich School of Medicine and Dentistry\Anatomy & Cell Biology,Western University

HSREB File Number: 105426
Study Title: Tissue Engineering with Adipose-derived Stem Cells
Sponsor: Canadian Institutes of Health Research

HSREB Initial Approval Date: August 13, 2014
HSREB Expiry Date: August 31, 2019

Documents Approved and/or Received for Information:

Document Name	Comments	Version Date
Other	Letter for OR and Clinic Staff to Introduce the Study (received June 2/14)	
Western University Protocol		2014/07/23
Letter of Information & Consent		2014/07/23

The Western University Health Science Research Ethics Board (HSREB) has reviewed and approved the above named study, as of the HSREB Initial Approval Datenoted above.

HSREB approval for this study remains valid until the HSREB Expiry Date noted above, conditional to timely submission and acceptance of HSREB ContinuingEthics Review. If an Updated Approval Notice is required prior to the HSREB Expiry Date, the Principal Investigator is responsible for completing andsubmitting an HSREB Updated Approval Form in a timely fashion.

The Western University HSREB operates in compliance with the Tri-Council Policy Statement Ethical Conduct for Research Involving Humans (TCPS2), theInternational Conference on Harmonization of Technical Requirements for Registration of Pharmaceuticals for Human Use Guideline for Good Clinical PracticePractices (ICH E6 R1), the Ontario Personal Health Information Protection Act (PHIPA, 2004), Part 4 of the Natural Health Product Regulations, Health CanadaMedical Device Regulations and Part C, Division 5, of the Food and Drug Regulations of Health Canada.

Members of the HSREB who are named as Investigators in research studies do not participate in discussions related to, nor vote on such studies when theyare presented to the REB.

The HSREB is registered with the U.S. Department of Health & Human Services under the IRB registration number IRB 00000940.

Ethics Officer, on behalf of Dr. Joseph Gilbert, HSREB Chair

Ethics Officer to Contact for Further Information

Erika Basile	Grace Kelly	Mina Mekhail	Vikki Tran
ebasile@uwo.ca	grace.kelly@uwo.ca	mmekhail@uwo.ca	vikki.tran@uwo.ca

This is an official document. Please retain the original in your files.

A.4 Immunohistochemistry controls

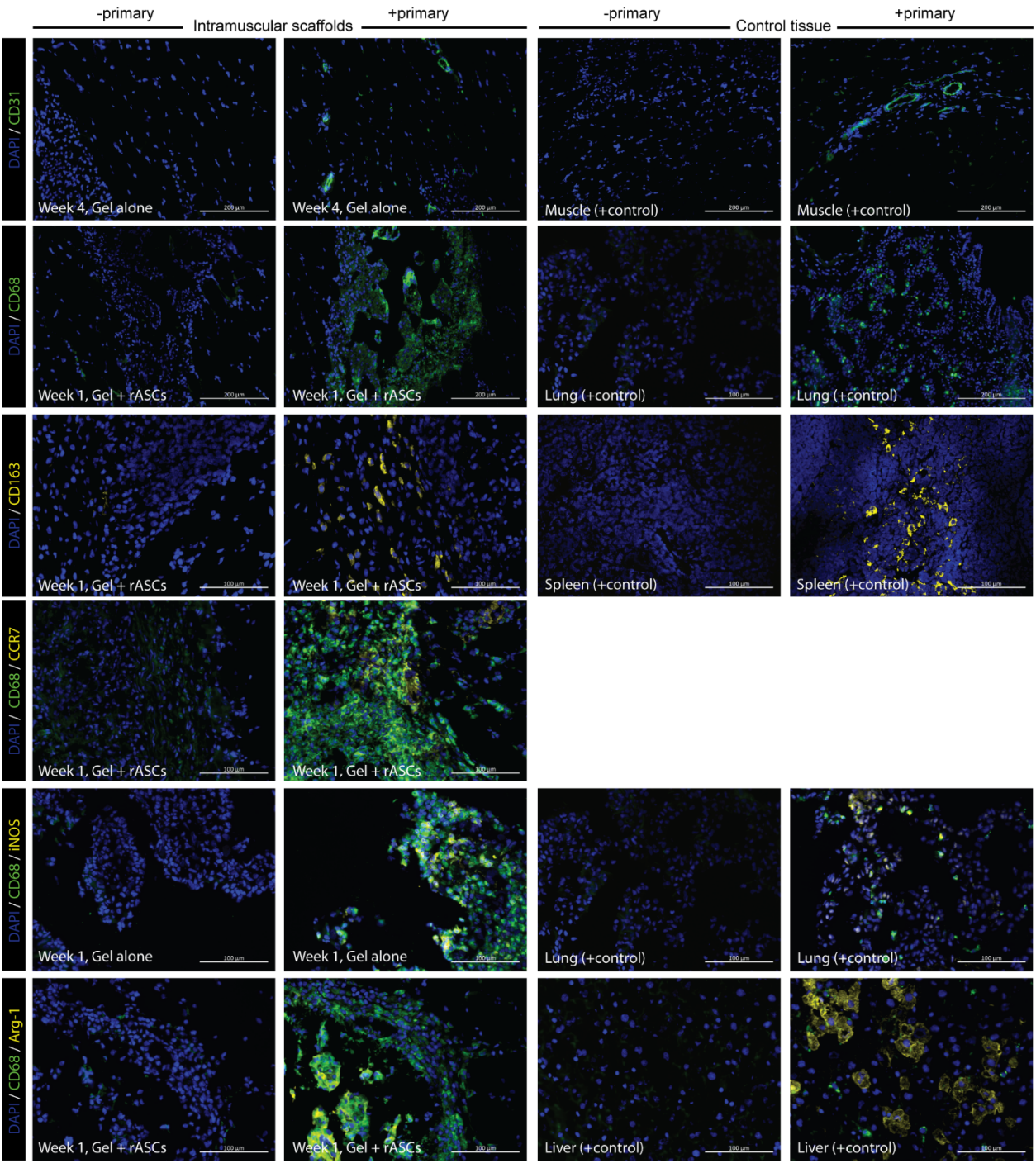

Figure A-11: Positive and negative controls for immunohistochemical staining of CD31, CD68, CD163, CCR7, iNOS, and Arg-1 in rat intramuscular implants. Negative primary controls were performed with the standard staining procedure, except no primary antibodies were added to the antibody dilution buffer for primary incubation.

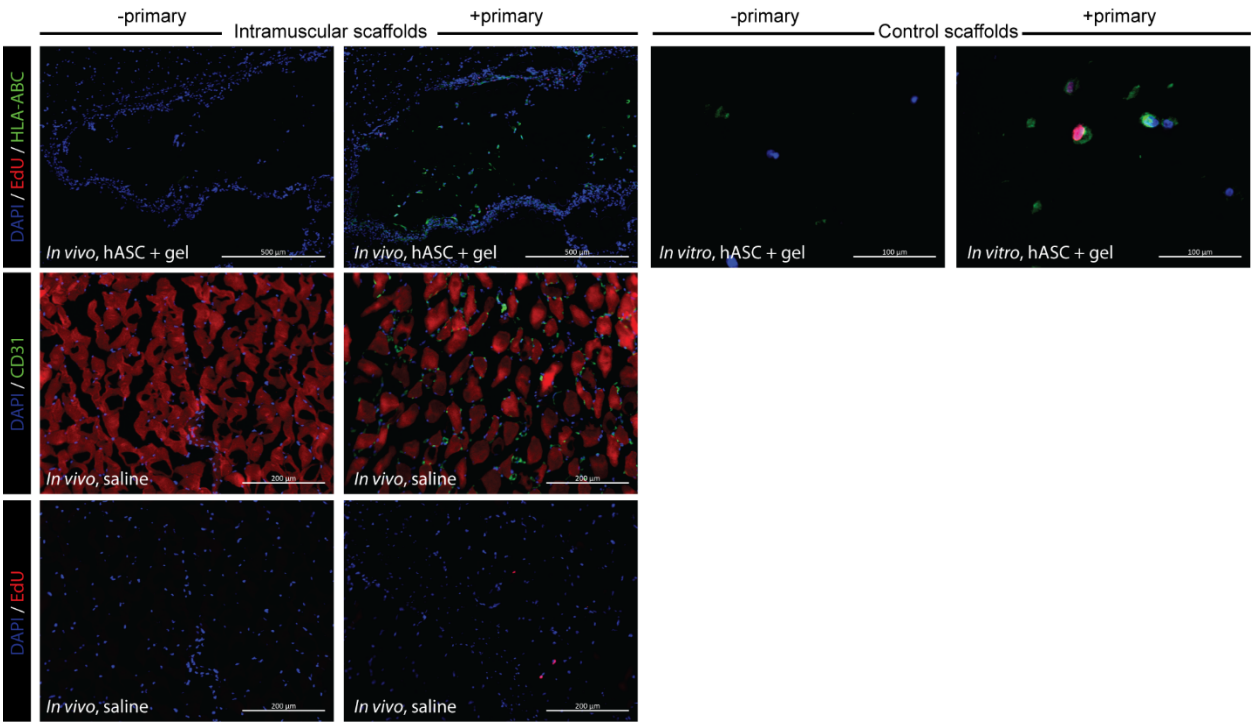

Figure A-12: Positive and negative controls for immunohistochemical staining of HLA-ABC, EdU, and CD31 in mouse intramuscular tissue. Negative primary controls were performed with the same staining procedure, except no primary antibodies were added to the antibody dilution buffer for primary incubation.